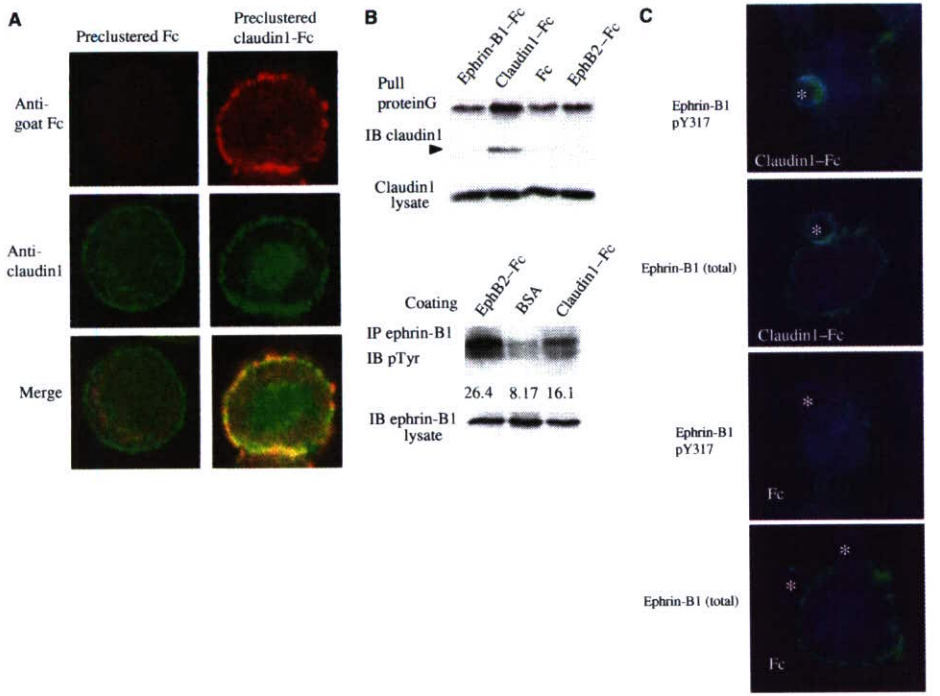

Figure 7 Clustered extracellular domains of claudin stimulate the phosphorylation of ephrin-B1. (**A**) HT29 cells were incubated with preclustered CLD1–Fc or the control Fc at 2 μg/ml for 1 h. The cells were immunostained with anti-CLD1 (green) and anti-Fc antibody (red). (**B**) Top: L CLD1 were incubated with Fc-fusion proteins as indicated. The cell lysates were precipitated with protein-G Sepharose, and subjected to IB with anti-CLD1 antibody. Bottom: L ephrin-B1 CLD1 were seeded at a low cell density on the plates coated with EphB2–Fc, BSA, or CLD1–Fc, as described in Materials and Methods. Ephrin-B1 was immunoprecipitated from the cell lysates 3 h after plating, and subjected to IB with 4G10. Values below each band are relative density of the bands. The same filter was re-hybridized with anti-ephrin-B1 antibody. (**C**) Microbeads precoated with claudin–Fc or control Fc were added to L ephrin-B1 CLD1. After 30 min incubation, cells were fixed, and immunostained with anti-pTyr ephrin-B1 or anti-ephrin-B1 (C18) antibody, which reacts with the C-terminal region of ephrin-B1 together with TOTO-3 iodide. The positions of the beads were marked with asterisks.

was detected on cell membrane contacting to the bead (Figure 7C). Moreover, ephrin-B1 was concentrated at the bead–cell contact sites (Figure 7C). On the other hand, we could not detect either phosphorylation or concentration of ephrin-B1 at the contact sites to the control Fc-coated beads.

Tyrosine phosphorylation of ephrin-B1 affects cell–cell adhesion

In order to understand the biological effects of the interaction of ephrin-B1 with claudins, we examined its potential influence on cell–cell adhesion. No significant morphological change in the confluent MDCK cells was observed even when ephrin-B1 expression was induced by doxycycline (Figure 8A, 'No Treatment'). On the other hand, apparent delay in the restoration of the cell–cell adhesion after calcium switch (see Materials and methods) was observed by inducible expression of ephrin-B1 (Figure 8A). To quantify this morphological observation, paracellular flux of fluorescence-labeled dextran was monitored in MDCK cells. The decrease in paracellular flux after calcium switch was also delayed in cells overexpressing ephrin-B1 (Figure 8B).

The effects of various ephrin-B1 mutants on cell adhesion were next compared by expressing wild type or mutants of ephrin-B1 through adenovirus-mediated gene transfer in confluent MDCK cells. Expression of wild-type ephrin-B1 slightly increased the permeability compared to expression of control GFP (Figure 8C, top). The difference was enhanced when the permeability was measured periodically during the weak treatment of the cells with calcium-chelating agent under the condition that phosphorylation of wild-type ephrin-B1 was still maintained (Figure 8C, bottom). On the other hand, the expression of ephrin-B1 lacking the cytoplasmic region (Δcyto) and the ephrin-B1 with the mutation of tyrosine residues in the cytoplasmic region (4YF) did not greatly affect the paracellular permeability (Figure 8C). In contrast, the expression of ephrin-B1 mutant lacking the valine at the carboxyl-tail (ΔV), which is reported to be critical for binding PDZ domain-containing proteins,

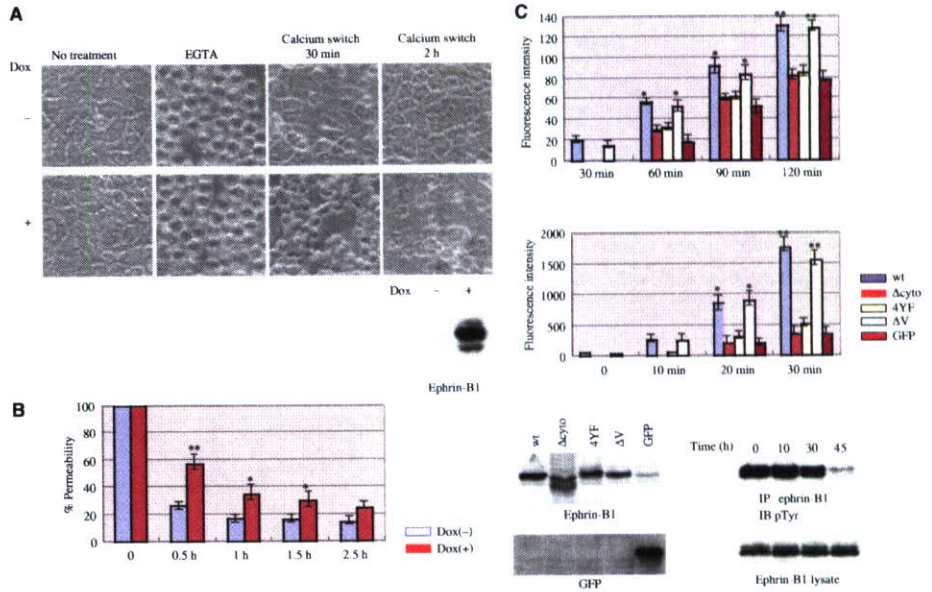

Figure 8 Tyrosine phosphorylation of ephrin-B1 affects intercellular adhesion: (**A**) MDCK ephrin-B1 Tet-ON cells were grown on culture dishes until confluent with (+) or without (−) the addition of doxycycline (Dox). The cells were incubated in $HBSS^{-}$-containing EGTA. The medium was then replaced by one containing calcium (calcium switch), and the cells were incubated for the indicated period. (**B**) MDCK ephrin-B1 Tet-ON cells grown in the Transwell chambers (Dox− or Dox+) were treated with EGTA to increase the initial permeability to almost the same levels. The monolayers were allowed to recover in the calcium-containing medium for the indicated period, then subject to FITC-dextran flux measurement. The results are presented in terms of the % fluorescence of the cells without recovery. Each bar represents the mean values ± s.d. from four independent experiments, each in duplicate. The asterisk indicates differences from Dox (−) cells at each time point. $^{*}P<0.05$, $^{**}P<0.01$. (**C**) Confluent MDCK cells grown in Transwells were infected with Ad-ephrin-B1, Ad-Δcyto ephrin-B1, Ad-4YF ephrin-B1, Ad- ΔV ephrin-B1 or Ad-GFP as described in Materials and methods. Top: The FITC-dextran flux during the indicated time was measured without pretreatment of EGTA. Bottom: The infected cells were treated with EGTA for the indicated period, and then FITC-dextran flux during the next 30 min was measured. This experiment was performed under the conditions of cell–cell contact remaining after treatment with EGTA, which was confirmed through the microscopic observation. Expression of ephrin-B1 from each construct in infected MDCK cells and the phosphorylation level of ephrin-B1 at each time point of EGTA treatment were shown at the bottom (left and right panels, respectively). The results from four independent experiments, each in duplicate, are shown as the mean values ± s.d. The asterisk indicates differences from the permeability of GFP-infected cells at each time point. $^{*}P<0.01$, $^{**}P<0.001$.

increased the permeability as well as wild-type ephrin-B1, suggesting that this residue is not crucial for the regulation of cell–cell adhesion. These results suggest that ephrin-B1 affects cell–cell adhesion depending on its tyrosine phosphorylation.

Discussion

Examination of the mode of association between claudin andephrin-B1 revealed that claudin associates with ephrin-B1 on the same cell surface. The formation of cell–cell contact remarkably enhances the phosphorylation of ephrin-B1 in a claudin-dependent manner. Our result further suggests that claudin–ephrin-B1 complex attenuates cell–cell adhesion through the phosphorylated cytoplasmic domain of ephrin-B1 (Figure 9). The association of ephrin-B1 with CLD1 and CLD4 was detected in the single cells. On the other hand, ephrin-B1–Fc did not bind to the CLD1 expressed on the cell membrane (Figure 7B), and, similarly, CLD1–Fc in the culture medium did not bind to ephrin-B1 (data not shown). Together with the observation that claudins did not stimulate the phosphorylation of ephrin-B1 in opposing membrane through the overlay coculture method (Supplementary data 3A), these results suggest that ephrin-B1 and claudins associate *in cis* on the same cell membrane, but not *in trans*.

In order to propose the novel mechanism for the activation of ephrin-B1 reverse signaling though claudins, we showed the ephrin-B1 phosphorylation in several cell lines in which the effects of cognate receptor EphB appear to be little or negligible. In COS1 cells, which were used to show the effect of claudin ECD1 on the phosphorylation of ephrin-B1, very little amount of EphB2 receptor was detected (Supplementary data 5A), there remaining a slight possibility that this receptor affects the phosphorylation state of ephrin-B1. Actually, there is a possibility that overexpressed claudin enhanced cell–cell interaction, which resulted in increased EphB2–ephrin-B1 interactions and enhanced ephrin-B1 phosphorylation. Therefore, HEK 293 cell, which according to several

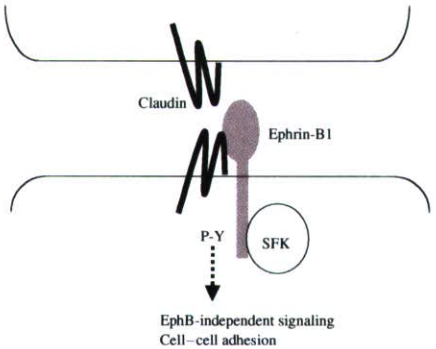

Figure 9 Diagram showing the possible relation between ephrin-B1 and claudin. The intercellular interaction of claudins stimulates the tyrosine phosphorylation of ephrin-B1 most probably through the activation of SFK, which may transduce signaling to the downstream effectors. The phosphorylation of ephrin-B1 directly or indirectly modifies the degree of cell–cell adhesion.

reports do not contain detectable levels of Eph receptors that bind ephrin-B1, was also used to confirm the results (Figure 3B) (Zisch *et al*, 2000; Miao *et al*, 2005).

The cognate receptors for ephrin-B1 were not detected in L cells and MDCK cells by ephrin-B1–Fc labeling (Supplementary data 5B), and at least EphB1, EphB2 and EphB3 were not detected by RT–PCR in L cells (data not shown). Moreover, ephrin-B1 phosphorylation level was not attenuated by the addition of soluble ephrin-B1 in L and MDCK cells (Supplementary data 5C), which was consistent with the observation that soluble ephrin-B1 blocks the EphB receptor-stimulated signaling, but does not affect the interaction between ephrin-B1 and claudin on the same cell membrane. Together with the observation that immobilized CLD1–Fc directly phosphorylated ephrin-B1, these results suggest that ephrin-B1 phosphorylation was enhanced by the interaction with claudins.

The phosphorylation of ephrin-B1 in claudin-expressing L cells was markedly increased in the existence of cell–cell adhesion. Although we cannot rule out the possibility that less amount of association between ephrin-B1 and claudin in single scattered cells may affect the phosphorylation level of ephrin-B1 (Figure 5A), clustered CLD1–Fc fusion protein coated on the plates or microbeads enhanced ephrin-B1 phosphorylation, suggesting that the intercellular interaction of claudins is most probably required for the phosphorylation of ephrin-B1. This increase in tyrosine phosphorylation cannot be explained by any other adhesion molecules or any cognate receptor for ephrin-B1, since the phosphorylation level of ephrin-B1 in parent L cells did not alter according to cell density (Figure 5). The fact that the incubation of the cells with soluble clustered CLD1–Fc was not as effective for the phosphorylation of ephrin-B1, suggests a functional difference between soluble clustered claudin and the endogenous claudin on the cell membrane. It is well known that the clustering of ephrin-B1 on the cell membrane represented the trigger of its phosphorylation when stimulated by the EphB2–Fc fusion protein. The intercellular interaction of claudins may enhance the local concentration of associating ephrin-B1, resulting in oligomerization and the activation of ephrin-B1 as a substrate of SFK. As the isolated ECD1 of CLD1 or CLD4 could not activate tyrosine phosphorylation of ephrin-B1, such concentration of ephrin-B1 may not be induced by the isolated ECD1 of claudins. Alternatively, the intercellular interaction of claudins may directly stimulate the activation of SFK, which in turn phosphorylate ephrin-B1 associating with the claudin. However, the presence of such activation of the SFK in response to the intercellular interaction of claudins is as yet unknown. In addition, the cause of the basal level of ephrin-B1 phosphorylation in parent L cells is not still clear. There still remains the possibility that some other mechanism causing the slight phosphorylation of ephrin-B1.

Ephrin-B1 increased the degree of paracellular permeability, which is a consequence of the tyrosine phosphorylation of the cytoplasmic domain of ephrin-B1. This result suggests that the interaction of claudins with ephrin-B1 attenuated cell–cell adhesion through a cellular signal transduction through phosphorylated ephrin-B1, rather than physical interference with claudins to make homophilic clusters. The measurement of the permeability of low-molecular-size dextran is commonly used for the assessment of tight junctions. However, phosphorylated ephrin-B1 does not seem to exclusively modify the function of tight junctions, because it affected the gross change of cell–cell adhesion. Although the phosphorylation of ephrin-B1 was induced by claudins, further precise examination is necessary to determine which adhesion molecule is the primary target of phosphorylated ephrin-B1. The ephrin-B1 phosphorylation does not regulate cell–cell adhesion through the modification of the expression levels of the proteins composing tight or adherence junctions. For example, the overexpression of ephrin-B1 in MDCK cells induced by doxycyline did not change the protein expression levels of CLD1, CLD4, ZO-1, E-cadherin and β-catenin (data not shown).

The expression of ephrin-B1 increased the permeability during both the processes of destabilizing the cell adhesion through EGTA treatment and restoring cell–cell adhesion after the calcium switch. The intracellular localization of claudins may therefore be important for the ephrin-B1-mediated regulation of cell–cell adhesion. When claudins are localized to tight junctions in a restrictive manner, ephrin-B1 may not be phosphorylated widely. In our assay of paracellular flux, overexpression of ephrin-B1 was induced in MDCK cells by adenovirus infection after the cells reached confluent, which might be the reason why ephrin-B1 did not increase the permeability effectively without treatment of the calcium-chelating agent. The disruption of tight junctions through calcium depletion leads to the presence of naive cell–cell contacts with the diffusion of claudins on the cell membrane, which may further stimulate ephrin-B1 phosphorylation more widely, and accelerate the cell dissociation. The intercellular interaction between claudins occurs also in naive-contact cells, which do not possess the mature tight junction strands. In the calcium-switching process, the formation of new cell–cell contact triggers the ephrin-B1 phosphorylation, which may then delay the construction of the firm cell–cell adhesion. Such mechanisms may be also involved in the event of epithelial-to-mesenchymal transition during the invasion and metastasis of some carcinoma cells. Alternately, ephrin-B1-expressing MDCK cells may be settled in a 'ready to dissociate' state when they are confluent. Upon the depletion of the extracellular calcium, the breaking up of cell–cell adhesion structures might be accelerated in these cells. The morphological observation of ephrin-B1-expressing MDCK cells (Figure 8A) also suggests that the phosphorylation of ephrin-B1 may affect the spreading of the cells resulting from the modification of cell-to-substrate adhesion.

Recent studies show that cell adhesion can trigger ligand-independent activation of growth factor receptors (Comoglio *et al*, 2003). For example, EGF receptor associates with E-cadherin. Following the cell–cell contact formation, an EGF receptor was found to be phosphorylated on tyrosine residues, which in turn activated MAP kinase and Rac in the absence of EGF stimulation (Pece and Gutkind, 2000; Betson *et al*, 2002). Claudins may play roles in translating environmental cues into intracellular signals through coupling with ephrin-B1 according to our results. Some of the claudins are frequently overexpressed in many cancer cells from the studies involving screening of the genes preferentially expressed in malignant cells. Therefore, claudins may play significant roles in carcinogenesis or the progression of cancers. In HT29 colon cancer cells, ephrin-B1 and claudins were found to be diffusely localized on the cell membrane, which may increase the chance of inducing ephrin-B1 phosphorylation. Novel signaling through the interaction of ephrin-B1 with claudins may inhibit the formation of tight adhesive structures during the process of cell–cell contact in some carcinoma cells, which may, in turn, affect malignant phenotypes such as invasion and metastasis of the carcinomas.

Materials and methods

Plasmids and antibodies, cDNA library, cell culture, IP and cell staining

Plasmids and antibodies used in this study and the methods of the library screening, cell culture, IP and cell staining are described in Supplementary data 1.

Preparation of CLD1–Fc-coated beads

Latex-sulfate microspheres (5.2 μm diameter; Interfacial Dynamics Corporation) were coated with CLD1–Fc fusion protein as reported (Honda *et al*, 2003). Briefly, beads were suspended in 0.1 M borate buffer, pH 8.0, and incubated with goat anti-mouse IgG (Fc-specific) antibody (ICN). After the beads were washed with PBS, the beads were then incubated with CLD1–Fc protein. After the incubation, the beads were washed three times with PBS, and resuspended in PBS containing 5 mg/ml bovine serum albumin (BSA).

Generation of adenoviruses and adenoviral infection

To generate recombinant adenoviruses, cDNAs encoding wild type or various mutants of ephrin-B1 were subcloned into the vector pShuttle-CMV (Stratagene). Transposition of the ephrin-B1 cDNAs from the pShuttle-CMV into pADEasy-1 (Stratagene) created the adenoviral vectors pAD-ephrin-B1 (wild type, Δcyto, 4YF, ΔV), where the transgenes were under the control of a CMV promoter. Recombinant adenoviral DNA was transfected into 293 human embryonic kidney cells to allow the production of adenoviral particles. The titer of adenovirus stocks was determined by an Adeno-X rapid titer kit (Clontech). Confluent MDCK cells grown on Transwell filters or glass coverslips were infected with adenoviruses at a multiplicity of infection (MOI) of 5 in medium containing 10% FBS. Following incubation for 12 h, the virus-containing medium was removed and fresh medium containing 10% FBS was added. The infected cells were used for the permeability assay 48 h after the infection.

Paracellular permeability assay

MDCK cells were grown until confluent in Transwell chambers, then the cells were either left untreated or treated with doxycycline (2 μg/ml) for 48 h prior to subject to the assay. In some experiments, the medium of both the upper and lower wells was replaced with Hank's balanced salt solutions (HBSS$^-$) containing 2 mM of EGTA for the indicated period. We performed the experiments under the conditions of cell–cell contact remaining after treatment with EGTA, which was confirmed through the microscopic observation. In some experiments, the monolayers were allowed to recover in the calcium-containing medium (calcium switch) with 0.5% FBS for the indicated period. Then, the upper well was replaced to the normal medium containing 0.5% FBS with FITC-dextran (MW 3000) at a concentration of 10 μg/ml. Following incubation for the indicated period, samples were taken from the lower compartment of the Transwell chambers. The amount of FITC-dextran in the lower wells was measured using Beacon 2000 (Takara), with an excitation wavelength of 490 nm and detection of emissions at 530 nm. Student's *t*-test was used to analyze data from four independent experiments, each in duplicate.

Supplementary data

Supplementary data are available at *The EMBO Journal* Online.

Acknowledgements

We thank Dr S Tsukita (Kyoto University) for providing the plasmids used in this study. This study was supported by the Program for the Promotion of Fundamental Studies in Health Science of the Organization for Pharmaceutical Safety and Research of Japan.

References

Batlle E, Henderson JT, Beghtel H, Van den Born MM, Sancho E, Huls G, Meeldijk J, Robertson J, Van de Wetering M, Pawson T, Clevers H (2002) β-catenin and TCF mediate cell positioning in the intestinal epithelium by controlling the expression of EphB/Ephrin-B. *Cell* **111:** 251–263

Betson M, Lozano E, Zhang J, Braga VM (2002) Rac activation upon cell–cell contact formation is dependent on signaling from the epidermal growth factor receptor. *J Biol Chem* **277:** 36962–36969

Bong YS, Park YH, Lee HS, Mood K, Ishimura A, Daar IO (2004) Tyr-298 in ephrinB1 is critical for an interaction with the Grb4 adaptor protein. *Biochem J* **377:** 499–507

Brantley-Sieders D, Parker M, Chen J (2004) Eph receptor tyrosine kinases in tumor and tumor microenvironment. *Curr Pharm Des* **10:** 3431–3442

Bruckner K, Pasquale EB, Klein R (1997) Tyrosine phosphorylation of transmembrane ligands for Eph receptors. *Science* **275:** 1640–1643

Comoglio PM, Boccaccio C, Trusolino L (2003) Interactions between growth factor receptors and adhesion molecules: breaking the rules. *Curr Opin Cell Biol* **15:** 565–571

Cowan CA, Henkemeyer M (2001) The SH2/SH3 adaptor Grb4 transduces B-ephrin reverse signals. *Nature* **413:** 174–179

Fujita M, Itoh M, Shibata M, Taira S, Taira M (2002) Gene expression pattern analysis of the tight junction protein, Claudin, in the early morphogenesis of *Xenopus* embryos. *Mech Dev* **119:** S27–S30

Furuse M, Sasaki H, Fujimoto K, Tsukita S (1998) A single gene product, claudin -1 or -2, reconstitutes tight junction strands and recruits occludin in fibroblasts. *J Cell Biol* **143:** 391–401

Himanen JP, Rajashankar KR, Lackmann M, Cowan CA, Henkemeyer M, Nikolov DB (2001) Crystal structure of an Eph receptor–ephrin complex. *Nature* **414:** 933–938

Holland SJ, Gale NW, Mbamalu G, Yancopoulos GD, Henkemeyer M, Pawson T (1996) Bidirectional signalling through the EPH-

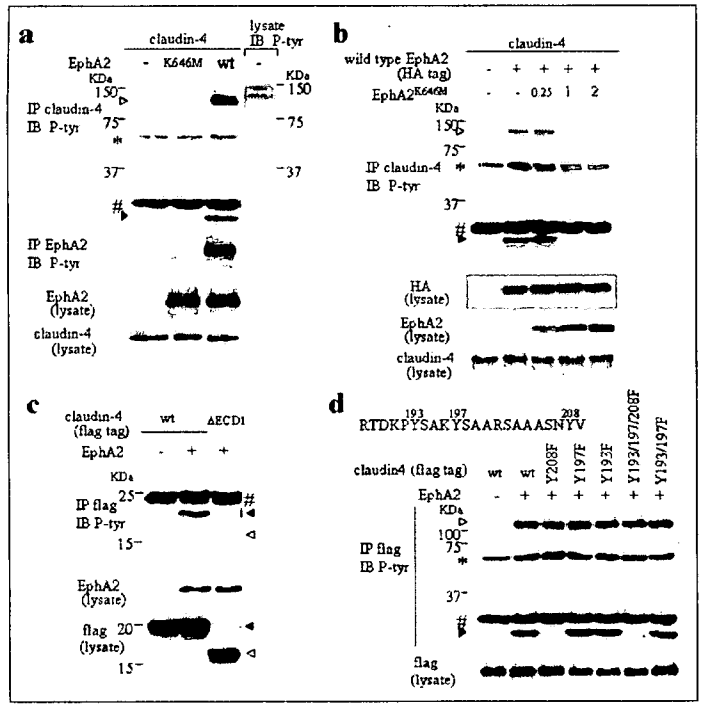

FIGURE 3. **Claudin-4 is tyrosine phosphorylated by the interaction with EphA2.** *a*, COS1 cells were transiently transfected with claudin-4 and wild type (*wt*) or a kinase-inactive mutant (*K646M*) of EphA2. *Upper panel*, claudin-4 was immunoprecipitated (*IP*) from cell lysates and subjected to immunoblotting with anti-phosphotyrosine (4G10). *Arrowheads* indicate tyrosine-phosphorylated EphA2 (*open*) and tyrosine-phosphorylated claudin-4 (*filled*). *Asterisk* and *sharp sign* indicate IgG heavy and light chains, respectively, which are not detected in the lysate of untransfected COS1 cells. *Middle panel*, EphA2 was immunoprecipitated (*IP*) from the cell lysates, and tyrosine phosphorylation of EphA2 was detected by immunoblotting (*IB*) with 4G10. *Bottom two panels*, EphA2 and claudin-4 detected in the lysate prior to immunoprecipitation. *b*, the kinase-inactive mutant of EphA2 competitively blocked the phosphorylation of claudin-4 by wild type EphA2. COS1 cells were transiently transfected with claudin-4 and hemagglutinin-tagged wild type EphA2 together with increasing amounts of kinase-inactive EphA2^{K646M} as indicated above the lanes. Assays were performed as in *panel a*. The expression level of wild type EphA2 (shown as immunoblotting with anti-hemagglutinin, *bottom panel*) was the same in each lysate. *Arrowheads* indicate tyrosine-phosphorylated EphA2 (*open*) and claudin-4 (*filled*). *Asterisk* and *sharp sign* indicate IgG heavy and light chains, respectively. *c*, claudin-4 lacking the binding region to EphA2 was not phosphorylated. COS1 cells were transiently transfected with wild type EphA2 and FLAG-tagged wild type claudin-4 or a mutant lacking the first extracellular domain of claudin-4 (*ΔECD1*) as indicated above the lanes. *Upper panel*, claudin-4 was immunoprecipitated (*IP*) with anti-FLAG from cell lysates, and tyrosine-phosphorylated claudin-4 was detected by immunoblotting (*IB*) with anti-phosphotyrosine (4G10). *Arrowheads* indicate wild type (*filled*) and ΔECD1 claudin-4 (*open*). *Sharp sign* indicates IgG light chain. *Lower panels*, EphA2 and FLAG-tagged claudin-4 detected in the lysate prior to immunoprecipitation. *d*, EphA2 phosphorylates claudin-4 at Tyr-208. The amino acid sequence of the carboxyl tail of human claudin-4 is shown at the top with the tyrosine residues numbered. COS1 cells were transiently transfected with EphA2 together with FLAG-tagged wild type (*wt*) claudin-4 or claudin-4 with mutations at the indicated tyrosine residues. Assays were performed as in *panel c*. *Upper panel*, *arrowheads* indicate phosphorylated EphA2 (*open*) and claudin-4 (*filled*). *Asterisk* and *sharp sign* indicate IgG heavy and light chains, respectively. *Lower panel*, FLAG-tagged claudin-4 detected in the lysate prior to immunoprecipitation.

right panel). These data demonstrated that ephrin-A1 and claudin-4 both bind to the amino-terminal region of EphA2 (amino acids 1–206), but in different manners.

Claudin-4 Is Phosphorylated in the Cytoplasmic Tail upon Interaction with EphA2—EphA2 is known to exhibit ligand-independent activation by homophilic dimer formation when overexpressed in COS1 cells. Claudin-4 was clearly phosphorylated on tyrosine residue when coexpressed with wild type EphA2, but not when coexpressed with EphA2^{K646M}, a kinase-inactive EphA2 mutant (Fig. 3*a*). Moreover, EphA2^{K646M} blocked tyrosine phosphorylation of claudin-4 induced by wild type EphA2 in a dose-dependent manner (Fig. 3*b*). It was also observed that the claudin-4 mutant that lacks the EphA2-binding site (amino acids 81–209, claudin-4 ΔECD1) was not phosphorylated (Fig. 3*c*). These results indicate that association of EphA2 with claudin-4 and EphA2 kinase activity is required for phosphorylation of claudin-4.

Claudin-4 has three tyrosine residues in the second (carboxyl-terminal) cytoplasmic domain, but there is no tyrosine in the first (amino-terminal) cytoplasmic domain. Among the three tyrosine residues in the second cytoplasmic domain, the one located at the carboxyl terminus is well conserved in most claudin families (22). EphA2-induced phosphorylation of claudin-4 was completely abolished when the tyrosine at the carboxyl terminus was replaced by phenylalanine (claudin-4^{Y208F}), whereas substitution of other tyrosine residues did not affect the phosphorylation level of claudin-4 (Fig. 3*d*).

It was next determined whether cell-cell contact stimulates tyrosine phosphorylation of claudin-4 by physiological activation of EphA2. HT29 cells were used because they express the ephrin-A1 ligand, which can activate EphA2 upon cell-cell adhesion (34). In HT29 cells, both EphA2 and claudin-4 were highly phosphorylated on tyrosine residues when the cells were plated at high density, whereas their phosphorylation level was very low when cell-cell interaction was disrupted by depletion of calcium in the medium (Fig. 4*a*). Treatment with nifedipine, a blocker of calcium channels, had no effect on the status of tyrosine phosphorylation of claudin-4 and EphA2 (data not shown), excluding the possibility that a decrease of intracellular calcium by EGTA affected the phosphorylation level of claudin. Treatment of HT29 cells with ephrin-A1-Fc enhanced phosphorylation of endogenous claudin-4 (Fig. 4*b*). Tyrosine phosphorylation of claudin-4 in HT29 cells was blocked by expression of EphA2-(1–563)-GFP, which does not contain the cytoplasmic region of EphA2 (Fig. 4*c*). These results suggest that claudin-4 is phosphorylated in HT29 cells when EphA2 is activated upon cell-cell interaction.

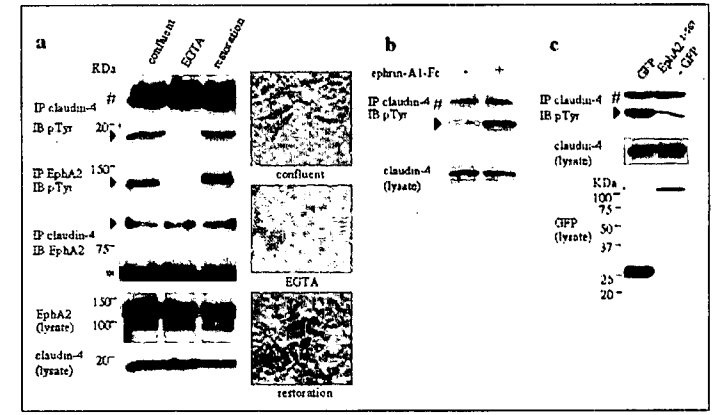

FIGURE 4. **Tyrosine phosphorylation of claudin-4 is induced by cell-cell contact.** *a*, HT29 cells were grown until confluent. The cells were either left untreated (*confluent*) or incubated in 2 mM EGTA in Hanks' balanced salt solution until cell-cell contacts were abolished but the cells remained attached to the plate (*EGTA*). EGTA was removed, and the cells were incubated in normal cell culture medium for 4 h (*restoration*). The cells were lysed at each time point and subjected to immunoprecipitation (*IP*) with anti-claudin-4 or anti-EphA2. Tyrosine-phosphorylated claudin-4 (*left column, top panel*) and tyrosine-phosphorylated EphA2 (*left column, second panel*) were detected by immunoblotting (*IB*) with anti-phosphotyrosine (4G10). EphA2 that coprecipitated with claudin-4 was detected by immunoblotting with anti-EphA2 (*left column, third panel*). Tyrosine-phosphorylated claudin-4, tryosine-phosphorylated EphA2, and coprecipitated EphA2 are indicated by *arrowheads*. *Sharp sign* and *asterisk* indicate IgG light and heavy chains, respectively. EphA2 and claudin-4 detected in the lysate prior to immunoprecipitation are shown in the *lower panels*. The appearance of the cells at each time point is shown in the *right panels*. *b*, HT29 cells plated at low cell density were treated with ephrin-A1-Fc for 10 min or left untreated (−). Claudin-4 was immunoprecipitated from each cell lysate, and tyrosine-phosphorylated claudin-4 was detected by immunoblotting (*IB*) with anti-phosphotyrosine (4G10). *Sharp sign* indicates IgG light chain. Claudin-4 detected in the lysate prior to immunoprecipitation is shown in the *lower panel*. *c*, confluent HT29 cells were infected with Ad-GFP or Ad-EphA2-(1–563)-GFP as indicated above the lanes. The infected cells were lysed, and the tyrosine phosphorylation of claudin-4 was examined as described in *panel b*. *Sharp sign* indicates IgG light chain. Claudin-4 and GFP and GFP-tagged EphA2 detected in the lysate prior to immunoprecipitation are shown in the *lower panels*.

Tyrosine Phosphorylation of Claudin-4 Attenuates Association with ZO-1—The carboxyl-terminal YV sequence of claudin associates with the PDZ domain of ZO-1 (22). We examined whether tyrosine phosphorylation of claudin-4 at the cytoplasmic tail affects interaction between claudin-4 and ZO-1. Non-phosphorylated and tyrosine-phosphorylated forms of recombinant GST-tagged claudin-4-(188–209), which contains the cytoplasmic tail, were purified using the TKX1 *E. coli* expression system (see "Experimental Procedures"). Non-phosphorylated claudin-4-(188–209) could effectively pull down the amino-terminal region of ZO-1 (N-ZO-1) expressed in COS1 cells. On the other hand, phosphorylated claudin-4 precipitated significantly lower amounts of N-ZO-1 (Fig. 5*a*, *lanes 1* and *2*). Because claudin-4-(188–209) contains three tyrosine residues (Fig. 3*d*), we also generated recombinant GST-claudin-4-(188–209)Y193/197F, in which two residual tyrosines were mutated, to confirm that phosphorylation of Tyr-208 of claudin-4 is responsible for attenuation of its binding ability with ZO-1. Non-phosphorylated wild type and the Y193/197F mutant of claudin-4-(188–209) equally coprecipitated ZO-1 (Fig. 5*a*, *lanes 1* and *3*), whereas phosphorylated claudin-4-(188–209)Y193/197F, in which only Tyr-208 was phosphorylated, did not effectively bind to ZO-1 (Fig. 5*a*, *lane 4*). Furthermore, neither claudin-4 lacking the carboxyl-terminal YV sequence nor GST alone bound to ZO-1 (Fig. 5*a*, *lanes 5* and *6*). Next, experiments were conducted to determine whether EphA2 activation leads to reduction of association between claudin-4 and ZO-1. The amount of claudin-4 coimmunoprecipitated with ZO-1 was reduced in EphA2-overexpressing COS1 cells (Fig. 5*b*). Association between claudin-4 and ZO-1 was also attenuated in MDCK cells expressing EphA2, and this association was further decreased by stimulation with ephrin-A1-Fc (Fig. 5*c*). From these results we conclude that EphA2 activation can reduce association of claudin-4 with ZO-1 by inducing phosphorylation of Tyr-208 of claudin-4 *in vivo*.

To examine the biological significance of EphA2-mediated attenuation of the binding affinity between claudin-4 and ZO-1, the change in localization of claudin-4 was monitored during the dynamic process of reestablishment of cell-cell adhesion. Wild type or the kinase-inactive mutant of EphA2 was expressed at high levels by adenovirus-mediated gene transfer in MDCK cells, which express endogenous claudin-4. When the cells were initially treated with calcium-chelating agent, ZO-1 and claudin-4 localization to cell-cell contact sites was completely abolished (data not shown). 30 min after replacing the calcium-free medium with normal growth medium (calcium switch), ZO-1 was found to relocalize to the cell-cell contact sites regardless of the presence of kinase-active or kinase-inactive EphA2 (Fig. 5*d*). On the other hand, in cells expressing kinase-dead EphA2, claudin-4 also relocalizes

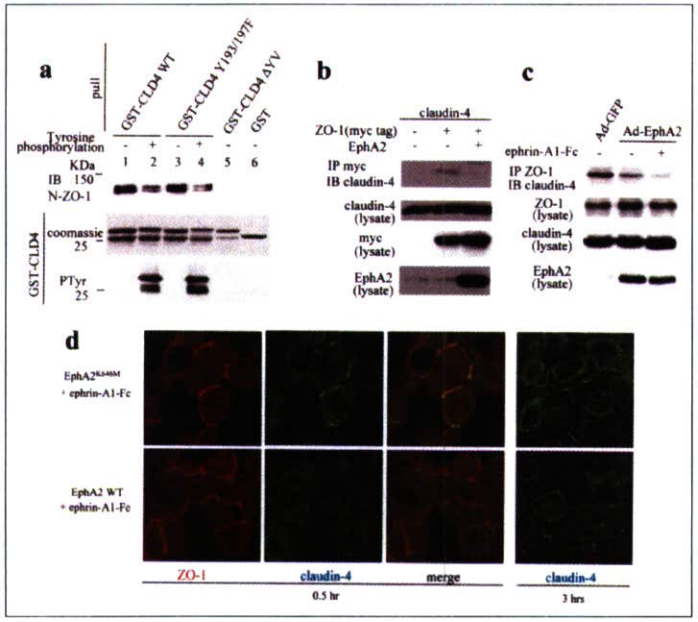

FIGURE 5. **Phosphorylation of claudin-4 at Tyr-208 inhibits interaction with ZO-1.** *a*, the second cytoplasmic domain of wild type (*WT*), the Y193/197F mutant, or the ΔYV mutant of claudin-4 was tagged with GST. The recombinant proteins were purified as either non-phosphorylated (−) or tyrosine phosphorylated (+) from TKX1-competent cells and incubated with lysate from N-ZO-1-transfected COS1 cells. The cell lysates were then incubated with protein G-Sepharose to precipitate claudin-4. *Upper panel*, coprecipitated N-ZO-1 was detected by immunoblotting (*IB*). *Middle panel*, purified GST fusion proteins added to the lysate are shown in a Coomassie Blue-stained gel. *Lower panel*, the tyrosine phosphorylation of recombinant GST-tagged claudin-4 was detected by immunoblotting with anti-phosphotyrosine (4G10). *b*, COS1 cells were transiently transfected with Myc-tagged ZO-1 and EphA2 as indicated above the lanes. ZO-1 was immunoprecipitated (*IP*) with anti-Myc antibody from cell lysates, and coprecipitated claudin-4 was detected by immunoblotting (*IB*). Claudin-4, ZO-1, and EphA2 detected in the lysates prior to immunoprecipitation are shown in the *lower panels*. *c*, MDCK cells infected with Ad-wild type EphA2 or control Ad-GFP were treated with EGTA. After removal of EGTA, the cells were incubated for 30 min in normal growth medium with (+) or without (−) ephrin-A1-Fc (4 μg/ml). ZO-1 was immunoprecipitated (*IP*) from the cell lysate, and coprecipitated claudin-4 was detected by immunoblotting (*IB*). ZO-1, claudin-4, and EphA2 detected in the lysates prior to immunoprecipitation are shown in the *lower panels*. *d*, MDCK cells infected with Ad-wild type EphA2 (*WT*) or Ad-EphA2^{K646M} were incubated with EGTA until cell-cell contacts were abolished. After removal of EGTA, the cells were incubated for 30 min or 3 h in normal growth medium with (+) or without (−) ephrin-A1-Fc (4 μg/ml) as indicated. The cells were then fixed and stained with anti-claudin-4 antibody or anti-ZO-1 antibody. Representative fields are shown.

to cell-cell contact sites 30 min after calcium switch, but in cells expressing kinase-active EphA2, claudin-4 did not relocalize to these sites (Fig. 5*d*). However, 3 h after calcium switch claudin-4 had relocalized to cell-cell contact sites in cells expressing kinase-active EphA2 (Fig. 5*d*). These results suggest that EphA2 causes a delay in reassembly of claudin-4 to tight junctions but has no effect on ZO-1.

EphA2 Affects Paracellular Permeability of Normal Epithelial Cells Depending on Its Kinase Activity—To examine the biological effect of the interaction of EphA2 with claudin-4 on tight junctions, paracellular permeability was measured using low molecular size dextran in MDCK epithelial cells. The amount of the dextran flux through a monolayer of confluent MDCK cells was almost undetectable even when EphA2 was overexpressed (data not shown). Therefore, we decided to examine the effect of EphA2 on reestablishment of the paracellular barrier after calcium switch. Overexpression of EphA2 effectively inhibited the prompt decrease of paracellular permeability through an MDCK monolayer after calcium switch, and this delay was further enhanced when cells were stimulated by ephrin-A1-Fc (Fig. 6*a*). On the other hand, kinase-inactive EphA2 did not affect paracellular permeability (Fig. 6*a*), indicating that the kinase activity of EphA2 affects permeability. In this experiment, the phosphorylation level of claudin-4 3 h after calcium switch had decreased to approximately the same level as in the confluent untreated cells (Fig. 6*b*, compare *lanes 2* and *4*). The paracellular flux of large molecular sized dextran (M_r 2,000) was below detectable levels at all time points shown in Fig. 6*a* (data not shown), indicating no massive destruction of junctional complexes had occurred in our experiment.

DISCUSSION

This is the first report showing tyrosine phosphorylation of claudin in relationship with its biological function. EphA2 induced the specific phosphorylation of Tyr-208 in the cytoplasmic tail of claudin-4 in COS1 cells, and endogenous claudin-4 was phosphorylated in response to EphA2 activation in HT29 cells. Both the kinase activity of EphA2 and association between EphA2 and claudin-4 are required for phosphorylation of claudin-4. Considering that EphA2 and claudin-4 associate on the same cell surface in *cis*, claudin-4 is most probably a direct substrate of EphA2. Our results indicate that activation of EphA2 by its ligand decreases integration of claudin-4 into tight junctions and enhances paracellular permeability.

Tyrosine phosphorylation of claudin-4 in its carboxyl-terminal tail inhibits binding to ZO-1. It is also reported that phosphorylation of the carboxyl-terminal tail of occludin by c-Src also attenuated its association with ZO-1, ZO-2, and ZO-3 *in vitro* (36). Thus, tyrosine phosphorylation within the PDZ domain-binding site is able to regulate protein-protein interaction.

Our results suggest that activation of EphA2 affects integration of claudin-4 into the sites of cell-cell contacts after calcium switch, thereby attenuating the barrier function of tight junctions. Although the mechanism of assembly of claudins and ZO-1 into tight junctions is not fully understood, ZO-1, which is primarily localized to tight junctions (35), presumably fails to recruit phosphorylated claudin-4 due to loss of physical association. This conclusion is consistent with the finding that claudin-4, but not ZO-1, localization to cell contacts is decreased after activation of EphA2 (Fig. 5*d*).

The EphA2-dependent increase of paracellular permeability was evident only during the dynamic process of tight junction reorganization triggered by calcium switch. On the other hand, expression of EphA2 did not effectively disrupt tight junctions, and junctional permeability and claudin-4 localization to cellular contacts were ultimately restored after calcium switch in MDCK cells even when claudin-4 was phosphorylated (Fig. 6*b*). These results suggest that phosphorylation of claudin-4 may affect the reassembly of tight junctions but not the maintenance of established tight junctions. One possibility is that the phosphorylation level of claudin-4 in confluent MDCK cells was relatively low and can be functionally compensated for by other members of the claudin family or by some other molecule. We are currently screening cell lines in which claudin-4 is highly phosphorylated at tight junctions to test this hypothesis.

Because of limitations in the availability of specific antibodies, the specificity of association between each member of the Eph family and the claudin family is still uncertain. At least one other Eph family member, EphA4, is likely to be involved in this cross-talk, as claudin-4 was also tyrosine phosphorylated by coexpression with EphA4 in COS1 cells (data not shown). Also, the tyrosine residue located at the carboxyl terminus is conserved among at least 8 claudin family members, claudin-1–8. Therefore, other claudins also have the potential to be phosphorylated by Eph receptors. We are currently testing this hypothesis.

In tumors overexpressing EphA2, assembly of tight junctions may be negatively regulated via phosphorylation of claudin. This has the potential to affect the malignant phenotype of the carcinoma, such as loss of cell polarity. Moreover, in tumors overexpressing both EphA2 and claudin-4, like HT29 colon cancer cells, phosphorylation of claudin-4 might transduce signals distinct from tight junction function. We are currently attempting to identify other downstream targets of signaling through tyrosine phosphorylation of claudin-4 and determine their roles in the regulation of epithelial cells and cancer cells.

Acknowledgments—We thank Dr. S. Tsukita (Kyoto University) for providing the plasmids used in this study. We thank Dr. B. J. Mayer (University of Connecticut Health Center) and Dr. D. B. Alexander (Dept. of Molecular Toxicology, Nagoya City University) for critically reading this manuscript.

REFERENCES

1. Blits-Huizinga, C., Nelersa, C., Malhotra, A., and Liebl, D. (2004) *IUBMB Life* **56**, 257–265
2. Murai, K. K., and Pasquale, E. (2003) *J. Cell Sci.* **116**, 2823–2832
3. Kullander, K., and Klein, R. (2002) *Nat. Rev. Mol. Cell. Biol.* **3**, 475–486
4. Poliakov, A., Cotrina, M., and Wilkinson, D. G. (2004) *Dev. Cell* **7**, 465–480

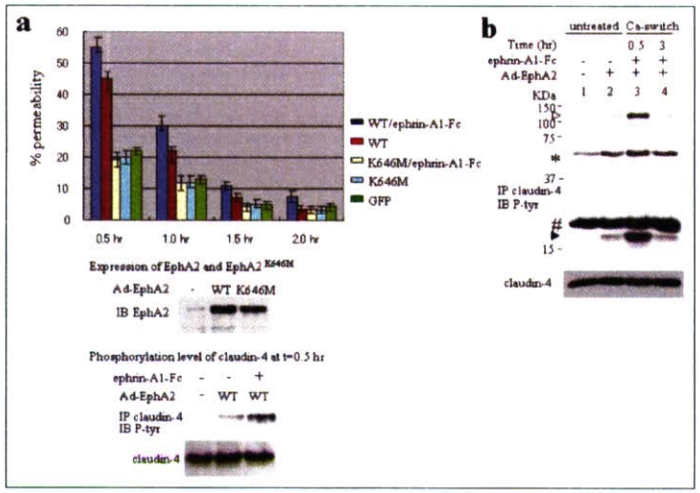

FIGURE 6. **EphA2 affects paracellular permeability and reassembly of claudin-4.** *a*, MDCK cells were grown until confluent in Transwell chambers. The cells were then infected with Ad-wild type EphA2 (*WT*), Ad-EphA2^{K646M} (*K646M*), or Ad-GFP. Two days later, the cells were treated with EGTA to disrupt cell-cell contacts, and then the EGTA was removed and replaced with normal growth medium (calcium switch). After the calcium switch, the cells were incubated in normal growth medium with (+) or without (−) ephrin-A1-Fc (4 μg/ml) for the indicated times. FITC-dextran was then added to the upper wells and the cells incubated for a further 30 min. After 30 min, the fluorescence of FITC-dextran in the lower wells was determined. The results are presented in terms of the % fluorescence in the lower wells when FITC-dextran was added to cell monolayers just after EGTA treatment. Each *bar* represents the mean value ± S.D. of three independent experiments. The expression of wild type EphA2 and EphA2^{K646M} is shown in the *middle panel*. The phosphorylation levels of claudin-4 in wild type EphA2-expressing cells with or without ephrin-A1-Fc 30 min after the calcium switch is shown in the *bottom panel*. *b*, confluent MDCK cells infected with Ad-wild type EphA2 (*lanes 2–4*) or not infected (*lane 1*) were either left untreated (*lanes 1* and *2*) or subjected to calcium switch as in *panel a* (*lanes 3* and *4*). After the calcium switch, the cells were incubated in normal growth medium containing ephrin-A1-Fc (4 μg/ml) for 30 min (*lane 3*) or 3 h (*lane 4*). The cells were then lysed, and claudin-4 was immunoprecipitated (*IP*) from the lysate. *Upper panel*, tyrosine-phosphorylated EphA2 and claudin-4 were detected by immunoblotting (*IB*) with anti-phosphotyrosine (4G10). *Arrowheads* indicate coprecipitated EphA2 phosphorylated on tyrosine (*open*) and immunoprecipitated claudin-4 phosphorylated on tyrosine (*filled*). *Asterisk* and *sharp sign* indicates IgG heavy chain and light chain, respectively. *Lower panel*, claudin-4 detected in the lysate prior to immunoprecipitation.

5. Huot, J. (2004) *Prog. Neuropsychopharmacol. Biol. Psychiatry* **28,** 813–818
6. Hinck, L. (2004) *Dev. Cell* **7,** 783–793
7. Mann, F., Harris, W. A., and Holt, C. E. (2004) *Int. J. Dev. Biol.* **48,** 957–964
8. Bolz, J., Uziel, D., Muhlfriedel, S., Gullmar, A., Peuckert, C., Zarbalis, K., Wurst, W., Torii, M., and Levitt, P. (2004) *J. Neurobiol.* **59,** 82–94
9. Klein, R. (2004) *Curr. Opin. Cell Biol.* **16,** 580–589
10. Brantley-Sieders, D., Parker, M., and Chen, J. (2004) *Curr. Pharm. Des.* **10,** 3431–3442
11. Surawska, H., Ma, P. C., and Salgia, R. (2004) *Cytokine Growth Factor Rev.* **15,** 419–433
12. Kinch, M. S., and Carles-Kinch, K. (2003) *Clin. Exp. Metastasis* **20,** 59–68
13. Brantley-Sieders, D. M., and Chen, J. (2004) *Angiogenesis* **7,** 17–28
14. Cheng, N., Brantley, D. M., and Chen, J. (2002) *Cytokine Growth Factor Rev.* **13,** 75–85
15. Kataoka, H., Igarashi, H., Kanamori, M., Ihara, M., Wang, J. D., Wang, Y. J., Li, Z. Y., Shimamura, T., Kobayashi, T., Maruyama, K., Nakamura, T., Arai, H., Kajimura, M., Hanai, H., Tanaka, M., and Sugimura, H. (2004) *Cancer Sci.* **95,** 136–141
16. Orsulic, S., and Kemler, R. (2000) *J. Cell Sci.* **113,** 1793–1802
17. Zantek, N. D., Azimi, M., Fedor-Chaiken, M., Wang, B., Brackenbury, R., and Kinch, M. S. (1999) *Cell Growth Differ.* **10,** 629–638
18. Jones T. L., Chong, L. D., Kim, J., Xu, R. H., Kung, H. F., and Daar, I. O. (1998) *Proc. Natl. Acad. Sci. U. S. A.* **95,** 576–581
19. Winning, R. S., Scales, J. B., and Sargent, T. D. (1996) *Dev. Biol.* **179,** 309–319
20. Morita, K., Furuse, M., Fujimoto, K., and Tsukita, S. (1999) *Proc. Natl. Acad. Sci. U. S. A.* **96,** 511–516
21. Tsukita, S., Furuse, M., and Itoh, M. (2001) *Nat. Rev. Mol. Cell. Biol.* **2,** 285–293
22. Itoh, M., Furuse, M., Morita, K., Kubota, K., Saitou, M., and Tsukita, S. (1999) *J. Cell Biol.* **147,** 1351–1363
23. Hamazaki, Y., Itoh, M., Sasaki, H., Furuse, M., and Tsukita, S. (2002) *J. Biol. Chem.* **277,** 455–461
24. Roh, M. H., Liu, C., Laurinec, S., and Margolis, B. (2002) *J. Biol. Chem.* **277,** 27501–27509
25. Aldred, M. A., Huang, Y., Livanarachchi, S., Pellegata, N. S., Gimm, O., Jhiang, S., Davuluri, R. V., de la Chapelle, A., and Eng, C. (2004) *J. Clin. Oncol.* **22,** 3531–3539
26. Nicols, L. S., Ashfag, R., and Lacobuzio-Donahue, C. A. (2004). *Am. J. Clin. Pathol.* **121,** 226–230
27. Rangel, L. B., Agarwal, R., D'Souza, T., Pizer, E. S., Alo, P. L., Lancaster, W. D., Gregoire, L., Schwartz, D. R., Cho, K. R., and Morin, P. J. (2003) *Clin. Cancer Res.* **9,** 2567–2575
28. Wang, Y., Ota, S., Kataoka, H., Kanamori, M., Li, Z., Band, H., Tanaka, M., and Sugimura, H. (2002) *Biochem. Biophys. Res. Commun.* **296,** 214–220
29. Tanaka, M., Ohashi, R., Nakamura, R., Shinmura, K., Kamo, T., Sakai, R., and Sugimura, H. (2004) *EMBO J.* **23,** 1075–1088
30. Palmer, A., Zimmer, M., Erdmann, K. S., Eulenburg, V., Porthin, A., Heumann, R., Deutsch, U., and Klein, R. (2002) *Mol. Cell.* **9,** 725–737
31. Cowan, C. A., and Henkemeyer, M. (2001) *Nature* **413,** 174–179
32. Cowan, C. A., and Henkemeyer, M. (2002) *Trends Cell Biol.* **12,** 339–346
33. Himanen, J. P., Rajashankar, K. R., Lackmann, M., Cowan, C. A., Henkemeyer, M., and Nikolov, D. B. (2001) *Nature* **414,** 933–938
34. Potla, L., Boghaert, E. R., Armellino, D., Frost, P., and Damle, N. K. (2002) *Cancer Lett.* **175,** 187–195
35. Rothen-Rutishauser, B., Riesen, F. K., Braun, A., Gunthert, M., and Wunderli-Allenspach, H. (2002) *J. Membr. Biol.* **188,** 151–162
36. Kale, G., Naren, A., Sheth, P., and Rao, R. K. (2003) *Biochem. Biophys. Res. Commun.* **302,** 324–329

Molecular Biology of the Cell
Vol. 17, 3187–3196, July 2006

The Docking Protein Cas Links Tyrosine Phosphorylation Signaling to Elongation of Cerebellar Granule Cell Axons[D]

Jinhong Huang,* Ryuichi Sakai,† and Teiichi Furuichi*

*Laboratory for Molecular Neurogenesis, Riken Brain Science Institute, Wako, Saitama 351-0198; and †Growth Factor Division, National Cancer Center Research Institute, Chuo-ku, Tokyo 104-0045, Japan

Submitted December 13, 2005; Revised April 25, 2006; Accepted May 1, 2006
Monitoring Editor: Richard Assoian

Crk-associated substrate (Cas) is a tyrosine-phosphorylated docking protein that is indispensable for the regulation of the actin cytoskeletal organization and cell migration in fibroblasts. The function of Cas in neurons, however, is poorly understood. Here we report that Cas is dominantly enriched in the brain, especially the cerebellum, of postnatal mice. During cerebellar development, Cas is highly tyrosine phosphorylated and is concentrated in the neurites and growth cones of granule cells. Cas coimmunoprecipitates with Src family protein tyrosine kinases, Crk, and cell adhesion molecules and colocalizes with these proteins in granule cells. The axon extension of granule cells is inhibited by either RNA interference knockdown of Cas or overexpression of the Cas mutant lacking the YDxP motifs, which are tyrosine phosphorylated and thereby interact with Crk. These findings demonstrate that Cas acts as a key scaffold that links the proteins associated with tyrosine phosphorylation signaling pathways to the granule cell axon elongation.

INTRODUCTION

Crk-associated substrate (Cas) docking protein was initially identified as a major phosphotyrosine-containing protein in fibroblasts transformed by *v-Src* or *v-Crk* oncogenes (Sakai *et al.*, 1994). It has an N-terminal Src homology 3 (SH3) domain, a substrate domain (SD) that consists of a cluster of tyrosine phosphorylation sites and a C-terminal Src-binding domain (SBD) that functions to directly bind the Src family protein tyrosine kinases (PTKs; Sakai *et al.*, 1994; Nakamoto *et al.*, 1996). In motile cells such as fibroblasts, Cas is tyrosine-phosphorylated by Src or Fak family PTKs after integrin stimulation, which induces Cas localization to focal adhesions. Tyrosine-phosphorylated Cas (YP-Cas) acts as a scaffold protein upstream of the Rho family small GTPase in focal adhesions (O'Neill *et al.*, 2000). Embryonic fibroblasts lacking the Cas gene exhibit impaired actin stress fiber bundling and cell motility, indicating that Cas is indispensable for actin cytoskeleton organization and cell migration (Honda *et al.*, 1998; Huang *et al.*, 2002). The function of Cas in neurons, however, is unknown.

Neurons extend neurites immediately after exiting from mitotic cycles. At the tip of the extending neurites, there are motile enlargements, growth cones that build the dynamic center for signaling of the mobility and direction of extending neurites. Filopodia and lamellipodia are two dynamic structures in the growth cone that rapidly extend and retract, providing the force to advance in response to extracellular cues. Filopodia are protrusions composed of bundled F-actin fibers, whereas lamellipodia are large fanlike structures composed of a cross-linked actin meshwork (Tanaka and Sabry, 1995; Luo, 2002). The signaling pathways from the surface to the actin cytoskeletal organization in growth cones are essential for neurite outgrowth (Dickson, 2001; Dent and Gertler, 2003; Pollard and Borisy, 2003). Protein tyrosine phosphorylation is the critical factor for the signaling cascades that control growth cone motility (Korey and Van Vactor, 2000).

Cerebellar granule cells are the most abundant cell population in the cerebellar circuit. Granule cells proliferate postnatally in the external granule layer (EGL). Postmitotic granule cells move into the inner half of the EGL (iEGL) where they begin to differentiate. While migrating further down the molecular layer (ML) to the internal granule layer (IGL), granule cells develop the characteristic morphologies of their axons, parallel fibers (Ono *et al.*, 1997). Granule cells settle in the IGL and develop their dendritic morphologies, forming synaptic glomerular rosettes with mossy fiber terminals and Golgi cell axon terminals. Src family PTKs such as Src, Fyn, Yes, Lyn, and Lck are highly expressed in the cerebellum, and their expression is developmentally regulated (Fults *et al.*, 1985; Cartwright *et al.*, 1988; Maness *et al.*, 1988; Sudol *et al.*, 1988, 1989; Zhao *et al.*, 1991; Chen *et al.*, 1996; Omri *et al.*, 1996). The PTK activity of Src in the developing cerebellum is ~6- to 10-fold that in fibroblasts (Cartwright *et al.*, 1988). High levels of Src, Fyn, and Yes are concentrated in the growth cones of cerebellar neurons (Maness *et al.*, 1988; Wu and Goldberg, 1993). Src family PTKs are implicated in the signaling pathways of cell adhesion molecule (CAM)-induced neurite outgrowth. Cultured cerebellar neurons prepared from mice lacking Fyn do not extend axons on neuronal cell adhesion molecule (NCAM)-

This article was published online ahead of print in *MBC in Press* (http://www.molbiolcell.org/cgi/doi/10.1091/mbc.E05-12-1122) on May 10, 2006.

[D] The online version of this article contains supplemental material at *MBC Online* (http://www.molbiolcell.org).

Address correspondence to: Teiichi Furuichi (tfuruichi@brain.riken.jp).

Abbreviations used: Cas, Crk associated substrate; YP-Cas, tyrosine phosphorylated Cas; SD, substrate domain; SBD, Src binding domain; PTK, protein tyrosine kinases; CAM, cell adhesion molecules; NCAM, neuronal cell adhesion molecule; EGL, external granule cell layer; ML, molecular layer; IGL, internal granule cell layer; PL, Purkinje cell layer; WM, white matter; EGFP, enhanced green fluorescent protein; GCP, growth cone particle.

coated culture matrix as rapidly as cells from wild-type littermates (Beggs *et al.*, 1994). Similarly, cerebellar granule cells from Src-deficient mutant mice show impaired neurite outgrowth on the neural adhesion molecule L1 (Ignelzi *et al.*, 1994). These results suggest that Src and Fyn have important roles in granule cell neurite extension. The signaling cascade from the CAMs and Src family PTKs to the cytoskeleton, however, remains to be clarified.

The present study demonstrates that among tissues of postnatally developing mice, Cas is most abundant in the brain, especially in the cerebellum. It is notable that YP-Cas peaked around the first postnatal week and was concentrated in the growth cone fractions. The Cas protein was immunocytochemically localized in the growth cones and neurites of granule cells. In the cerebellum, Cas coimmunoprecipitated with Src family PTKs, Crk, and CAM proteins N-cadherin and NCAM. Granule cell axon elongation was impaired by either RNA interference (RNAi) knockdown of Cas or overexpression of Cas mutants with deletion of the multiple tyrosine phosphorylation sites that confer the Crk-binding property. Our results suggest that YP-Cas acts as an important scaffold in the signaling of axon elongation of cerebellar neurons, linking extracellular signals to the cytoskeleton through tyrosine phosphorylation.

MATERIALS AND METHODS

Primary Dissociated Cerebellar Cell Culture

Cerebellar cells were prepared from postnatal day 0 (P0) ICR mouse cerebella as described previously (Shiraishi *et al.*, 1999). In brief, the cerebella from P0 mice were treated with 0.1% trypsin (Sigma Chemical, St. Louis, MO) and 0.05% DNase I (Roche Diagnostics, Indianapolis, IN) in Ca^{2+}-Mg^{2+}-free Hanks' balanced salt solution (HBSS), dissociated by repeated passage through a micropipette tip in Ca^{2+}-Mg^{2+}-free HBSS containing 0.05% DNase I and 12 mM $MgSO_4$, and then rinsed with the culture medium. Dispersed cells (4×10^5) were plated onto poly-L-lysine (Sigma)-coated glass coverslips (12-mm diameter; Matsunami, Tokyo, Japan) in serum-free defined medium: Eagle's medium supplemented with 1 mg/ml bovine serum albumin, 10 μg/ml insulin, 0.1 nM L-thyroxine, 0.1 mg/ml transferrin, 1 μg/ml aprotinin (all from Sigma), 30 nM selenium (Merck, Darmstadt, Germany), 0.25% (wt/vol) glucose, 2 mM glutamine, 2 mg/ml sodium bicarbonate, 0.1 mg/ml streptomycin (Meiji Seika KK, Tokyo, Japan), and 100 U/ml penicillin (Banyu Pharmaceutical, Tokyo, Japan). The cultures were maintained in a humidified atmosphere of 5% CO_2 in air at 37°C.

Primary Cerebellar Neuron Transfection and Axon Length Analysis

Cas mutants produced as described previously (Huang *et al.*, 2002) were constructed in a plasmid vector that contains the CAG promoter. Short interfering RNA (siRNA) of Cas was generated using the BLOCK-iT RNAi TOPO Transcription and BLOCK-iT Complete Dicer RNAi kits (Invitrogen, Carlsbad, CA) according to the manufacturer's instructions (Azuma *et al.*, 2005). siRNA of LacZ was generated using the same procedure as for Cas siRNA and was used as a negative control. Transfection of cerebellar neurons was performed soon after the neurons were dissociated using the Mouse Neuron Nucleofector kit and the Nucleofector device (Amaxa, Cologne, Germany; Liu *et al.*, 2003; Hama *et al.*, 2004). The transfection efficiency was 5%. The calcium phosphate method using a CellPhect Transfection Kit (Amersham Biosciences, Buckinghamshire, United Kingdom) was also used to transfect cerebellar neurons on day 1 in vitro (DIV1) in serum-free defined medium on poly-L-lysine–coated glass coverslips. The length of the longest axon was quantified in granule cells (marked by immunolabeling with antibody against Pax6) expressing the Cas mutant or siRNA. Axons were also confirmed by immunolabeling with antibody against Tau-1. Axons could be easily distinguished from dendrites because granule cells at DIV2 exhibit a representative morphology with a long single or bipolar axon with multiple short dendrites (Powell *et al.*, 1997). The percentage of granule cells with axons longer than 200 μm in each transfection case was quantified in at least 20 fields randomly selected from three independent experiments. Student's *t* test was used to compare results between the mutant and the control cells. $p < 0.05$ was considered significant.

RT-PCR Analysis

A series of first-strand cDNAs was produced by reverse-transcription (RT) from 20 ng of total cerebellar RNAs at the various developmental stages, using an oligo-dT primer. The cDNA sequence corresponding to the nucleotide positions 583-1182 (amino acids 175–394) of p130Cas was amplified using the primers 5′-ACATCTACCAAGTCCCTCCA-3′ (forward primer) and 5′-AGGCACGTCATACAGTGTTC-3′ (reverse primer). The cycling conditions were as follows: denaturing at 94°C for 3 min, amplification by 25 cycles of 94°C (15 s), 55°C (2 min), and 72°C (1 min), and extension at 72°C for 5 min. To analyze tissue distribution, total RNAs prepared from various tissues of P7 or P21 mice were used for RT-PCR. The RT-PCR of glyceraldehyde-3-phosphate dehydrogenase with primers 5′-GCCATCAACGACCCCTTCATTGACCTC-3′ (forward primer) and 5′-GCCATGTAGGCCATGAGGTCCACCAC-3′ (reverse primer) were used as an internal control.

In Situ Hybridization

In situ hybridization brain histochemistry was basically performed as described previously(Shiraishi *et al.*, 1999). The cDNA sequence corresponding to nucleotide positions 583-1182 (amino acids 175–394) of the p130Cas cDNA was used as a template to prepare the digoxigenin-labeled antisense riboprobes using a digoxigenin-dUTP labeling kit (Roche Diagnostics). Paraffin sections of mouse brain (10 μm thick) were fixed in 4% paraformaldehyde for 5 min, washed twice in phosphate-buffered saline (PBS), and treated with freshly prepared 10 μg/ml proteinase K (Invitrogen) at room temperature. After acetylation, the sections were subjected to digoxigenin-based hybridization procedures. Briefly, the sections were incubated in a hybridization buffer containing 0.2 μg/ml digoxigenin-labeled riboprobes at 60°C overnight in a humid chamber. The hybridized sections were washed by successive immersion in 1× SSC (150 mM NaCl and 15 mM sodium citrate, pH 7.0, 60°C, 10 min, twice), 2× SSC (37°C, 10 min), 2× SSC containing 20 μg/ml RNase A (37°C, 30 min), 2× SSC (37°C, 10 min), and 0.2× SSC (60°C, 30 min, twice). The hybridization signals were detected using the digoxigenin detection kit (Roche Diagnostics).

Immunoprecipitation and Immunoblotting

Protein extraction and Western blotting analysis were performed as described previously (Huang *et al.*, 2002). Briefly, mouse cerebella or cerebra were lysed in 1% Triton X-100 buffer (50 mM HEPES, 150 mM NaCl, 10% glycerol, 1% Triton X-100, 1.5 mM $MgCl_2$, 1 mM EGTA, 100 mM NaF, 1 mM Na_3VO_4, 10 μg/ml aprotinin, 10 μg/ml leupeptin, and 1 mM phenylmethylsulfonyl fluoride). Aliquots of protein lysates were separated by SDS-PAGE and probed with diluted antibodies. For immunoprecipitation, protein (500 μg) was mixed with 1 μg primary antibody and incubated for 1 h on ice. The mixtures were rotated with protein A- or protein G-Sepharose (Amersham) for 1 h at 4°C. The Sepharose were washed four times with 1% Triton X-100 buffer and boiled in sample buffer before being subjected to SDS-PAGE analysis.

Antibodies

Antibodies against mouse Cas were used as described previously (Sakai *et al.*, 1994). A phospho-specific polyclonal antibody (αCas-pYDxP) that specifically recognizes YP-Cas was generated by immunizing rabbits with a synthetic peptide, CAEDV(pY)DVP (a.a. 456–463), which is representative of the repetitive tyrosine-containing motifs in the Cas SD, after being conjugated with thyroglobulin (Miyake *et al.*, 2005). Antibodies against Src family tyrosine kinases, N-cadherin, L1, β-integrin, NCAM140/180, hemagglutinin (HA), and Crk were from BD Bioscience (Franklin Lakes, NJ). The antibodies against Fyn (Fyn3), c-Src (N-16), NCAM120, and JNK1 were from Santa Cruz Biotechnologies (Santa Cruz, CA). The antibody anti-GAP43 was from Innogenetics (Alpharetta, GA). The antibodies against phosphotyrosine 4G10 was from Upstate Biotechnology (Waltham, MA), antibodies against Map2 (AP20) and calbindin were from Sigma, the antibody against Pax-6 was from Covance (Princeton, NJ), and the antibody against tau-1 was from Chemicon International (Temecula, CA).

Subcellular Fractionation and Isolation of Growth Cone Particles

P7 and P21 mouse cerebella were homogenized in the homogenization buffer (0.32 M sucrose, 5 mM Tris-HCl, 1 mM EGTA, 1 mM DTT, 1 mM pepstatin A, 1 mM leupeptin, and 1 mM Na_3VO_4). The protein homogenates were centrifuged at 1000 × *g* for 10 min. The pellet was lysed in 1% Triton X-100 buffer (PPt1). The supernatant was recentrifuged at 105,000 × *g* for 1 h. The pellet was lysed in 1% Triton X-100 buffer (PPt2 + 3), and the supernatant was used as Sup3. Growth cone particles (GCP) were prepared essentially as described previously (Pfenninger *et al.*, 1983; Helmke *et al.*, 1998). P7 mouse cerebella were homogenized in ~8 volumes of 0.32 M sucrose containing 1 mM $MgCl_2$ and 1 mM TES buffer, pH 7.3. The homogenate was centrifuged at 2000 rpm for 10 min (pellet, PPt1), and the resulting low-speed supernatant (cytosol) was loaded onto a discontinuous density gradient with steps of 0.75 and 1 M sucrose in the same buffer. The gradients were spun to equilibrium at 28,000 rpm for 1 h in a swing rotor SW-28 (Beckman Coulter, Fullerton, CA). The fraction at the 0.32/0.75 M sucrose interface containing the GCPs was collected. This fraction was diluted 3- to 4-fold with 0.32 M sucrose, and GCPs were pelleted at 40,000 rpm for 30 min (TLA-100, Beckman) and extracted with 1% Triton X-100 buffer for 30 min at 4°C (GCP).

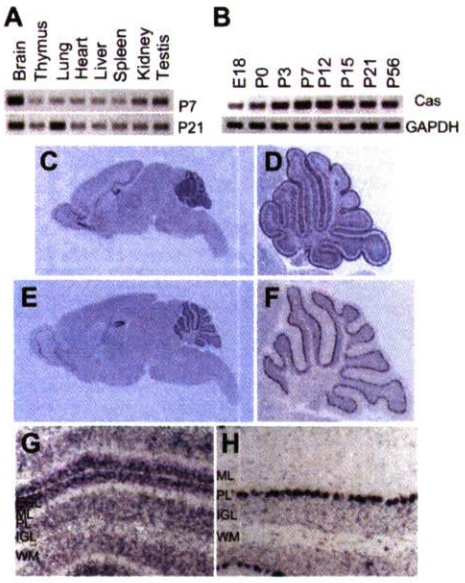

Figure 1. Expression of Cas mRNA in developing mouse cerebella. (A) Semiquantitative RT-PCR analysis of Cas mRNA expression in P7 or P21 mouse tissue. (B) RT-PCR analysis of Cas mRNA expression in postnatal cerebella at six different postnatal stages. RT-PCR for GAPDH was used as an internal control. (C–H) In situ hybridization analysis of Cas distribution in the P7 (C, D, and G) and P21 (E, F, and H) mouse brains. C, P7 brain; D, P7 cerebellum; E, P21 brain; F, P21 cerebellum; G, P7 cerebellar cortex; H, P21 cerebellar cortex. EGL, external granule cell layer; ML, molecular layer; IGL, internal granule cell layer; PL, Purkinje cell layer; WM, white matter.

Immunohistochemistry and Fluorescent Microscopy

The cells were fixed with 4% paraformaldehyde for 1 h, washed three times with PBS, and then permeabilized with 0.2% Triton X-100/PBS for 5 min before incubation with 5% normal goat serum in PBS (−). For native tissues, ICR mice were transcardically perfused with 4% paraformaldehyde in PBS (−), and the dissected brains were immersed for 2 h in the same fixative buffer and cryosectioned (20 μm thick). For immunoreaction, fixed cultured cells or brain sections were preincubated with 5% normal goat serum in PBS (−) for 1 h and then incubated with primary antibody (anti-Cas, 1 μg/ml), for 1 h at room temperature. After washing with PBS (−), the samples were incubated with Alexa-conjugated secondary antibody (Invitrogen). Immunofluorescence was observed using a Zeiss (Oberkochen, Germany) Meta-510 confocal laser microscope. Conventional immunostaining reaction was also performed using a diaminobenzidine and horseradish peroxidase–conjugated secondary antibody.

RESULTS

Cas mRNA Is Abundantly Expressed in Developing Mouse Cerebella

To examine the functional role of Cas in the mouse CNS, we first analyzed the expression of Cas mRNA in mice at P7 and P21 using RT-PCR technique. Of the eight tested tissues of P7 mice, the expression level of Cas mRNA was highest in the brain (Figure 1A). Cas mRNA was also expressed abundantly in P21 brain. In situ hybridization analysis revealed strong Cas mRNA labeling in the cerebellum, hippocampus,

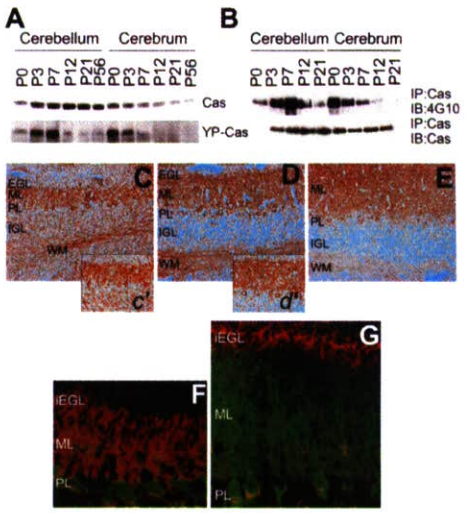

Figure 2. Expression and tyrosine phosphorylation of Cas protein in developing mouse cerebella. (A) Immunoblotting of Cas and YP-Cas in the postnatal cerebella. Approximately equal amounts of protein lysates from six different postnatal stages (P0, P3, P7, P12, P21, and P56) were subjected to immunoblotting analysis by an antibody against Cas or YP-Cas. (B) Immunoprecipitation with the Cas antibody followed by immunoblotting with the phospho-tyrosine antibody 4G10. (C–E) Immunohistochemical staining of Cas in the P7 (C and c′), P12 (D and d′), and P21 (E) mouse cerebella sections. (F and G) Immunohistochemical analysis of YP-Cas detected by the specific antibody (red) in P7 (F) and P12 (G) mouse cerebella. Purkinje cells were immunostained with anti-calbindin antibody (green). iEGL, the inner half of EGL.

and olfactory bulb at P7 (Figure 1C) and P21 (Figure 1E). The cerebellum was the predominant region with Cas mRNA expression at P7 (Figure 1D) and P21 (Figure 1F). During postnatal cerebellar development, Cas mRNA expression was up-regulated, with the peak occurring from P7 to P12 (Figure 1B). In the P7 cerebella, Cas mRNA was primarily concentrated in the EGL, and was also present in the IGL, Purkinje cell layer (PL), and white matter (WM; Figure 1G). In P21 cerebella, on the other hand, it was predominantly localized in the PL and present in only low levels in the IGL and WM (Figure 1H). These results suggested that Cas has a functional role(s) in cerebellar development.

Cas Protein Is Highly Tyrosine-phosphorylated during Cerebellar Development

We investigated the expression and tyrosine phosphorylation of Cas protein in developing mouse brains at six different postnatal stages (P0, P3, P7, P12, P21, and P56) by immunoblotting analysis (Figure 2A). The tyrosine-phosphorylated Cas (YP-Cas) was immunodetected by an antibody that recognizes the tyrosine-phosphorylated YDxP motifs of Cas (Miyake *et al.*, 2005). In the cerebella, Cas protein expression was up-regulated to a peak level at around P21 and then slightly down-regulated, which almost paralleled the mRNA expression profile (Figure 1B). In contrast to this developmental profile of Cas expression, YP-Cas

rapidly increased after birth to reach a peak level at P7 and then sharply decreased. This steep increase of YP-Cas within the first postnatal week was also confirmed by an immunoprecipitation assay with the anti-Cas antibody followed by immunoblotting with the anti-phospho-tyrosine antibody 4G10 (Figure 2B). In the cerebra, on the other hand, both Cas and YP-Cas proteins were most abundant at P0 and then markedly decreased (Figure 2, A and B).

We then immunohistochemically analyzed the cellular distribution of Cas protein in the developing cerebella (Figure 2, C–E). In P7 cerebella, there was intense Cas immunolabeling in the ML and PL and weak immunolabeling in the EGL, IGL, and WM (Figure 2C). In P12 cerebella, there was high density labeling in the ML, PL, and WM and low density labeling in the IGL (Figure 2D). In P21 cerebella, there was strong Cas staining in the ML and PL and weak staining in the WM (Figure 2E). On the other hand, YP-Cas had characteristic cellular distribution patterns in the developing cerebella (Figure 2, F and G). Intense YP-Cas immunolabeling was distributed primarily in the iEGL and ML at P7 (F) and in the iEGL at P12 (G), and moderate labeling was observed in the WM at P7 and P12 (unpublished data). In the P12 ML, there was weak YP-Cas immunolabeling around the growing dendrites of Purkinje cells, which were coimmunostained for calbindin (a Purkinje cell marker; Figure 2G). At P21, there was very weak immunostaining in the ML and IGL (unpublished data). These data indicate that Cas is highly tyrosine-phosphorylated in postmitotic premigratory granule cells within the iEGL, in outgrowing Purkinje cell dendrites within the ML, and in the WM (probably in Purkinje cell axons), at the first and second postnatal stages.

Cas Is Enriched in the Growth Cones of Developing Cerebellar Neurons

We performed subcellular fractionation of Cas protein from P7 and P21 mouse cerebella. Cas immunoreactivity was recovered in the precipitation fractions, PPt1 (nuclei and cytoskeleton fractions) and PPt2 + 3 (membrane fraction containing mitochondria and microsomes), and the supernatant fraction Sup3 (cytosolic; Figure 3A, bottom). On the other hand, YP-Cas immunoreactivity was enriched in the precipitation fractions: in the PPt1 and PPt2 + 3 at P7 and in the PPt2 + 3 at P21 (Figure 3A, top). Moreover, YP-Cas was concentrated in the GCP fraction prepared from P7 cerebella, in which a growth cone marker, growth-associated protein 43 (GAP43), was recovered (Figure 3B).

We next analyzed the subcellular localization of Cas protein in cultured cerebellar neurons (Figure 3, C–I). Cas was detected in axons of granule cells at DIV1, and was largely concentrated in their fanlike tips, growth cones (Figure 3, C–L). Although the fine structure of granule cell growth cones was difficult to observe because of their thin and tiny morphology, Cas was localized in both the central and peripheral domains (Figure 3, F–I), and colocalized with actin bundles (Figure 3, J–L'). In cultured Purkinje cells (DIV14), Cas immunoreactivity was observed in the tips of the dendritic arbors as well as in their dendrites, axons, and soma (unpublished data). These data indicate that Cas is subcellularly localized in outgrowing neurites and growth cones of cerebellar neurons. The subcellular fractionation analysis implied that Cas in growth cones is highly tyrosine-phosphorylated.

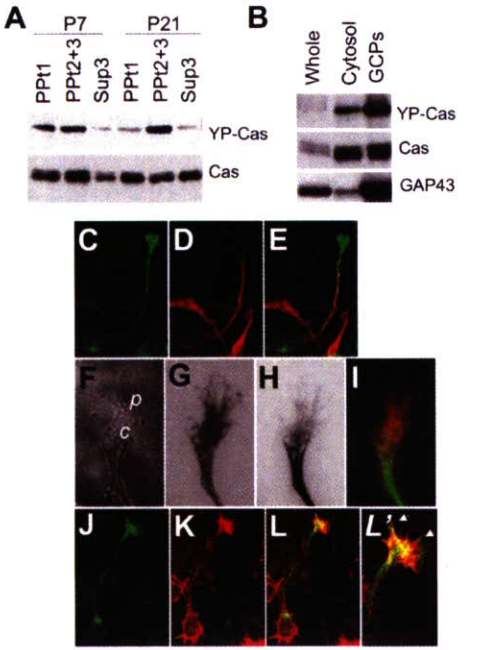

Figure 3. Cas is enriched in the growth cones of cerebellar granule cells. (A) Immunoblotting of Cas in subcellular protein fractions from P7 and P21 mouse cerebella. (B) Immunoblotting of Cas and YP-Cas in growth cone fractions from P7 mouse cerebella. Equal amounts of proteins were loaded in each lane and immunoblotted with antibodies against YP-Cas, Cas, and GAP43 (as a control of growth cone proteins). (C–E) Confocal images of Cas (C) and Map2 (D) in the granule cells (DIV1). (E) Merged image of C and D. (F–I) Phase-contrast images (F) of Cas (G) and Map2 (H) in the granule cell growth cones. (I) Merged image of G and H. (J–L'), Immunostaining of Cas (J) and F-actin (by phalloidin staining; K) in granule cells. (L) Merged image of J and K. (L') Magnified views of the growth cones. Arrows indicate colocalization of Cas and F-actin.

RNAi Knockdown of Cas Inhibits Axon Extension of Granule Cells

We examined whether interference of the endogenous Cas by RNAi affects granule cell axon extension (Figure 4A). The effectiveness of siRNAs was first evaluated in DLD-1 cells (human colon tumor cells), in which more than 90% of Cas protein expression was knocked down within 72 h after transfection (Supplementary Figure 1A). Then, the siRNA efficiency was confirmed by cotransfection of CasFL and Cas siRNA in cerebellar primary cultures (Supplementary Figure 1, B and C). Because of the transfection ratio and the difficulty in quantifying the Cas expression level changes in the primary culture by immunoblotting, the number of cells expressing the exogenous CasFL construct carrying the HA epitope in each observation field was quantified by HA immunostaining. HA-positive cells were decreased by cotransfection of Cas siRNA (~3 in each field), in comparison with that of the control LacZ (*Escherichia coli* β-galactosidase gene) siRNA (~10 in each field), demonstrating that Cas siRNA specifically knocked down Cas proteins in granule cells.

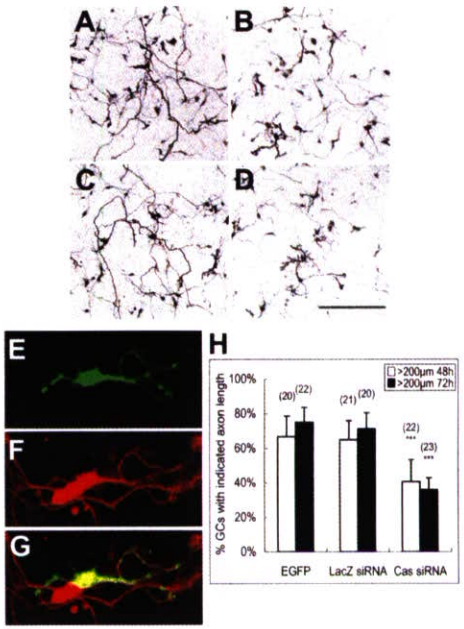

Figure 4. RNAi knockdown of Cas impairs axon extension of cerebellar granule cells. (A–D) Confocal images of cerebellar granule cells transfected with Cas siRNA or LacZ siRNA. Cerebellar granule cells were cotransfected soon after cell dissociation by either Cas siRNA or LacZ siRNA with pCAG-EGFP. Cells were fixed and observed 48 or 72 h after the transfection. (A) LacZ siRNA 48 h; (B) Cas siRNA 48 h; (C) LacZ siRNA 72 h; (D) Cas siRNA 72 h. Scale bar, 200 μm. (E–G) Granule cells (stained by anti-Pax6 antibody; F) with multiple short axons observed in Cas siRNA transfection (E). (H) Percentage of cells with axons longer than 200 μm within each observation field 48 or 72 h after transfection. Data are presented as mean ± SEM. Values in the parentheses above the column indicate the number of observation fields from at least three independent experiments. ***$p < 0.001$, compared with the EGFP control (*t* test).

The knockdown effect of Cas siRNA on neurite extension of granule cells was analyzed by counting cells with an axon length of more than 200 μm cotransfected with Cas siRNA and enhanced green fluorescent protein (EGFP) in comparison with controls. The control granule cells, which were cotransfected with LacZ siRNA and EGFP, exhibited an almost normal neurite pattern with long axons at 48 and 72 h (Figure 4, A and C, respectively) after transfection. In contrast, cells cotransfected with the Cas siRNA and EGFP had an impaired axon pattern at 48 and 72 h (Figure 4, B and D, respectively) after transfection. Pax6 (a granule cell marker)-positive cells coexpressing Cas siRNA and EGFP formed a complex neurite pattern with short, branched axons (Figure 4, E–G), indicating that Cas knockdown affected the granule cells. Long axons (>200 μm) extended from 65 and 72% LacZ siRNA-expressing granule cells at 48 and 72 h after transfection, respectively (Figure 4H). These ratios were almost comparable with those in cells expressing EGFP alone. The number of long axons (>200 μm) was significantly reduced in Cas siRNA-expressing granule cells to 40 and 35% at 48 and 72 h after transfection, respectively (Figure 4H). This Cas siRNA knockdown effect was observed even in granule cells overexpressing exogenous CasFL protein (Supplementary Figure 1D). Therefore, our data suggest that Cas is related to granule cell axon elongation.

Deletions of the YDxP Motifs or the Cas Substrate Domain Impairs Axon Elongation of Granule Cells

Cas consists of three major protein-protein interaction domains (Figure 5A): the N-terminal SH3 domain (binds to the PxxP motif of Fak, Pyk2, PTP1B, etc.), the SD (consists of a cluster of YxxP motifs that are tyrosine-phosphorylated by PTKs, leading to binding to Crk, Nck, SHIP-2, etc.), and SBD (containing motifs RPLPSPP [a.a.733–739] and YDYV [a.a.762–765], which bind to Src family PTKs; Sakai *et al.*, 1994). To assess the structure and function relationship of Cas protein in granule cell development, we constructed four Cas mutants: three deletion mutants lacking the SH3 (ΔSH3), SD (ΔSD), or only YDxP motifs within the SD (ΔYDxP), and a substitution mutant of the RPLPSPP and YDYV motifs within the SBD to RLGSSPP and FDYV, respectively (mSBD; Figure 5A). Either the full-length Cas (CasFL) or mutant Cas was coexpressed with the EGFP vector in cultured granule cells by transfection (Figure 5B). Expressed EGFP fluorescence was generally widespread over the soma and neurites of granule cells. Granule cells transfected with the CasFL, ΔSH3, or mSBD exhibited a representative morphology with single or bipolar long extending axons at this stage (DIV2; Ono *et al.*, 1997; Powell *et al.*, 1997), whereas cells transfected with the ΔSD or ΔYDxP tended to have significantly shorter, and sometimes branching, axons (Figure 5B), similar to that observed in Cas knockdown cells by Cas siRNA (Figure 4, E–H). These short axons were immunopositive for Tau-1 (unpublished data). The average length of the longest axon, in cells expressing CasFL, ΔSH3, or mSBD was nearly 250 μm, whereas that of cells expressing the ΔSD (~58 μm) or ΔYDxP (~76 μm) was very short (Figure 5C). Long axons (>200 μm) extended from more than 70% of CasFL, ΔSH3, mSBD, and EGFP-expressing cells, whereas they were observed in fewer than 40% of ΔSD or ΔYDxP-expressing cells (Figure 5D). These results suggest that the SD containing the YDxP motifs is involved in the axon elongation of granule cells and that the ΔSD and ΔYDxP act as dominant negatives to endogenous Cas in this process. The F-actins in the granule cells overexpressing Cas mutants were labeled (Supplementary Figure 4); however, there were no significant differences in the quantity of F-actins in the growth cones of cells expressing ΔYDxP and other mutants.

Cas Is the Substrate of Src Family Tyrosine Kinases in the Developing Mouse Cerebella

In fibroblasts, Cas binds to both Src and Fak family PTKs and is consequently phosphorylated by them (Nakamoto *et al.*, 1996; Cary *et al.*, 1998). To elucidate the molecular basis of Cas tyrosine phosphorylation during mouse cerebellar development, we investigated the association of Cas with nine PTKs belonging to the Src or Fak family (Figure 6). Seven Src family (Src, Fyn, Lyn, Yes, Hck, Lck, and Zap70) and the two Fak family (Fak and Pyk2) PTKs tested were expressed in the mouse cerebella (unpublished data). Only Src family PTKs, however, coimmunoprecipitated with Cas in P7 cerebellar extracts (Figure 6A), suggesting that the Src

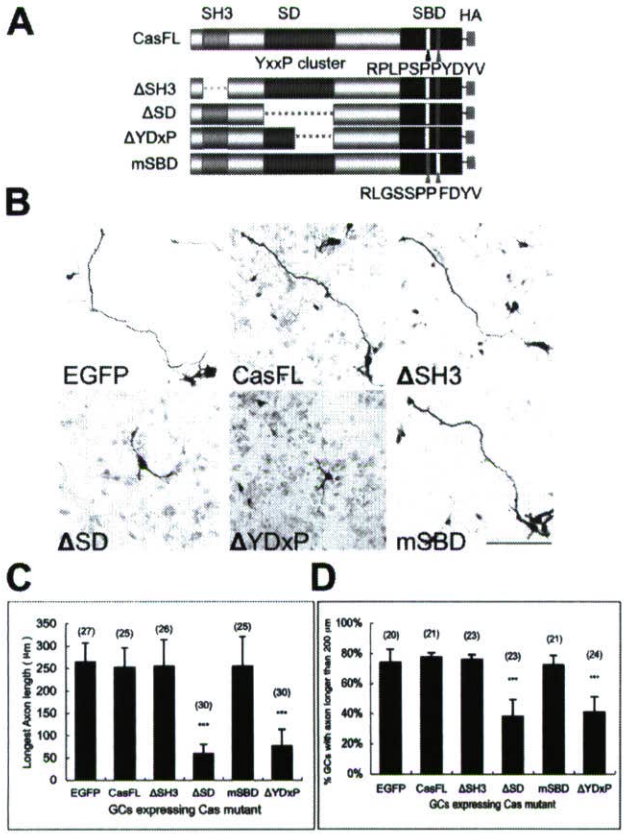

Figure 5. Overexpression of the Cas mutant lacking Crk binding ability inhibits axon elongation of granule cells. (A) Cas mutants with domain deletion or mutation. ΔSH3, deletion of the SH3 domain; ΔSD deletion of a cluster of tyrosine phosphorylation sites; ΔYDxP, deletion of YDxP motifs; mSBD, double mutations RLGSSPP and FDYV at the Src binding domain. (B) Confocal images of cerebellar granule cells expressing Cas mutants. Cerebellar granule cells were double-transfected by electroporation with a Cas mutant with an EGFP vector soon after dissociation of cerebellar cells. The cells were stained with the antibody against HA 48 h after plating. Bar, 100 μm. (C) Average length of the axons in the EGFP and Cas mutants coexpressing cells. (D) Percentage of transfected cells with axon length more than 200 μm. Cerebellar granule cells (DIV1) were transfected with Cas mutants using the calcium phosphate method. Cells were fixed, stained with the antibody against HA, and observed at DIV2. Data are indicated as mean ± SEM. Values in the parentheses above the column indicate the number of the transfected cells from at least three independent experiments. ***$p < 0.001$, compared with the EGFP control (*t* test).

family, but not the Fak family, associates with Cas in the mouse cerebella at the early stage. This result was confirmed by in vitro experiments using a Src family PTK inhibitor PP2. In contrast to the ineffective structural analog PP3, PP2 inhibited the tyrosine phosphorylation of Cas in cultured cerebellar cells (Figure 6B). YP-Cas was reduced to an almost undetectable level by treatment with 25 μM PP2, indicating that Src family PTKs are responsible for the tyrosine phosphorylation of Cas in these cells. Src and Fyn were enriched in the GCP fraction of the P7 cerebella (Supplementary Figure 2A), and their tyrosine phosphorylation levels were high in the P3–P7 cerebella (Supplementary Figure 2B). Immunocytochemical analysis of cultured granule cells (DIV1) revealed colocalization of Cas with Src and Fyn in the growth cones (Figure 6C). In addition, Cas was colocalized with Src, Fyn, or Yes in the cerebellar cortex at P12 (Supplementary Figure 2C). Moreover, there was a punctate accumulation pattern of the mSBD along the neurites (Supplementary Figure 3A). There were similar phenotypes in cells expressing ΔSBD (unpublished data). Although the underlying mechanism of punctuate distribution on neurites is unclear, it might be related to tyrosine phosphorylation, because exogenously expressed CasFL had a similar punctate accumulation pattern when PTK activity was inhibited with PP2 for 1 h (Supplementary Figure 3B).

Developmental Stage-specific Interaction of the Tyrosine-phosphorylated Cas with Adaptor Protein Crk in the Mouse Cerebellum

Crk is an adaptor protein that regulates actin cytoskeleton organization and cell migration (Klemke *et al.*, 1998). CrkII directly binds with YP-Cas in PC12 cells stimulated with nerve growth factor (Ribon and Saltiel, 1996). Our previous study indicated that YDxP motifs within the SD domain of Cas are involved in binding to CrkII in fibroblasts (Zhou *et al.*, 1993; Huang *et al.*, 2002). We examined whether there is an interaction between Cas and Crk in developing mouse cerebella (Figure 7, A and B). Crk protein was almost constantly expressed throughout cerebellar development (Figure 7A). Cas protein, however, was more efficiently coimmunoprecipitated with anti-Crk antibody from cerebellar extracts at P7 than from those at other stages tested (Figure 7B, top). In addition, the coimmunoprecipitated Cas was tyrosine phosphorylated (Figure 7B, middle). This P7 stage,

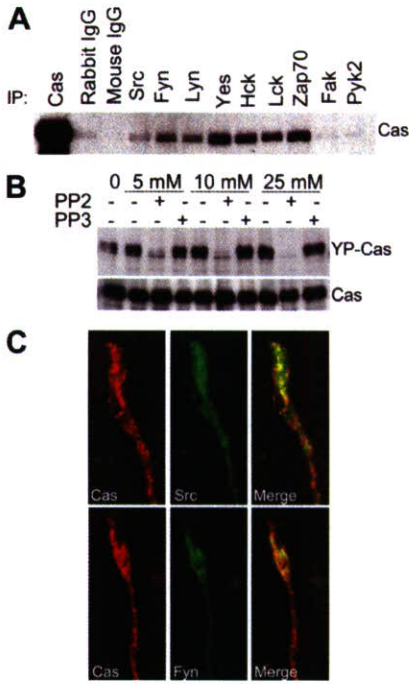

Figure 6. Cas is a substrate of Src family tyrosine kinases in the developing mouse cerebella. (A) Coimmunoprecipitation of Cas with the Src family PTKs in the mouse cerebella. An equal quantity of protein lysates from P7 cerebella was first immunoprecipitated by Src, Fyn, Yes, Lyn, Hck, Lck, Zap70, Fak, or Pyk2 antibodies and then immunoblotted by the Cas antibody. (B) Src family PTK inhibitor PP2 inhibited tyrosine phosphorylation of Cas in cerebellar neurons. Primary cultured cerebellar neurons were treated with dimethyl sulfoxide, PP2, or a noninhibitory analog, PP3, at the indicated concentrations for 20 min, and the cell lysates were immunoblotted for YP-Cas. The same membrane was reblotted to indicate the quantity of Cas in each lane. (C) Cas (red) colocalizes with Src or Fyn (green) in the growth cones of cultured cerebellar granule cells. Cerebellar granule cells were fixed at DIV1, stained, and imaged using confocal microscopy.

in which there is a tight interaction between Cas and Crk, was consistent with the peak stage for tyrosine phosphorylation of Cas (Figure 2A). Moreover, both Cas and Crk immunolabels were codistributed in growth cones and neurites of cultured granule cells and were colocalized with actin bundles at the peripheral and central domains of growth cones (Figure 7C).

Because there is a direct interaction between CrkII and JNK1 (c-Jun N-terminal kinase 1; Girardin and Yaniv, 2001), we next investigated the Crk-JNK1 association. JNK1 expression was up-regulated with a peak at P7 and then down-regulated during mouse cerebellar development (Figure 7A). In immunoprecipitates with anti-Crk antibody, JNK1 was abundant in the early stages (P3–P7; Figure 7B). Taken together, these results suggest that the YP-Cas-Crk-JNK1

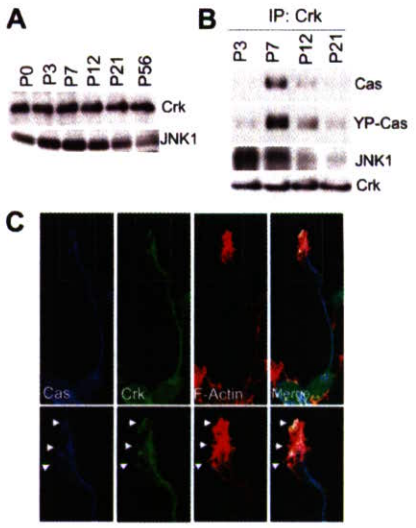

Figure 7. YP-Cas forms a complex with Crk-JNK1 in P7 mouse cerebella. (A) Immunoblotting of Crk and JNK1 protein in the mouse cerebella at different development stages. (B) Coimmunoprecipitation of Crk with Cas and JNK1 in developing mouse cerebella. An equal quantity of cerebella protein lysates from P3, P7, P12, and P21 mice were immunoprecipitated with the anti-Crk antibody and then immunoblotted with the antibody against Cas, YP-Cas, or JNK1. (C) Colocalization of Cas (blue), Crk (green), and F-actin (red, phalloidin staining) in the growth cones of cultured cerebellar granule cells (DIV1). Arrows indicate the colocalized structure.

protein interaction is involved in the signaling pathway regulating actin organization of growth cones in granule cells.

Association of Cas with N-Cadherin and NCAM in the Developing Mouse Cerebellum

There are three major classes of CAMs in the nervous system: integrin, cadherin, and the IgG superfamily of CAM (IgCAM), which serve as plasma membrane sensors for extracellular cues, leading to the activation of intracellular signaling events related to the cytoskeleton (Walsh and Doherty, 1997). Cas is tyrosine-phosphorylated by Fak or Src family PTKs after integrin stimulation (O'Neill *et al.*, 2000). Therefore, we examined whether Cas is associated with CAMs in the mouse cerebella. Anti-Cas antibody coimmunoprecipitated with N-cadherin, NCAM, and L1, but not β-integrin, from P7 cerebellar extracts (Supplementary Figure 2D). The specific antibody for N-cadherin and NCAM coimmunoprecipitated with Cas protein from cerebellar extracts in the early developmental stage (Figure 8A). N-cadherin and NCAM140/180 mRNA were expressed in the EGL and IGL in postnatal mouse cerebella at P7 (Supplementary Figure 5), which coincides with the expression of Cas mRNA (Figure 1). Both N-cadherin and NCAM protein were enriched in the GCP fraction of P7 cerebella (Supplementary Figure 2A). Moreover, N-cadherin and NCAM colocalized with Cas in the growth cones and neurites of cultured granule cells (Figure 8B). Taken together, our data suggest that

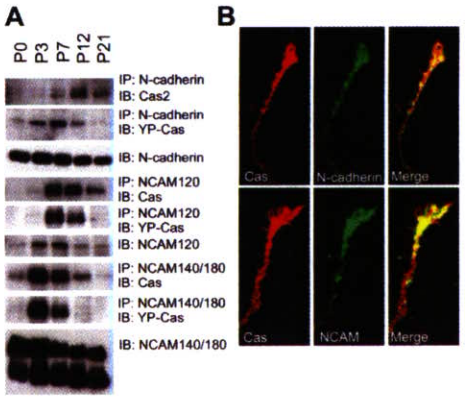

Figure 8. Cas and YP-Cas are developmentally associated with N-cadherin, NCAM120, or NCAM140/180 in mouse cerebella. (A) Cas and YP-Cas were coimmunoprecipitated with N-cadherin and NCAM in postnatal developing mouse cerebella. Equal amounts of protein lysate from the P0, P3, P7, P12, and P21 mouse cerebella were immunoprecipitated by antibodies against N-cadherin, NCAM120, or NCAM140/180. The immunoprecipitants were immunoblotted by the antibody against Cas. The same immunoprecipated protein blots were reused for immunoreaction with the antibody against YP-Cas. (B) Confocal images of colocalization of Cas (Red) with N-cadherin and NCAM140/180 (green) in the growth cones of cultured cerebellar granule cells (DIV1).

N-cadherin and NCAM interact with the Cas-mediated signaling complex and act as a cell surface signaling complex in granule cell neuritogenesis.

DISCUSSION

Cas acts as an indispensable scaffold for the signaling proteins involved in tyrosine phosphorylation–coupled actin cytoskeleton reorganization pathways and regulates cell morphology and migration in fibroblasts (Honda *et al.*, 1998; Huang *et al.*, 2002). The function of Cas in the nervous system, however, is unclear. Cas-deficient mice are embryonic lethal at 11.5–12.5 d after coitum because of impaired heart development (Honda *et al.*, 1998), making it difficult to investigate its role in the brain, which functionally develops later. The present findings demonstrate the functional importance of Cas as a signaling interface among the proteins involved in axon elongation of cerebellar granule cells during postnatal development.

The neural circuitry of the cerebellum develops through a coordinated program of neuronal migration, neurite outgrowth, and synaptic interconnections (Hatten and Heintz, 1995). To accomplish this circuit development, both granule cells and Purkinje cells undergo drastic morphological changes, in which actin cytoskeletal reorganization is very active (Ono *et al.*, 1997). The results of the present study demonstrated that both Cas mRNA and protein predominate in the cerebellum during this postnatal period in mice. Cas is enriched in the neurites and growth cones of developing granule cells and Purkinje cells. The specific binding of Cas to Src PTKs and consequent tyrosine phosphorylation, by which Cas acquires the critical ability to bind with downstream signaling proteins, peak in the early postnatal stage. This developmental profile of YP-Cas apparently coincides with the time window during which neurite extension of the granule cells and Purkinje cells are more active. In addition, YP-Cas is largely distributed around the iEGL, where postmitotic granule cells start to differentiate by axonal extension and migration, and the ends of Purkinje cell dendrites are actively sprouting. These results indicate that tyrosine phosphorylation of Cas is closely associated with the postnatal development of cerebellar neurons.

In fibroblasts, Cas interacts with Fak family PTKs through the N-terminal SH3 domain and also directly binds to Src family PTKs via the C-terminal SBD, which contains the YDYV and RPLPSPP motifs (Sakai *et al.*, 1994; Ruest *et al.*, 2001), resulting in the tyrosine-phosphorylation of Cas, the production of YP-Cas. Src family PTKs are highly expressed in the cerebellum and their expression and activity is developmentally regulated (Fults *et al.*, 1985; Cartwright *et al.*, 1988; Maness *et al.*, 1988; Sudol *et al.*, 1988, 1989; Chen *et al.*, 1996; Omri *et al.*, 1996). A previous study indicated that Fak has important roles in axon extension and polarization of cerebellar Purkinje cells (Rico *et al.*, 2004). There are no reports, however, of a role for Fak in cerebellar granule cell development. Our study demonstrated that Cas has no tight association with Fak and Pyk2 compared with Src family PTKs in early postnatal developing cerebella. Cas associates with Src family PTKs in developing mouse cerebella and colocalizes with Src and Fyn in the growth cones of granule cells. Moreover, the Src family PTK inhibitor PP2 almost completely blocks the tyrosine phosphorylation of Cas in in vitro cerebellar cell cultures. These findings support the idea that Src, but not Fak, family PTKs are responsible for the tyrosine phosphorylation of Cas in cerebellar neurons.

Cas is constitutively tyrosine-phosphorylated after binding to the Src family PTKs, and the major tyrosine phosphorylation sites are the SD, including four YQxP motifs and nine YDxP motifs in fibroblasts (Pellicena and Miller, 2001; Ruest *et al.*, 2001). We previously reported that Cas null fibroblasts have defective actin stress fiber organization and that the ΔYDxP Cas mutant fails to restore the actin stress fiber organization (Huang *et al.*, 2002). In the present study, knockdown of Cas protein expression with the Cas siRNA impaired axonal growth, and dominant-negative effects of Cas mutants, ΔSD and ΔYDxP, in axon elongation were also observed. Granule cells expressing exogenous ΔSD or ΔYDxP have abnormally truncated axonal protrusions, whereas no abnormal axon elongation was observed in cells expressing the other mutants ΔSH3 and mSBD, indicating the importance of the interaction of Cas with the SD-binding proteins for axon extension of granule cells. On the other hand, the overexpressed mSBD mutant tended to distribute in a punctate pattern in the dendrites and soma (Supplementary Figure 3), suggesting that a defect in the binding of Cas to Src family PTKs affects the subcellular distribution of Cas proteins. Loss of the dominant negative effect of mSBD on axon extension might be due to its aberrant subcellular accumulation. Taken together, these results indicate that Cas has an important role in the signaling of axon elongation through interactions with its binding partners via the tyrosine-phosphorylated YDxP motifs.

Phospho-tyrosines within the YDxP motifs are essential for binding Cas to the SH2 domain of the adaptor protein Crk (Zhou *et al.*, 1993; Huang *et al.*, 2002), which subsequently regulates the actin reorganization during fibroblast migration (Klemke *et al.*, 1998). A recent study reported that Crk is recruited to the lipid rafts in growing neurites and mediates lamellipodia formation in PC12 cells (Haglund *et al.*, 2004). Our present data indicate that the interaction between Cas and Crk occurs within the time window when Cas is highly tyrosine-phosphorylated during cerebellar development. In addition, Cas and Crk are subcellularly colocalized with F-actin bundles in the peripheral region of growth cones of cultured granule cells. These results suggest that the impaired axon elongation induced by Cas knockdown with siRNA or overexpression of the ΔYDxP mutant in granule cells might be due to a deficiency in the regulation of the actin-cytoskeletal organization through the YP-Cas-Crk interaction.

Our data demonstrate that JNK1 interacts with the YP-Cas-Crk complex in mouse cerebellum during the early postnatal stage. JNK1 interacts with the SH3 domain of CrkII (Girardin and Yaniv, 2001) and is involved in signaling of neuronal microtubule dynamics through the phosphorylation of microtubule-associated proteins (Chang *et al.*, 2003; Bjorkblom *et al.*, 2005). Another downstream effector of Crk is a small GTPase Rac1 that mediates the actin cytoskeletal dynamics during axonal outgrowth (Luo, 2002). Rac1 is activated by DOCK180, a Crk SH3-binding protein, leading to the lamellipodia formation by fibroblasts (Tanaka *et al.*, 1997; Kiyokawa *et al.*, 1998). It is notable that high Rac activity is present in early postnatal cerebellum (Arakawa *et al.*, 2003). In our primary dissociation cultures, the growth cones of granule cells were very tiny and unstable, and they grew out very rapidly soon after plating on culture dishes. Even if there are subtle changes, it would be very difficult to observe actin dynamics within the growth cone after incubating to obtain effective cellular levels of recombinant Cas proteins, which are exogenously expressed by cDNA transfection. Therefore, we primarily analyzed the length of extending neurites after transfection experiments. Similarly, we did not focus our study on fillopodia and lamellipodia, which are more dynamic structures within the growth cones.

NCAMs actively participate in neurite elongation and dendritic and axonal arbor pathfinding (Walsh and Doherty, 1997; Rougon and Hobert, 2003). The importance of the CAMs, including NCAM, N-cadherin, and L1 for axonal growth was established by a large number of antibody perturbation experiments (Lindner *et al.*, 1983; Hoffman *et al.*, 1986; Walsh and Doherty, 1997; Sakurai *et al.*, 2001; He and Meiri, 2002). A recent study demonstrated that mice deficient for both Nr-CAM and L1 exhibit severe cerebellar folial defects and reduced IGL thickness (Sakurai *et al.*, 2001), indicating that Nr-CAM and L1 have a role in cerebellar granule cell development. Although, to our knowledge, there are no reports of NCAM or N-cadherin knockout mice with defects in cerebellar granule cell development, this might be due to a CAM redundancy. Our data indicate that the developmental expression of N-cadherin and NCAM140/180 mRNA in postnatal mouse cerebella at P7 coincides with that of Cas in the EGL and IGL at the same developmental stage. YP-Cas associates with N-cadherin and NCAMs in the early stage (P3–P12) of cerebellar development, and NCAM and N-cadherin are concentrated in the growth cones of granule cells. Integrin, however, did not coimmunoprecipitate with Cas, which seems to be consistent with a recent study in which NCAM and L1, but not β1 integrin, were detected in the detergent-resistant membranes of cerebellar granule cells (Nakai and Kamiguchi, 2002). NCAM and L1 are implicated in the underlying signaling cascades via the activation of Src and Fyn (Beggs *et al.*, 1994; Ignelzi *et al.*, 1994; Beggs *et al.*, 1997). Whether Cas is tyrosine-phosphorylated after association with CAMs or Cas is tyrosine-phosphorylated before the association with CAMs remain unclear. Cell surface signals via CAMs might activate Src family PTKs, followed by Src PTK binding to and subsequent tyrosine-phosphorylation of Cas protein, leading to the axonal outgrowth of granule cells.

Although Cas mRNAs are localized in both the outer (mitotic) and inner (postmitotic) layer of the EGL, Cas proteins, including phosphorylated form, predominantly distribute in the inner EGL where postmitotic granule cells are settled and begin with their differentiation before cell migration toward the ML. Therefore, we think that Cas is mainly involved in the differentiation of granule cells rather than in the proliferation of their precursors. It is possible, however, that a small amount of Cas protein is involved in granule cell growth.

In conclusion, our data provide functional evidence that the tyrosine-phosphorylated docking protein Cas acts as a signaling interface from the protein tyrosine phosphorylation toward the axonal outgrowth in cerebellar granule cells. The present findings demonstrate that Cas is most abundant in developing mouse cerebellum and is highly tyrosine-phosphorylated in the early postnatal stage, probably by its binding partner Src PTKs. YP-Cas binds Crk, which further recruits downstream proteins such as JNK1. This sequential signaling event likely regulates granule cell axonal outgrowth.

ACKNOWLEDGMENTS

Jinhong Huang was a postdoctoral fellowship recipient of the Japan Society for the Promotion of Science (JSPS). We thank Dr. Noriyuki Morita for the cerebellar dissociation cell cultures and immunohistochemistry, Dr. Fumio Yoshikawa for subcellular fractionation of the growth cone particles, and Dr. Hiroshi Hama for DNA transfection into primary cerebellar neurons. We also thank Dr. Tamae Asawa (National Cancer Research Center) for the Cas siRNA study.

REFERENCES

Arakawa, Y., Bito, H., Furuyashiki, T., Tsuji, T., Takemoto-Kimura, S., Kimura, K., Nozaki, K., Hashimoto, N., and Narumiya, S. (2003). Control of axon elongation via an SDF-1alpha/Rho/mDia pathway in cultured cerebellar granule neurons. J. Cell. Biol. *161*, 381–391.

Azuma, K., Tanaka, M., Uekita, T., Inoue, S., Yokota, J., Ouchi, Y., and Sakai, R. (2005). Tyrosine phosphorylation of paxillin affects the metastatic potential of human osteosarcoma. Oncogene *24*, 4754–4764.

Beggs, H. E., Baragona, S. C., Hemperly, J. J., and Maness, P. F. (1997). NCAM140 interacts with the focal adhesion kinase p125(fak) and the SRC-related tyrosine kinase p59(fyn). J. Biol. Chem. *272*, 8310–8319.

Beggs, H. E., Soriano, P., and Maness, P. F. (1994). NCAM-dependent neurite outgrowth is inhibited in neurons from Fyn-minus mice. J. Cell. Biol. *127*, 825–833.

Bjorkblom, B., Ostman, N., Hongisto, V., Komarovski, V., Filen, J. J., Nyman, T. A., Kallunki, T., Courtney, M. J., and Coffey, E. T. (2005). Constitutively active cytoplasmic c-Jun N-terminal kinase 1 is a dominant regulator of dendritic architecture: role of microtubule-associated protein 2 as an effector. J. Neurosci. *25*, 6350–6361.

Cartwright, C. A., Simantov, R., Cowan, W. M., Hunter, T., and Eckhart, W. (1988). pp60c-src expression in the developing rat brain. Proc. Natl. Acad. Sci. USA *85*, 3348–3352.

Cary, L. A., Han, D. C., Polte, T. R., Hanks, S. K., and Guan, J. L. (1998). Identification of p130Cas as a mediator of focal adhesion kinase-promoted cell migration. J. Cell. Biol. *140*, 211–221.

Chang, L., Jones, Y., Ellisman, M. H., Goldstein, L. S., and Karin, M. (2003). JNK1 is required for maintenance of neuronal microtubules and controls phosphorylation of microtubule-associated proteins. Dev. Cell *4*, 521–533.

Chen, S., Ren, Y. Q., and Hillman, D. E. (1996). Transient expression of lyn gene in Purkinje cells during cerebellar development. Brain Res. Dev. Brain Res. *92*, 140–146.

Dent, E. W., and Gertler, F. B. (2003). Cytoskeletal dynamics and transport in growth cone motility and axon guidance. Neuron *40*, 209–227.

Dickson, B. J. (2001). Rho GTPases in growth cone guidance. Curr. Opin. Neurobiol. *11*, 103–110.

Fults, D. W., Towle, A. C., Lauder, J. M., and Maness, P. F. (1985). pp60c-src in the developing cerebellum. Mol. Cell. Biol. *5*, 27–32.

Girardin, S. E., and Yaniv, M. (2001). A direct interaction between JNK1 and CrkII is critical for Rac1-induced JNK activation. EMBO J. *20*, 3437–3446.

Haglund, K., Ivankovic-Dikic, I., Shimokawa, N., Kruh, G. D., and Dikic, I. (2004). Recruitment of Pyk2 and Cbl to lipid rafts mediates signals important for actin reorganization in growing neurites. J. Cell. Sci. *117*, 2557–2568.

Hama, H., Hara, C., Yamaguchi, K., and Miyawaki, A. (2004). Protein kinase C signaling mediates global enhancement of excitatory synaptogenesis in neurons triggered by local contact with astrocytes. Neuron *41*, 405–415.

Hatten, M. E., and Heintz, N. (1995). Mechanisms of neural patterning and specification in the developing cerebellum. Annu. Rev. Neurosci. *18*, 385–408.

He, Q., and Meiri, K. F. (2002). Isolation and characterization of detergent-resistant microdomains responsive to NCAM-mediated signaling from growth cones. Mol. Cell. Neurosci. *19*, 18–31.

Helmke, S., Lohse, K., Mikule, K., Wood, M. R., and Pfenninger, K. H. (1998). SRC binding to the cytoskeleton, triggered by growth cone attachment to laminin, is protein tyrosine phosphatase-dependent. J. Cell. Sci. *111*(Pt 16), 2465–2475.

Hoffman, S., Friedlander, D. R., Chuong, C. M., Grumet, M., and Edelman, G. M. (1986). Differential contributions of Ng-CAM and N-CAM to cell adhesion in different neural regions. J. Cell. Biol. *103*, 145–158.

Honda, H. *et al.* (1998). Cardiovascular anomaly, impaired actin bundling and resistance to Src-induced transformation in mice lacking p130Cas. Nat. Genet. *19*, 361–365.

Huang, J., Hamasaki, H., Nakamoto, T., Honda, H., Hirai, H., Saito, M., Takato, T., and Sakai, R. (2002). Differential regulation of cell migration, actin stress fiber organization, and cell transformation by functional domains of Crk-associated substrate. J. Biol. Chem. *277*, 27265–27272.

Ignelzi, M. A., Jr., Miller, D. R., Soriano, P., and Maness, P. F. (1994). Impaired neurite outgrowth of src-minus cerebellar neurons on the cell adhesion molecule L1. Neuron *12*, 873–884.

Kiyokawa, E., Hashimoto, Y., Kobayashi, S., Sugimura, H., Kurata, T., and Matsuda, M. (1998). Activation of Rac1 by a Crk SH3-binding protein, DOCK180. Genes Dev. *12*, 3331–3336.

Klemke, R. L., Leng, J., Molander, R., Brooks, P. C., Vuori, K., and Cheresh, D. A. (1998). CAS/Crk coupling serves as a "molecular switch" for induction of cell migration. J. Cell Biol. *140*, 961–972.

Korey, C. A., and Van Vactor, D. (2000). From the growth cone surface to the cytoskeleton: one journey, many paths. J. Neurobiol. *44*, 184–193.

Lindner, J., Rathjen, F. G., and Schachner, M. (1983). L1 mono- and polyclonal antibodies modify cell migration in early postnatal mouse cerebellum. Nature *305*, 427–430.

Liu, J. J., Ding, J., Kowal, A. S., Nardine, T., Allen, E., Delcroix, J. D., Wu, C., Mobley, W., Fuchs, E., and Yang, Y. (2003). BPAG1n4 is essential for retrograde axonal transport in sensory neurons. J. Cell. Biol. *163*, 223–229.

Luo, L. (2002). Actin cytoskeleton regulation in neuronal morphogenesis and structural plasticity. Annu. Rev. Cell Dev. Biol. *18*, 601–635.

Maness, P. F., Aubry, M., Shores, C. G., Frame, L., and Pfenninger, K. H. (1988). c-src gene product in developing rat brain is enriched in nerve growth cone membranes. Proc. Natl. Acad. Sci. USA *85*, 5001–5005.

Miyake, I., Hakomori, Y., Misu, Y., Nakadate, H., Matsuura, N., Sakamoto, M., and Sakai, R. (2005). Domain-specific function of ShcC docking protein in neuroblastoma cells. Oncogene *24*, 3206–3215.

Nakai, Y., and Kamiguchi, H. (2002). Migration of nerve growth cones requires detergent-resistant membranes in a spatially defined and substrate-dependent manner. J. Cell Biol. *159*, 1097–1108.

Nakamoto, T., Sakai, R., Ozawa, K., Yazaki, Y., and Hirai, H. (1996). Direct binding of C-terminal region of p130Cas to SH2 and SH3 domains of Src kinase. J. Biol. Chem. *271*, 8959–8965.

O'Neill, G. M., Fashena, S. J., and Golemis, E. A. (2000). Integrin signalling: a new Cas. (t) of characters enters the stage. Trends Cell Biol. *10*, 111–119.

Omri, B., Crisanti, P., Marty, M. C., Alliot, F., Fagard, R., Molina, T., and Pessac, B. (1996). The Lck tyrosine kinase is expressed in brain neurons. J. Neurochem. *67*, 1360–1364.

Ono, K., Shokunbi, T., Nagata, I., Tokunaga, A., Yasui, Y., and Nakatsuji, N. (1997). Filopodia and growth cones in the vertically migrating granule cells of the postnatal mouse cerebellum. Exp. Brain Res. *117*, 17–29.

Pellicena, P., and Miller, W. T. (2001). Processive phosphorylation of p130Cas by Src depends on SH3-polyproline interactions. J. Biol. Chem. *276*, 28190–28196.

Pfenninger, K. H., Ellis, L., Johnson, M. P., Friedman, L. B., and Somlo, S. (1983). Nerve growth cones isolated from fetal rat brain: subcellular fractionation and characterization. Cell *35*, 573–584.

Pollard, T. D., and Borisy, G. G. (2003). Cellular motility driven by assembly and disassembly of actin filaments. Cell *112*, 453–465.

Powell, S. K., Rivas, R. J., Rodriguez-Boulan, E., and Hatten, M. E. (1997). Development of polarity in cerebellar granule neurons. J. Neurobiol. *32*, 223–236.

Ribon, V., and Saltiel, A. R. (1996). Nerve growth factor stimulates the tyrosine phosphorylation of endogenous Crk-II and augments its association with p130Cas in PC-12 cells. J. Biol. Chem. *271*, 7375–7380.

Rico, B., Beggs, H. E., Schahin-Reed, D., Kimes, N., Schmidt, A., and Reichardt, L. F. (2004). Control of axonal branching and synapse formation by focal adhesion kinase. Nat. Neurosci. *7*, 1059–1069.

Rougon, G., and Hobert, O. (2003). New insights into the diversity and function of neuronal immunoglobulin (Ig) superfamily molecules. Annu. Rev. Neurosci. *26*, 207–238.

Ruest, P. J., Shin, N. Y., Polte, T. R., Zhang, X., and Hanks, S. K. (2001). Mechanisms of CAS substrate domain tyrosine phosphorylation by FAK and Src. Mol. Cell. Biol. *21*, 7641–7652.

Sakai, R., Iwamatsu, A., Hirano, N., Ogawa, S., Tanaka, T., Mano, H., Yazaki, Y., and Hirai, H. (1994). A novel signaling molecule, p130, forms stable complexes in vivo with v-Crk and v-Src in a tyrosine phosphorylation-dependent manner. EMBO J. *13*, 3748–3756.

Sakurai, T., Lustig, M., Babiarz, J., Furley, A. J., Tait, S., Brophy, P. J., Brown, S. A., Brown, L. Y., Mason, C. A., and Grumet, M. (2001). Overlapping functions of the cell adhesion molecules Nr-CAM and L1 in cerebellar granule cell development. J. Cell Biol. *154*, 1259–1273.

Shiraishi, Y., Mizutani, A., Bito, H., Fujisawa, K., Narumiya, S., Mikoshiba, K., and Furuichi, T. (1999). Cupidin, an isoform of Homer/Vesl, interacts with the actin cytoskeleton and activated rho family small GTPases and is expressed in developing mouse cerebellar granule cells. J. Neurosci. *19*, 8389–8400.

Sudol, M., Alvarez-Buylla, A., and Hanafusa, H. (1988). Differential developmental expression of cellular yes and cellular src proteins in cerebellum. Oncogene Res. *2*, 345–355.

Sudol, M., Kuo, C. F., Shigemitsu, L., and Alvarez-Buylla, A. (1989). Expression of the yes proto-oncogene in cerebellar Purkinje cells. Mol. Cell. Biol. *9*, 4545–4549.

Tanaka, E., and Sabry, J. (1995). Making the connection: cytoskeletal rearrangements during growth cone guidance. Cell *83*, 171–176.

Tanaka, S., Ouchi, T., and Hanafusa, H. (1997). Downstream of Crk adaptor signaling pathway: activation of Jun kinase by v-Crk through the guanine nucleotide exchange protein C3G. Proc. Natl. Acad. Sci. USA *94*, 2356–2361.

Walsh, F. S., and Doherty, P. (1997). Neural cell adhesion molecules of the Ig superfamily: role in axon growth and guidance. Annu. Rev. Cell Dev. Biol. *13*, 425–456.

Wu, D. Y., and Goldberg, D. J. (1993). Regulated tyrosine phosphorylation at the tips of growth cone filopodia. J. Cell Biol. *123*, 653–664.

Zhao, Y. H., Baker, H., Walaas, S. I., and Sudol, M. (1991). Localization of p62c-yes protein in mammalian neural tissues. Oncogene *6*, 1725–1733.

Zhou, S., Shoelson, S. E., Chaudhuri, M., Gish, G., Pawson, T., Haser, W. G., King, F., Roberts, T., Ratnofsky, S., and Lechleider, R. J. (1993). SH2 domains recognize specific phosphopeptide sequences. Cell *72*, 767–778.

Cell

Force Sensing by Mechanical Extension of the Src Family Kinase Substrate p130Cas

Yasuhiro Sawada,[1,*] Masako Tamada,[1] Benjamin J. Dubin-Thaler,[1] Oksana Cherniavskaya,[1] Ryuichi Sakai,[2] Sakae Tanaka,[3] and Michael P. Sheetz[1]

[1] Department of Biological Sciences, Columbia University, Sherman Fairchild Center Room 715, MC-2416, 1212 Amsterdam Avenue, New York, NY 10027, USA

[2] Growth Factor Division, National Cancer Center Research Institute, 5-1-1 Tsukiji, Chuo-ku, Tokyo 104-0045, Japan

[3] Department of Orthopaedic Surgery, Graduate School of Medicine, The University of Tokyo, 7-3-1 Hongo, Bunkyo-ku, Tokyo 113-0033, Japan

*Contact: ys454-ind@umin.ac.jp

DOI 10.1016/j.cell.2006.09.044

SUMMARY

How physical force is sensed by cells and transduced into cellular signaling pathways is poorly understood. Previously, we showed that tyrosine phosphorylation of p130Cas (Cas) in a cytoskeletal complex is involved in force-dependent activation of the small GTPase Rap1. Here, we mechanically extended bacterially expressed Cas substrate domain protein (CasSD) in vitro and found a remarkable enhancement of phosphorylation by Src family kinases with no apparent change in kinase activity. Using an antibody that recognized extended CasSD in vitro, we observed Cas extension in intact cells in the peripheral regions of spreading cells, where higher traction forces are expected and where phosphorylated Cas was detected, suggesting that the in vitro extension and phosphorylation of CasSD are relevant to physiological force transduction. Thus, we propose that Cas acts as a primary force sensor, transducing force into mechanical extension and thereby priming phosphorylation and activation of downstream signaling.

INTRODUCTION

Cellular responses to mechanical force underlie many critical functions, from normal morphogenesis to carcinogenesis, cardiac hypertrophy, wound healing, and bone homeostasis. Recent studies indicate that various signaling pathways are involved in force transduction, including MAP kinases, small GTPases, and tyrosine kinases/phosphatases (Geiger and Bershadsky, 2002; Giannone and Sheetz, 2006; Katsumi et al., 2002; Sawada et al., 2001). A variety of primary force-sensing mechanisms could be postulated, including mechanical extension of cytoplasmic proteins, activation of ion channels, and formation of force-stabilized receptor-ligand bonds (catch bonds) (Vogel and Sheetz, 2006), which would then activate downstream signaling pathways. At a biochemical level, tyrosine phosphorylation levels appear to be linked to mechanically induced changes controlling many other cellular functions (Giannone and Sheetz, 2006). One protein involved in mechanically induced phosphorylation-dependent signaling is the Src family kinase substrate Cas (Crk-associated substrate), which is involved in various cellular events such as migration, survival, transformation, and invasion (Defilippi et al., 2006). Stretch-dependent tyrosine phosphorylation of Cas by Src family kinases (SFKs) occurs in detergent-insoluble cytoskeletal complexes and is involved in force-dependent activation of the small GTPase Rap1 (Tamada et al., 2004). Rap1 is activated by distinct types of guanine nucleotide exchange factors coupled with various receptors or second messengers and plays an important role in a number of signaling pathways, including integrin signaling (Hattori and Minato, 2003).

The Cas substrate domain, which is located in the center of Cas, is flanked by the amino-terminal SH3 and the carboxy-terminal Src-binding domains. These amino- and carboxy-terminal domains are involved in Cas localization at focal adhesions, while the substrate domain itself is not (Nakamoto et al., 1997), suggesting that these flanking domains anchor Cas molecules to the cytoskeletal complex and that the substrate domain could be extended upon cytoskeleton stretching. Furthermore, the Cas substrate domain has 15 repeats of a tyrosine-containing motif (YxxP) (Mayer et al., 1995), and multiple sequence repeats are found in molecules with mechanical functions such as titin (Rief et al., 1997).

Cell stretching could increase tyrosine phosphorylation by (1) directly activating the kinase, (2) inactivating the phosphatase, (3) mechanically bringing the kinase to the substrate, or (4) enhancing the susceptibility of the substrate to phosphorylation. To test between these possibilities, we have analyzed the mechanisms of stretch-dependent

enhancement of Cas phosphorylation. In intact cells, Cas phosphorylation by c-Src is significantly increased by cell stretching with no detectable change in c-Src kinase activity. Cas phosphorylation mediates physiological force transduction through stretch-dependent activation of Rap1 in intact cells. With *in vitro protein extension* (IPE) experiments, we find that phosphorylation of CasSD by specific kinases is increased upon extension. Further, an antibody that recognizes extended CasSD in vitro preferentially recognizes Cas molecules at the periphery of late spreading cells where higher traction forces are predicted and Cas is phosphorylated, indicating that the in vitro extension and phosphorylation of CasSD is relevant to force transduction through Cas phosphorylation in intact cells. Thus, we suggest that Cas serves as a direct mechanosensor where force induces a mechanical extension of the substrate domain that primes it for phosphorylation. We propose that such "substrate priming" is a general mechanism for force transduction.

RESULTS

Cell Stretching Enhances SFK-Dependent Phosphorylation of Cas without a Detectable Increase in Src Kinase Activity

We first examined whether the phosphorylation of Cas increased upon intact cell stretching, using the cell stretching system that we developed (Sawada et al., 2001). Cells were cultured on a stretchable substrate (collagen-coated silicone), and the substrate was stretched uniformly and biaxially (10% in each dimension) and held stretched. To analyze the primary responses to cell stretching, samples were prepared from the cells lysed shortly (1 min) after stretching. Immunoblotting using an anti-phospho-Cas antibody (pCas-165) that specifically recognizes multiple phosphorylated YxxP motifs in the substrate domain (Fonseca et al., 2004) revealed a stretch-dependent increase in tyrosine phosphorylation of Cas in HEK293 cells (Figure 1A). When the selective SFK inhibitor CGP77675 (Missbach et al., 1999) (Novartis Pharma AG, Switzerland) was added prior to stretching, stretch-dependent tyrosine phosphorylation of Cas was inhibited (Figure 1A). Furthermore, stretch-dependent phosphorylation of Cas was greatly attenuated in SYF cells that lacked the major SFKs, c-Src, c-Yes, and Fyn (Klinghoffer et al., 1999), and was restored in SYF cells stably expressing c-Src (Figure 1B), c-Yes, or Fyn (data not shown). Thus, stretching intact cells increased tyrosine phosphorylation of Cas by SFKs.

To determine if stretch-dependent increases in Cas phosphorylation correlated with SFK activation, the levels of c-Src phosphorylation at either activating or inhibiting tyrosine residue (Y416 and Y527, respectively) were examined in SYF cells stably expressing c-Src, either stretched or left unstretched. We observed no changes in phosphorylation levels of those tyrosines (pY416 and pY527) (Figure 1B, lanes 3 and 4). Since the levels of pY416 and pY527 indicate Src kinase inhibition and activation, respectively (Thomas and Brugge, 1997), cell stretching did not appear to affect c-Src activity, while Cas phosphorylation significantly increased. This was further confirmed by an in vitro kinase assay of immunoprecipitated c-Src (Figure 1C). Thus, stretching intact cells increased tyrosine phosphorylation of Cas by c-Src without detectable enhancement of c-Src kinase activity.

Tyrosine Phosphorylation of Cas Is Involved in Stretch-Dependent Rap1 Activation

To explore the role of Cas in physiological force transduction pathways, we analyzed the involvement of Cas in the stretch-dependent activation of Rap1 in cells (Sawada et al., 2001). When the level of Cas protein and phosphorylated Cas was selectively decreased by small interfering RNA (siRNA) in HEK293 cells (Figure 2A, upper panel), Rap1 activity in cells, either stretched or unstretched, was significantly attenuated (Figure 2A, lower panel). Thus, Cas plays a significant role in the stretch-dependent activation of Rap1 in intact cells. However, there is likely more than one pathway for Rap1 activation, considering the fold decrease of Rap1 activity (~50%) in Cas knockdown cells (Figure 2A) as well as the stretch-dependent Rap1 activation observed in Cas-deficient fibroblasts (data not shown).

To further examine the role of phosphorylation of Cas in stretch-dependent Rap1 activation, we overexpressed Cas together with Rap1 in HEK293 cells. Upon coexpression of monomeric red fluorescent protein (RFP)-tagged wild-type Cas (RFP-Cas) with green fluorescent protein (GFP)-tagged Rap1 (GFP-Rap1), stretch-dependent activity of GFP-Rap1 was enhanced over the cells coexpressing RFP alone or RFP-Cas15YF that had all 15 YxxP motifs in the substrate domain mutated to FxxP (Figure 2B). The fold increase of Rap1 activity by cell stretching appeared to be smaller in the case of RFP-Cas-expressing cells, probably due to the less efficient incorporation of "overexpressed" Cas into physiological signaling complexes. However, we conclude that tyrosine phosphorylation of Cas is responsible for a significant fraction of the stretch-dependent Rap1 activation.

In Vitro Extension of CasSD

Because kinase activation did not appear to be the primary mechanism regulating Cas phosphorylation in response to cell stretching (Figures 1B and 1C), we tested whether the mechanical extension of the Cas substrate domain modulated its susceptibility to phosphorylation by SFKs. To eliminate the involvement of any extraneous molecules, we performed biochemical analysis, using an IPE system. In that system, bacterially expressed Cas substrate domain protein, CasSD (Cas115–420), was biotinylated on both amino and carboxy termini (designated NC-biotinylated CasSD, Figure 3A, top) and was bound to avidin covalently immobilized on a latex substrate (Figure 3A). After stretching of the latex membrane (Figure 3A), biochemical analyses were performed.

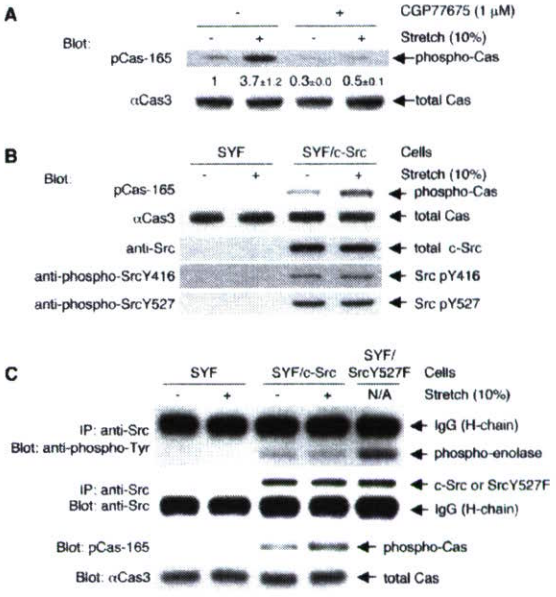

Figure 1. SFK- and Stretch-Dependent Tyrosine Phosphorylation of Cas In Vivo

(A) Stretch-dependent tyrosine phosphorylation of Cas in intact cells. HEK293 (2×10^5) cells on the collagen (type I)-coated stretchable silicone dish were treated with either CGP77675 (1 μM) or its vehicle (0.01% DMSO) and were either stretched (biaxially, 10% in each dimension) or left unstretched. One minute after stretching or without stretching, the cells were solubilized with 1× SDS sample buffer containing 20 mM DTT and analyzed for Cas phosphorylation by anti-phospho-Cas (pCas-165) and anti-Cas (αCas3) immunoblotting. Quantification of phosphorylation (phospho-Cas/total Cas) was scaled with unstretched control set at 1 and noted below the pCas-165 blot with SD ($n = 4$).

(B) Cell stretching increases Src-dependent phosphorylation of Cas without apparent change in phosphorylation levels of activating and inhibiting tyrosines of c-Src. SYF cells (triple knockout cells of c-src, c-yes, and fyn) or SYF cells stably expressing c-Src (4×10^5) were either stretched or left unstretched. One minute after stretching or without stretching, cells were solubilized with SDS sample buffer, and equivalent portions of each sample were subjected to SDS-PAGE followed by pCas-165, αCas3, anti-Src, anti-phospho-Src Y416, and anti-phospho-Src Y527 immunoblotting.

(C) Cell stretching increases Src-dependent phosphorylation of Cas without apparent change in Src kinase activity. SYF cells or SYF cells stably expressing c-Src (4×10^5) were either stretched or left unstretched. One minute after stretching or without stretching, cells were lysed and subjected to immunoprecipitation followed by an in vitro kinase assay using acid-treated enolase as a substrate. Src kinase activity was analyzed by measuring the phosphorylation of enolase with anti-phospho-tyrosine immunoblotting (top panel). Immunoprecipitated Src, i.e., Src protein in the kinase reaction, was quantified by anti-Src immunoblotting (second panel). Equivalent small portions of each lysate were mixed with SDS sample buffer and subjected directly to SDS-PAGE followed by pCas-165 and αCas3 immunoblotting to analyze for Cas phosphorylation (third and fourth panels). Kinase reactions for the lane 3 and 4 samples appeared not to be saturated because the sample prepared from SYF/SrcY527F cells (SYF cells expressing SrcY527F, the highly active mutant form of c-Src) cultured on a plastic plate following the same protocol gave more phosphorylation of enolase (lane 5). The intense bands above enolase (top panel) and below Src (second panel) represent IgG (heavy chain) from the anti-Src antibody.

To determine if stretching of the latex membrane actually extended NC-biotinylated CasSD, we developed the yellow fluorescent protein (YFP) amino-terminal swapping assay based on the interaction between the amino- and carboxy-terminal regions of YFP. In this assay, CasSD extension was detected by the separation of YFP components attached to the ends of CasSD, causing the binding of an exogenous YFP component. When the two halves of a split YFP, YFP-N and YFP-C, were fused to the amino- and carboxy-terminal ends of NC-biotinylated CasSD, respectively (NY/CY-NC-biotinylated CasSD, Figure 3B), we observed yellow fluorescence in both NY/CY-NC-biotinylated CasSD-expressing bacteria and the purified protein, as expected (Hu et al., 2002). When we added purified His_6-YFP-N to bind to YFP-C in NY/CY-NC biotinylated CasSD (Figure 3B, top), His_6-YFP-N binding was not observed without latex membrane stretching (Figure 3C, lane 1). However, we observed His_6-YFP-N binding upon stretching (Figure 3C, lane 2). Furthermore, His_6-YFP-N did not bind to NY/CY-C-biotinylated CasSD (the unextendable mono-biotinylated control, Figure 3B, bottom) or NC-biotinylated CasSD (extendable, but with no YFP component, Figure 3A, top) even following stretching (Figure 3C, lanes 3–6). Using His_6-YFP-N together with YFP-C fused to glutathione *S*-transferase (GST) in a GST pull-down experiment, we found that YFP-N bound to YFP-C under the same buffer conditions used in the YFP amino-terminal swapping assay (data not shown). Thus, stretching of the latex membrane separated the YFP halves in NY/CY-NC-biotinylated CasSD and allowed His_6-YFP-N to bind, indicating the extension of CasSD (Figure 3B, top).

Extension-Dependent Phosphorylation of CasSD by Recombinant Tyrosine Kinases In Vitro

Since CasSD could be extended by the IPE system, we examined the effect of extension on tyrosine phosphorylation of CasSD by recombinant active c-Src. While the level of phosphorylation was low without stretching (Figure 4A, lane 1), CasSD phosphorylation increased in proportion

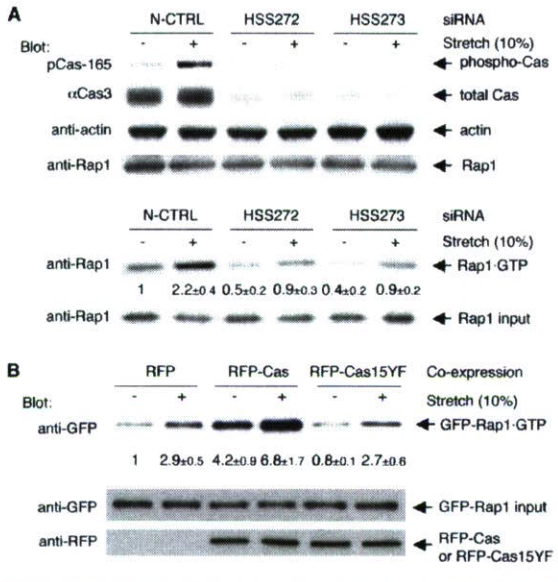

Figure 2. Significant Role of Cas Phosphorylation in Physiological Force Transduction

(A) Cas is involved in stretch-dependent Rap1 activation in intact cells. RNAi experiments were performed as described in the Experimental Procedures. siRNAs used were Stealth RNAi Negative Control Med GC (N-CTRL: lanes 1 and 2), BCAR1-HSS114272 (HSS272: lanes 3 and 4), and BCAR1-HSS114273 (HSS273: lanes 5 and 6) (Invitrogen). Twenty-four hours after transfection, HEK293 cells were either stretched or left unstretched. To determine the level of Cas expression and phosphorylation, cells were solubilized with SDS sample buffer 1 min after stretching or without stretching, and equivalent portions of each sample were subjected to SDS-PAGE followed by anti-phospho-Cas (pCas-165), anti-Cas (αCas3), anti-Rap1, and anti-actin immunoblotting (upper panel). To measure stretch-dependent Rap1 activity, cells were solubilized with lysis buffer for GST pull-down assay (see Experimental Procedures) 5 min after stretching or without stretching. Rap1 was quantified by anti-Rap1 immunoblotting. Rap1 activity (Rap1•GTP/Rap1 input) was scaled with the unstretched control set at 1 and noted below the Rap1•GTP blot with SD (n = 4) (lower panel). The data shown in Figure 2A (upper and lower panels) were obtained with siRNA transfection performed at the same time.

(B) Significant role of tyrosine phosphorylation of Cas in stretch-dependent Rap1 activation. RFP, RFP-Cas, or RFP-Cas15YF was cotransfected with GFP-Rap1 into HEK293 cells (1×10^6/dish). Twenty-four hours after transfection, cells were either stretched or left unstretched. Five minutes after stretching or without stretching, cells were solubilized and subjected to the GST pull-down assay. GFP-Rap1 was quantified by anti-GFP immunoblotting. GFP-Rap1 activity (GFP-Rap1•GTP/GFP-Rap1 input) was scaled with the unstretched RFP-transfected cells set at 1 and noted below the GFP-Rap1•GTP blot with SD (n = 4).

to the magnitude of latex membrane stretching (25%, 50%, 75%, 100%, and 150%) (Figure 4A, lanes 2–6). An unextendable mono-biotinylated CasSD (C-biotinylated CasSD, see Figure 3A, top) was poorly tyrosine phosphorylated either with or without stretching (Figure 4A, lanes 7 and 8). To test if c-Src kinase activity was modulated in the IPE experiments, we added acid-treated enolase to the kinase mixture at the time of kinase reaction and measured its phosphorylation. In the same reaction that gave an extension-dependent increase in CasSD phosphorylation, neither the level of enolase phosphorylation nor the phosphorylation levels of Y416 and Y527 of c-Src kinase were affected by stretching (data not shown). These results indicated that extension-dependent tyrosine phosphorylation of CasSD resulted from CasSD extension and not from an increase in the kinase activity of recombinant c-Src.

We also asked whether or not other kinases phosphorylated CasSD in an extension-dependent manner in IPE experiments. Neither the non-SFK tyrosine kinase Csk (C-terminal Src kinase) nor ZAP-70 phosphorylated NC-biotinylated CasSD, even after stretching (Figure 4B). However, in the same kinase reaction protocol, both Csk and ZAP-70 were able to phosphorylate their known substrates, acid-treated enolase (Bougeret et al., 1993) and the cytoplasmic fragment of human erythrocyte band 3 (cdb3) (Isakov et al., 1996), respectively (data not shown). On the other hand, a known Cas kinase, Abl (Mayer et al., 1995) and another SFK, FynT, phosphorylated CasSD in an extension-dependent manner (Figure 4B). Thus, extension-dependent phosphorylation of CasSD in vitro is caused in a kinase-specific manner, and not by a nonspecific effect of the IPE system.

Although neither the force needed for CasSD extension nor its effect on individual YxxP motifs in CasSD is known, the IPE experiments revealed that different extents of extension induced the phosphorylation of different regions. When we used two different anti-phospho-Cas antibodies (pCas-165 and pCas-410) that had different, though not strictly specific, binding preferences for YxxPs in the Cas substrate domain (Shin et al., 2004) to measure the in vitro CasSD phosphorylation, pCas-410 immunoblotting gave significantly greater fold increase than pCas-165 blots by 40% latex membrane stretching (Figure 4C, left panel). However, pCas-165 and pCas-410 blots showed a similar fold increase by 100% stretching (Figure 4C, right panel). These results suggest that the pCas-410 sites are more efficiently exposed and phosphorylated than pCas-165 sites by smaller extent of CasSD extension.

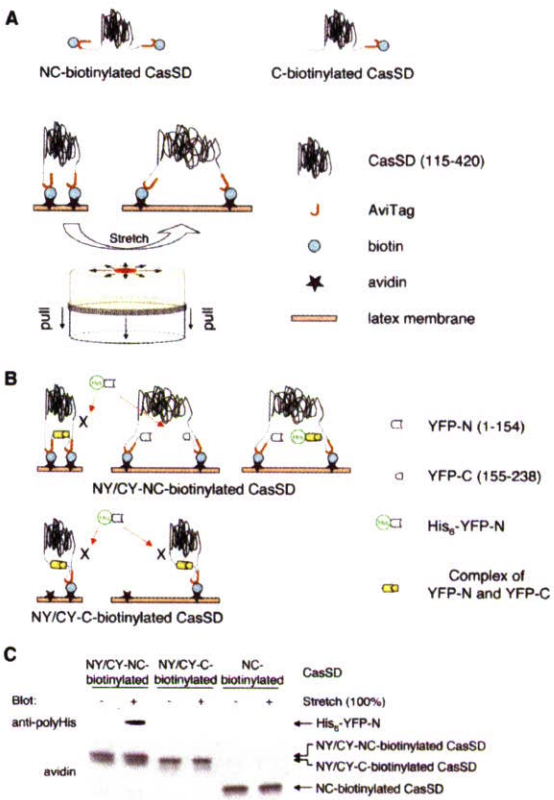

Figure 3. IPE System

(A) Scheme of NC-biotinylated CasSD, C-biotinylated CasSD, and the process of mechanical extension of CasSD in the IPE system.

(B) Schematic description of YFP amino-terminal swapping.

(C) His_6-YFP-N binds to extended NY/CY-NC-biotinylated CasSD, but not to NY/CY-C-biotinylated CasSD or NC-biotinylated CasSD. Biotinylated CasSD proteins, either extended or unextended on latex membrane, were incubated with His_6-YFP-N in the buffer containing 1% Triton X-100 and 1% BSA. After washing, bound complex was solubilized and subjected to SDS-PAGE followed by anti-polyHistidine immunoblotting or avidin affinity blotting.

αCas1, an Antibody that Recognizes Extended CasSD

In order to test if Cas was extended in regions of cell traction forces, we utilized an antibody, αCas1, which was raised against a peptide sequence in the Cas substrate domain (Sakai et al., 1994) (Figure S1A). We found that αCas1 recognized the extended NC-biotinylated CasSD and not the unextended control, C-biotinylated CasSD in the IPE system (Figure 5A). Further, αCas1 bound to SDS-denatured CasSD regardless of its phosphorylation state (Figure S1B), as well as full-length Cas in the SDS-denatured cell lysates (Figure S1C). Thus, αCas1 binding appeared to require the exposure of its epitope in the Cas substrate domain by either extension or denaturation.

Extension of Cas in Triton Cytoskeletons

Using αCas1, we examined whether Cas was extended by stretching Triton cytoskeletons where tyrosine phosphorylation of Cas was observed (Tamada et al., 2004). When we stretched Triton cytoskeletons from Cas-deficient fibroblasts expressing RFP-Cas, we observed a significant increase in αCas1 binding (Figure 5B, lower panel, lanes 1 and 2). Triton cytoskeletons from Cas-deficient fibroblasts expressing RFP alone did not bind αCas1 (Figure 5B, lower panel, lanes 3 and 4). Further, another anti-Cas antibody, αCas3, the epitope of which did not involve the substrate domain (Figure S1A) (Sakai et al., 1994), did not change its binding to Cas in Triton cytoskeletons upon stretching (Figure 5B, lower panel, lanes 5 and 6). These results indicate that the extension of the Cas substrate domain is enhanced by cytoskeleton stretching.

Cas Is Extended at the Sites of High Traction Forces Where Cas Is Phosphorylated In Vivo

Cas extension was difficult to observe in intact cells, since the cell stretching system could not fit onto a total internal

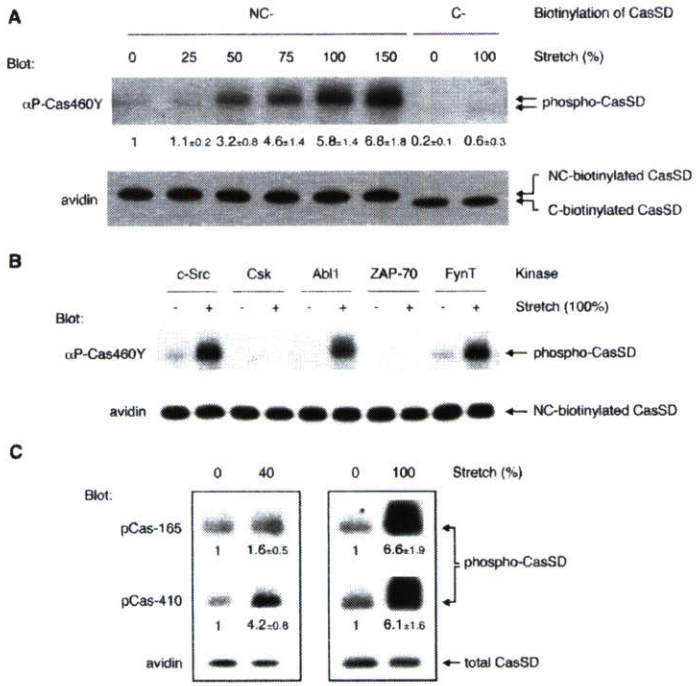

Figure 4. Extension-Dependent Phosphorylation of CasSD by Tyrosine Kinases In Vitro

(A) CasSD is tyrosine phosphorylated by recombinant c-Src in an extension-dependent manner. NC-biotinylated or C-biotinylated CasSD was either extended or left unextended on latex membrane, incubated with recombinant c-Src for 2 min, washed, solubilized, and analyzed for tyrosine phosphorylation by anti-phospho-Cas (αP-Cas460Y) immunoblotting and avidin affinity blotting. The magnitude of the latex membrane stretching is described as the percent change of length in each dimension. Quantification of phosphorylation of CasSD was scaled with unextended NC-biotinylated CasSD set at 1 and noted below the anti-phospho-Cas blot with SD (n = 4).

(B) Kinase specificity of extension-dependent tyrosine phosphorylation of CasSD. NC-biotinylated CasSD was either extended (100%) or left unextended and then incubated with recombinant c-Src, Csk, Abl1, ZAP-70, or FynT for 2 min at room temperature. Tyrosine phosphorylation of CasSD was analyzed as in (A).

(C) Extension-dependent phosphorylation of CasSD by c-Src measured by two different anti-phospho-Cas antibodies. Samples were prepared as in (A) except for the extent of the latex membrane stretching (40% in the left panel and 100% in the right panel). Equivalent portions of each sample were subjected to SDS-PAGE followed by pCas-165 and pCas-410 immunoblotting and avidin affinity blotting. Quantification of phosphorylation of CasSD was scaled with unextended NC-biotinylated CasSD set at 1 and noted below the anti-phospho-Cas blots with SD (n = 4).

reflection fluorescence (TIRF) or confocal microscope. Further, the stretchable substrate (silicone) had high background fluorescence. Therefore, we looked at αCas1 immunostaining of intact cells during the late phase of spreading on collagen-coated glass coverslips (20 min after plating), when the fast movement of actin cytoskeletons at the periphery is observed (Dubin-Thaler et al., 2004) and the forces required for continuous spreading are generated (Giannone et al., 2004). In RFP-Cas-expressing Cas-deficient fibroblasts, we found that αCas1 staining primarily colocalized with RFP-Cas in the peripheral regions (Figure 5C, top). An anti-phospho-Cas antibody (pCas-165) also exhibited a peripheral staining in the late spreading cells (Figure 5C, bottom), confirming that Cas extension correlated with phosphorylation. These staining patterns did not appear to be artifacts of antibody staining, since αCas3 staining always colocalized with RFP-Cas (Figure 5C, middle). Considering the specificity of αCas1 and αCas3 in immunoblotting (Figure S1C), both αCas1 and αCas3 staining most likely represent the distribution of their Cas epitopes, and not the crossreaction with other cellular protein(s). Indeed, we observed

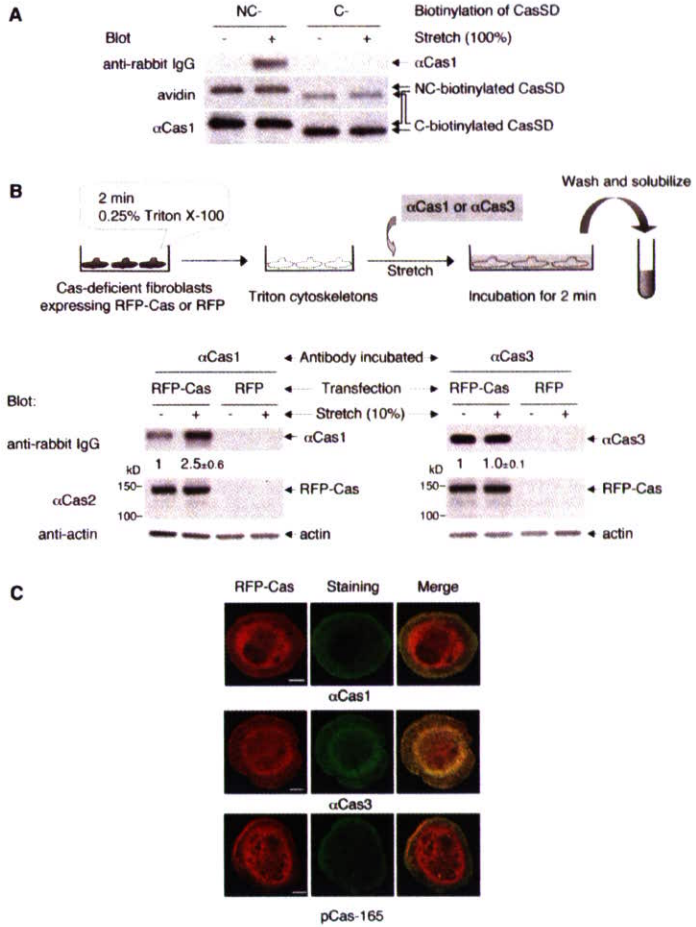

Figure 5. Extension of Cas In Situ and In Vivo

(A) αCas1 recognizes extended CasSD in vitro. NC-biotinylated or C-biotinylated CasSD was either extended (100%) or left unextended in the IPE system. After blocking, CasSD proteins were incubated with αCas1, washed, and solubilized with SDS sample buffer containing 0.12 M DTT. Equivalent portions of each sample were analyzed for quantification of bound αCas1 by anti-rabbit IgG immunoblotting. The amount of NC-biotinylated and C-biotinylated CasSD in each sample was quantified by avidin affinity blotting and αCas1 immunoblotting. Note that the difference in the relative signal intensity between avidin and αCas1 blots is consistent with the molar ratio of biotinylation (NC-biotinylated CasSD:C-biotinylated CasSD = 2:1).

(B) Stretch dependence of αCas1 and αCas3 binding to Cas in Triton cytoskeletons. Triton cytoskeletons were prepared from Cas-deficient fibroblasts transfected with RFP-Cas or RFP alone, either stretched or left unstretched, and incubated with either αCas1 or αCas3 as shown in the diagram. Quantification of bound antibody by anti-rabbit IgG immunoblotting was scaled with unstretched control set at 1 and noted with SD (n = 4).

(C) αCas1 preferentially binds to Cas, where higher traction forces are expected in vivo. Cas-deficient fibroblasts expressing RFP-Cas were plated, fixed after 20 min, and then stained with αCas1, αCas3, or pCas-165. Confocal images are shown for RFP-Cas (left, red channel) and immunostaining (center, green channel) and are merged on the right. Scale bars, 10 μm.

only faint background staining in untransfected Cas-deficient fibroblasts with either αCas1 or αCas3 (data not shown).

These in situ (cytoskeleton stretching) (Figure 5B) and in vivo (intact cell spreading) (Figure 5C) results, together with the observed preference of αCas1 binding for extended CasSD in vitro (Figure 5A), suggest that the in vitro extension of CasSD causes the conformational change of CasSD that is relevant to the force-dependent conformational change of Cas protein in vivo. Therefore, the extension-dependent phosphorylation of CasSD in vitro (Figure 4) appears to be relevant to the force-dependent phosphorylation of Cas in vivo (Figures 1, 2, and 5C).

DISCUSSION

Tyrosine Phosphorylation of Cas Is Involved in Physiological Force Transduction

Cas appears to act as a force transducer in vivo, since the knockdown of Cas expression by siRNA significantly attenuated stretch-dependent Rap1 activity (Figure 2A) and overexpression of wild-type Cas, but not coexpression of the phosphorylation-defective Cas mutant (Cas15YF) enhanced stretch-dependent Rap1 activity (Figure 2B). Phosphorylation by SFK is critical since stretch-dependent Cas phosphorylation was inhibited by the SFK inhibitor CGP77675 (Figure 1A) and attenuated in SYF cells (Figures 1B and 1C). These findings conform to our previous observation of stretch-dependent Cas phosphorylation by SFK in cytoskeletal complexes (Triton cytoskeletons) (Tamada et al., 2004) and indicate that tyrosine phosphorylation of Cas upon cell stretching constitutes a significant pathway for stretch-dependent Rap1 activation in intact cells (Sawada et al., 2001).

Possible Mechanisms for Stretch-Increased Cas Phosphorylation

Although Src was shown to be mechanically activated using genetically engineered reporters (Wang et al., 2005), it is not clear how endogenous c-Src is activated or if it is indirectly activated by force. We observed that Src-dependent phosphorylation of Cas was significantly increased by stretching in c-Src-expressing SYF cells without causing Src kinase activation (Figures 1B and 1C). These findings suggest that activation of the kinase is not primarily responsible for stretch-dependent increase of Cas phosphorylation in vivo. Since the SFK inhibitor greatly attenuated the stretch-dependent increase of Cas phosphorylation (Figure 1A), stretch-dependent alteration of phosphatase activity is also unlikely to be the cause. Further, the tyrosine phosphatase inhibitor sodium orthovanadate did not inhibit stretch-dependent tyrosine phosphorylation of Cas in Triton cytoskeletons (Tamada et al., 2004).

It is unlikely that stretching causes the spatial interaction between the kinase and the substrate, considering the constraints that such a mechanism places on the geometry of the cytoskeleton (Tamada et al., 2004). Since a mechanical modification of the substrate (Cas) was sufficient to increase Cas phosphorylation in vitro, we have focused on the analysis of that possibility.

Extension of Cas by Cellular Force

Both the amino-terminal SH3 and carboxy-terminal Src-binding domains are required for Cas localization at focal adhesions (Nakamoto et al., 1997), where cellular force is expected to be concentrated, and force-dependent signaling involving tyrosine phosphorylation occurs (Geiger and Bershadsky, 2002; Tamada et al., 2004). Since different proteins are known to associate with SH3 and Src-binding domains of Cas (Defilippi et al., 2006), an individual Cas molecule would be anchored to the cytoskeleton-adhesion complex via two distinct sites. In addition, the SH3 domain of Cas binds to FAK (focal adhesion kinase) (Harte et al., 1996). FAK has a FERM (erythrocyte band 4.1-*ezrin*-*r*adixin-*m*oesin) domain commonly found in actin-binding proteins (Lee et al., 2004), associates with an actin-binding protein, talin (Chen et al., 1995), and is involved in the dynamic variation in tyrosine phosphorylation within focal adhesions (Ballestrem et al., 2006). Thus, we speculate that the amino-terminal anchor of Cas to the focal adhesion complex is more closely linked to the actin cytoskeleton than the carboxy-terminal anchor and that Cas is subjected to traction forces generated by the actin cytoskeleton (Figure 6).

Although the structures of the SH3 and the serine-rich domains of Cas were reported (Briknarova et al., 2005; Wisniewska et al., 2005), no structural analysis of the substrate domain has been reported, and the structure prediction algorithms (available at the Network Protein Sequence Analysis site) do not give a clear prediction for the structure of Cas substrate domain. We speculate that the intramolecular interactions within the substrate domain constrain its conformation in the absence of traction force and that traction force is required to expose YxxP sites to kinases.

Because our model centers on extension of Cas, the magnitude of force needed for extension is a concern. The force per integrin molecule in the adhesion site was estimated to be on the order of 1 pN (Balaban et al., 2001; Jiang et al., 2003), an order of magnitude below the force needed to reversibly unfold single domains of proteins such as spectrin by AFM (atomic force microscope) (Fisher et al., 1999). However, it has been shown that the protein unfolding force depends exponentially on the loading rate (Carrion-Vazquez et al., 1999), and at a low loading rate, proteins can be unfolded by forces even orders of magnitude below the forces required for unfolding at a high loading rate (Merkel et al., 1999). Further, extension of Cas may not require the force needed to cause "unfolding," i.e., linearization of a mechanically stable distinct structure. Thus, extension of Cas probably can occur by physiological forces at focal contact sites (order of a few pN). Further details of force-dependent extension and phosphorylation of the Cas substrate domain in vitro as well as in vivo are under study.

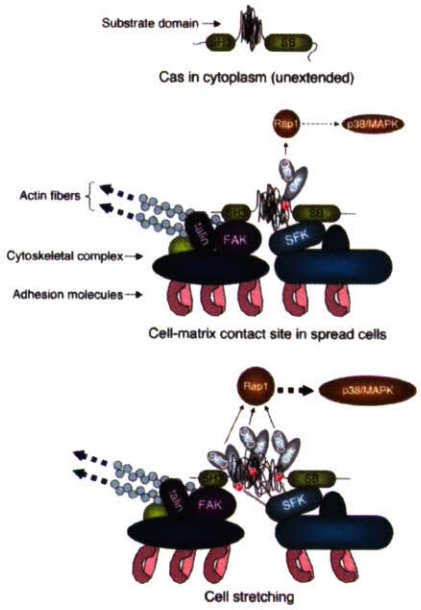

Figure 6. Model of Extension of Cas and Signaling at Cell-Matrix Contact Sites

The top and middle panels represent a Cas molecule with unextended configuration of substrate domain in the cytoplasm and a Cas molecule with moderate extension of substrate domain at the cell-matrix contact site of spread cells, respectively. The bottom panel represents the extension-dependent phosphorylation of the Cas substrate domain by SFK and enhancement of its downstream signaling. SH3 and SB represent the SH3- and the Src-binding domains of Cas, respectively.

Physiological Role of Extension and Phosphorylation of Cas in Force Transduction

Several different experimental approaches indicate that Cas extension plays a role in the direct sensing of traction forces in vivo. In vitro, extension of NC-biotinylated CasSD remarkably enhanced its phosphorylation by exogenous c-Src, FynT, or Abl1 (Figure 4). Extension of CaSD was confirmed by measuring the separation of two halves of YFP linked to the ends of the CasSD (Figure 3B). Stretch-dependent phosphorylation of Cas in cytoskeletons and in intact cells further supports the idea that it is involved in physiological force sensing. Antibody binding to epitopes exposed by extension in regions of higher traction forces shows that Cas is extended in vivo. Although many force-dependent effects are observed within cells, extension of Cas appears to be a primary force-sensing process and not part of a secondary force-response pathway, since extension-dependent phosphorylation of CasSD by active kinases was observed in vitro, where any extraneous biochemical interactions or signaling pathways were completely eliminated. While extracellular matrix proteins also respond to force by unfolding (Oberhauser et al., 2002) and exhibit different functional effects (Zhong et al., 1998), we show here that a cytoplasmic protein, Cas, has a gain of function upon cell stretching in terms of increase in phosphorylation and activation of Crk/C3G-Rap1 signaling.

A much greater percentage extension is required to observe the increase of in vitro phosphorylation of CasSD (Figure 4A, lanes 2–6) than the percentage of cell stretching to observe an increase of in vivo Cas phosphorylation (Figures 1 and 2). In vivo, cytoskeletal filaments will not stretch significantly, and cytoskeletal networks are believed to be strain hardened by cell-generated traction forces; therefore, molecular complexes at "stress-bearing" sites will be greatly extended upon even mild cell stretching. Moreover, cell traction forces will pre-extend the cytoskeleton-bound Cas molecules in spread cells even without stretching (Figure 6, middle). Thus, 10% stretching of intact cells can cause more than 10% extension of "unextended" Cas (Figure 6, top), since traction forces are concentrated at cell-matrix contact sites (Geiger and Bershadsky, 2002). In addition, αCas1 immunostaining shows that Cas is extended in the high-traction force regions of cells where Cas is phosphorylated (Figure 5C).

In other studies, shear stress increases Cas phosphorylation by SFK in vascular endothelial cells (Okuda et al., 1999). Since shear stress is known to modulate the cell contractility (Chien et al., 2005) in which Cas has been shown to play a role (Tang and Tan, 2003), extension of Cas caused by the increased cell contractility might result in shear stress-dependent phosphorylation. Thus, local extension of Cas is likely to be involved in the local response to various types of "mechanical stress" and can possibly account for the versatile function of Cas (Defilippi et al., 2006).

Substrate Priming as a General Mechanism of Cell Signaling

Enhancement of a substrate's susceptibility to phosphorylation by mechanical extension is designated as extension-dependent "substrate priming." The transduction of cell forces into a biochemical signal by mechanical substrate priming could be highly flexible and dynamic. The extent of substrate extension in vivo will depend upon the extent of strain produced locally in the cell, resulting in a graded extent of substrate phosphorylation and, consequently, gradations in the magnitude of downstream signaling events. Substrate priming by mechanical force might be generally involved in kinase signaling, particularly in light of our observation that a number of other cytoskeletal proteins are tyrosine phosphorylated in a stretch-dependent manner (Tamada et al., 2004) and since substrate conformation is a critical determinant in phosphorylation of other SFK substrates (Cooper et al., 1984). Thus, we suggest that substrate priming by localized protein

extension provides a simple mechanism for sensing the level of force on a cell as well as the location at which force is applied.

EXPERIMENTAL PROCEDURES

Antibodies

Polyclonal antibodies against Cas protein (αCas1, αCas2, and αCas3) were described previously (Sakai et al., 1994). The polyclonal anti-phospho-Cas antibodies pCas-165 and pCas-410, a polyclonal anti-phospho-SrcY416 antibody, and a polyclonal anti-phospho-SrcY527 antibody were purchased from Cell Signaling. The polyclonal anti-phospho-Cas antibody αP-Cas460Y (Miyake et al., 2005) was used for in vitro experiments with CasSD. Monoclonal anti-GFP (JL-8) and anti-RFP (anti-DsRed) antibodies were purchased from Clontech and BD Pharmingen, respectively. Monoclonal anti-Src (GD11) and anti-polyHistidine antibodies were purchased from Upstate Biotechnology and Sigma, respectively. Polyclonal anti-actin and anti-Rap1 antibodies were purchased from Santa Cruz Biotech.

Cells and DNA Plasmid Transfection

Human embryonic kidney (HEK) 293 cells, Cas-deficient fibroblasts (Huang et al., 2002), and SYF cells that lack c-Src, c-Yes, and Fyn were cultured in DMEM supplemented with 10% fetal bovine serum (FBS) and penicillin/streptomycin (100 IU/ml and 100 μg/ml) at 37°C and 5% CO_2. DNA plasmid transfection was performed with Fugene 6 (Roche) according to the manufacturer's protocol. To isolate stably transfected cell lines, pPUR that carried a puromycin-resistant gene (Clontech) was cotransfected, and clones were selected using puromycin (Clontech).

Immunoprecipitation and In Vitro Kinase Assay of Src

To measure the Src kinase activity in SYF cells and stable transfectant cells derived from SYF cells, Src was immunoprecipitated, and an in vitro kinase assay was performed using acid-treated enolase as a substrate. Phosphorylation of enolase was analyzed by anti-phospho-tyrosine immunoblotting. Details of the in vitro kinase assay of immunoprecipitated Src are described in the Supplemental Data section.

RNA Interference Experiments

To decrease the endogenous expression of Cas protein, two different siRNAs, BCAR1-HSS114272 and BCAR1-HSS114273 (Stealth RNAi, Invitrogen), were transfected into HEK293 cells (1×10^5/dish) using Lipofectamine RNAiMAX according to the manufacturer's protocol (180 pmol RNA interference [RNAi] and 9 μl Lipofectamine RNAiMAX/dish) (Invitrogen). Six hours after transfection, culture medium was replaced with fresh DMEM containing 10% FBS. Twenty-four hours after transfection, cells were either stretched or left unstretched and subjected to biochemical analyses.

Quantification of Rap1 Activity

A GST pull-down assay was performed to measure the Rap1 activity using GST-RalGDS-RBD that preferentially bound to Rap1·GTP (Sakakibara et al., 2002). To measure the Rap1 input, equivalent portions of each lysate were directly subjected to SDS-PAGE followed by immunoblotting.

Kinases and Substrates

Recombinant c-Src, FynT, Abl1, Csk, and ZAP-70 were purchased from Invitrogen. Specific kinase activities of c-Src, FynT, Csk, and ZAP-70 were determined by an in vitro kinase assay using poly-Glu/Tyr (4:1) as a substrate (Invitrogen). Abl1 kinase activity was determined by an in vitro kinase assay using Abl1 substrate (Invitrogen). Enolase (rabbit muscle) was purchased from Sigma. Bacterially expressed cdb3 was used as a substrate to measure the ZAP-70 activity.

Preparation of Biotinylated Proteins

Various forms of biotinylated CasSD were prepared using Biotin AviTag technology (Avidity). The Biotin AviTag sequence consists of 15 residues (GLNDIFEAQKIEWHE) and is specifically and efficiently biotinylated by the protein biotin ligase BirA. Biotinylated AviTag-fused proteins were obtained by coexpression with BirA in bacteria (BL21 Star, Invitrogen) cultured in NZCYM medium containing d-biotin (50 μM; Research Organics) at the time of IPTG induction. The molar ratio of biotin to AviTag-fused protein was confirmed to be 2:1 in NC-biotinylated CasSD and NY/CY-NC-biotinylated CasSD, and 1:1 in C-biotinylated CasSD and NY/CY-C-biotinylated CasSD. Details of biotinylated protein preparation are given in the Supplemental Data section.

For chimeric proteins of biotinylated CasSD and YFP components (NY/CY-NC-biotinylated CasSD and NY/CY-C-biotinylated CasSD), yellow fluorescence was observed and estimated in bacteria and in solution by quantitative fluorescence microscopy. Solutions containing NY/CY-NC-biotinylated CasSD or NY/CY-C-biotinylated CasSD were as fluorescent as solutions containing bacterially expressed full-length YFP at the same concentration (0.8 μM).

Plasmids

Plasmids used in this work are described in the Supplemental Data section.

Stretching of Intact Cells

Cells plated on collagen (type I; Sigma-Aldrich)-coated stretchable silicone dishes (Sawada et al., 2001) were either stretched biaxially (and kept stretched) or left unstretched in our cell stretching system (Sawada et al., 2001; Tamada et al., 2004).

Covalent Avidin Coating of Latex Membrane and Preparation of Biotinylated Proteins Specifically Bound to Avidin-Coated Latex Membrane

Avidin (Neutravidin) was covalently immobilized onto the surface of latex membrane by introducing the amine-reactive groups using Friedal-Crafts chemistry, and biotinylated proteins were bound to the immobilized avidin. Details of preparation of biotinylated protein bound to latex membrane are described in the Supplemental Data section.

IPE System

A biotinylated protein-bound latex membrane set in an adjustable tension ring was placed on a lubricated round-shaped glass stage and stretched biaxially and uniformly by pulling down the tension ring (Figure 3A, bottom). Magnitude of the latex membrane stretching was described as percent change of length in each dimension. For example, 100% stretching represented 2-fold expansion in each dimension. To recover the protein for analysis, the protein-bound membrane (Figure 3A, bottom) was incubated with 1× SDS sample buffer containing 0.12 M DTT at 95°C for 5 min. Using amine-reactive, photocleavable biotin analog (NHS-PC-LC-Biotin, PIERCE) (Sawada and Sheetz, 2002), we confirmed that this procedure recovered the majority (>95%) of biotinylated proteins bound to the immobilized avidin.

YFP Amino-Terminal Swapping Assay

NY/CY-NC-biotinylated, NY/CY-C-biotinylated (Figure 3B), or NC-biotinylated CasSD (Figure 3A) bound to avidin-coated latex membrane was prepared as described above. After stretching of latex membrane (100%) or without stretching, biotinylated CasSD proteins were washed two times with 1% BSA and 1% Triton X-100 in PBS and incubated with 2 μM His_6-YFP-N in 1% BSA and 1% Triton X-100 in PBS containing 1 mM DTT for 10 min at room temperature. The bound protein complex on the latex membrane was washed four times with 1% BSA and 1% Triton X-100 in PBS and two times with 1% Triton X-100 in PBS, recovered with 1× SDS sample buffer containing 0.12 M DTT. The samples were subjected to SDS-PAGE followed by anti-polyHistidine immunoblotting and avidin affinity blotting.

In Vitro Extension and Phosphorylation of CasSD

NC-biotinylated or C-biotinylated CasSD bound to avidin-coated latex membrane was prepared as described above. After stretching of latex membrane or without stretching, biotinylated CasSD proteins were washed three times with 0.25% Triton X-100 and 2% BSA in buffer A (20 mM HEPES [pH 7.5], 150 mM NaCl, 4 mM $MgCl_2$, 1 mM DTT, 1 mM PMSF, 20 μg/ml aprotinin, 0.5 mM EGTA) and three times with 0.1% BSA in buffer A and incubated with recombinant kinases (specific activity of each kinase used: 700 pmol/min phosphate transfer) in 350 μl of kinase reaction buffer (20 mM HEPES [pH 7.5], 0.9 mM ATP, 0.1% BSA, 140 mM NaCl, 10 mM $MgCl_2$, 3 mM $MnCl_2$, 0.5 mM EGTA, 20 μg/ml aprotinin, 1.5 mM DTT, 1.5 mM Na_3VO_4, 0.03% Brij-35) for 2 min at room temperature. After kinase reaction, biotinylated CasSD proteins were washed three times with ice-cold 1% Triton X-100 in PBS containing 1 mM Na_3VO_4, recovered, and solubilized by incubation with 1× SDS sample buffer containing 0.12 M DTT at 95°C for 5 min. Tyrosine phosphorylation of CasSD was determined by anti-phospho-Cas immunoblotting and avidin affinity blotting.

In Vitro Binding of αCas1 to Extended CasSD

NC-biotinylated or C-biotinylated CasSD bound to avidin-coated latex membrane was either extended (100%) or left unextended in PBS containing 1% Triton X-100, 2% BSA, 5% FBS, 1 mM DTT, 20 μg/ml aprotinin, and 0.5 mM EGTA. After 10 min, CasSD proteins on the latex surface were washed three times and incubated for 30 min with PBS containing 2% BSA, 5% FBS, 1 mM DTT, 20 μg/ml aprotinin, and 0.5 mM EGTA to block nonspecific binding and then incubated for 2 min with αCas1 diluted at 1:1200 in the same buffer. After six washes with PBS containing 0.1% Tween-20 and 1 mM DTT, bound proteins were solubilized with 1× SDS sample buffer containing 0.12 M DTT and subjected to SDS-PAGE followed by anti-rabbit IgG or αCas1 immunoblotting and avidin affinity blotting.

Binding of Two Different Anti-Cas Antibodies, αCas1 and αCas3, to Triton Cytoskeletons

Triton cytoskeletons were prepared from Cas-deficient fibroblasts transiently expressing RFP-Cas or RFP alone as described previously (Sawada and Sheetz, 2002). After two washes with buffer A containing 2% BSA and 5% FBS, the buffer was replaced with the buffer A containing 0.5 mM ATP, 2% BSA, 5% FBS, and either αCas1 or αCas3 (1:400 dilution), and Triton cytoskeletons were either stretched or left unstretched. After 2 min of incubation, samples were washed two times with buffer A containing 2% BSA and 5% FBS and four times with buffer A, solubilized with 1× SDS sample buffer containing 20 mM DTT, and subjected to SDS-PAGE followed by anti-rabbit IgG, αCas2, and anti-actin immunoblotting (Figure 5B, upper panel).

Immunofluorescence Staining, Fluorescence Microscopy, and Image Display

Twenty minutes after being plated on collagen (Type-I)-coated coverslips, Cas-deficient fibroblasts expressing RFP-Cas were washed with PBS; fixed with 3.7% formaldehyde in PBS; permeabilized with 0.1% Triton X-100 in PBS; stained using αCas1, αCas3, or pCas-165 as a primary antibody (1:400 dilution for αCas1 and αCas3 and 1:100 dilution for pCas-165) and Alexa Fluor 488 anti-rabbit IgG as a secondary antibody; and then viewed with a confocal microscope (Olympus IX-81 with FV500 system). Image intensity from the green channel (immunofluorescence with αCas1, αCas3, or pCas-165) and the red channel (RFP-Cas) was displayed with the contrast enhanced by setting the highest intensity in each image at the maximum value of the dynamic range and the background (cell-free area) at zero in ImageJ, a free open source Java imaging platform (http://rsb.info.nih.gov/ij/).

Statistical Analysis

Statistical analysis was performed with the paired Student's t test, and $p < 0.05$ was defined as significant.

Supplemental Data

The Supplemental Data include Supplemental Experimental Procedures and one supplemental figure and can be found with this article online at http://www.cell.com/cgi/content/full/127/5/1015/DC1/.

ACKNOWLEDGMENTS

We thank S. Ohkubo, T. Mandai, M. Cull, M. Galbmillion, and M.L. Bushey for assisting in the construction of the IPE system; P.S. Low, S.K. Hanks, T. Yamamoto, and M. Matsuda for the plasmids; J.M. Fernandez, M. Edidin, T.D. Perez, A. Sakakibara, C.D. Hu, H. Takayanagi, T. Miyazaki, T. Tezuka, M. Saitoh, K. Takeda, H. Ichijo, and K. Nakamura for helpful discussions and consistent support. This work was supported by NIH grant R01 EB001480.

Received: June 9, 2006
Revised: August 20, 2006
Accepted: September 25, 2006
Published: November 30, 2006

REFERENCES

Balaban, N.Q., Schwarz, U.S., Riveline, D., Goichberg, P., Tzur, G., Sabanay, I., Mahalu, D., Safran, S., Bershadsky, A., Addadi, L., and Geiger, B. (2001). Force and focal adhesion assembly: A close relationship studied using elastic micropatterned substrates. Nat. Cell Biol. *3*, 466–472.

Ballestrem, C., Erez, N., Kirchner, J., Kam, Z., Bershadsky, A., and Geiger, B. (2006). Molecular mapping of tyrosine-phosphorylated proteins in focal adhesions using fluorescence resonance energy transfer. J. Cell Sci. *119*, 866–875.

Bougeret, C., Rothhut, B., Jullien, P., Fischer, S., and Benarous, R. (1993). Recombinant Csk expressed in Escherichia coli is autophosphorylated on tyrosine residue(s). Oncogene *8*, 1241–1247.

Briknarova, K., Nasertorabi, F., Havert, M.L., Eggleston, E., Hoyt, D.W., Li, C., Olson, A.J., Vuori, K., and Ely, K.R. (2005). The serine-rich domain from Crk-associated substrate (p130Cas) is a four-helix bundle. J. Biol. Chem. *280*, 21908–21914.

Carrion-Vazquez, M., Oberhauser, A.F., Fowler, S.B., Marszalek, P.E., Broedel, S.E., Clarke, J., and Fernandez, J.M. (1999). Mechanical and chemical unfolding of a single protein: A comparison. Proc. Natl. Acad. Sci. USA *96*, 3694–3699.

Chen, H.C., Appeddu, P.A., Parsons, J.T., Hildebrand, J.D., Schaller, M.D., and Guan, J.L. (1995). Interaction of focal adhesion kinase with cytoskeletal protein talin. J. Biol. Chem. *270*, 16995–16999.

Chien, S., Li, S., Shiu, Y.T., and Li, Y.S. (2005). Molecular basis of mechanical modulation of endothelial cell migration. Front. Biosci. *10*, 1985–2000.

Cooper, J.A., Esch, F.S., Taylor, S.S., and Hunter, T. (1984). Phosphorylation sites in enolase and lactate dehydrogenase utilized by tyrosine protein kinases in vivo and in vitro. J. Biol. Chem. *259*, 7835–7841.

Defilippi, P., Di Stefano, P., and Cabodi, S. (2006). p130Cas: A versatile scaffold in signaling networks. Trends Cell Biol. *16*, 257–263.

Dubin-Thaler, B.J., Giannone, G., Dobereiner, H.G., and Sheetz, M.P. (2004). Nanometer analysis of cell spreading on matrix-coated surfaces reveals two distinct cell states and STEPs. Biophys. J. *86*, 1794–1806.

Fisher, T.E., Oberhauser, A.F., Carrion-Vazquez, M., Marszalek, P.E., and Fernandez, J.M. (1999). The study of protein mechanics with the atomic force microscope. Trends Biochem. Sci. *24*, 379–384.

Fonseca, P.M., Shin, N.Y., Brabek, J., Ryzhova, L., Wu, J., and Hanks, S.K. (2004). Regulation and localization of CAS substrate domain tyrosine phosphorylation. Cell. Signal. *16*, 621–629.

Geiger, B., and Bershadsky, A. (2002). Exploring the neighborhood: Adhesion-coupled cell mechanosensors. Cell *110*, 139–142.

Giannone, G., and Sheetz, M.P. (2006). Substrate rigidity and force define form through tyrosine phosphatase and kinase pathways. Trends Cell Biol. *16*, 213–223.

Giannone, G., Dubin-Thaler, B.J., Dobereiner, H.G., Kieffer, N., Bresnick, A.R., and Sheetz, M.P. (2004). Periodic lamellipodial contractions correlate with rearward actin waves. Cell *116*, 431–443.

Harte, M.T., Hildebrand, J.D., Burnham, M.R., Bouton, A.H., and Parsons, J.T. (1996). p130Cas, a substrate associated with v-Src and v-Crk, localizes to focal adhesions and binds to focal adhesion kinase. J. Biol. Chem. *271*, 13649–13655.

Hattori, M., and Minato, N. (2003). Rap1 GTPase: Functions, regulation, and malignancy. J. Biochem. (Tokyo) *134*, 479–484.

Hu, C.D., Chinenov, Y., and Kerppola, T.K. (2002). Visualization of interactions among bZIP and Rel family proteins in living cells using bimolecular fluorescence complementation. Mol. Cell *9*, 789–798.

Huang, J., Hamasaki, H., Nakamoto, T., Honda, H., Hirai, H., Saito, M., Takato, T., and Sakai, R. (2002). Differential regulation of cell migration, actin stress fiber organization, and cell transformation by functional domains of Crk-associated substrate. J. Biol. Chem. *277*, 27265–27272.

Isakov, N., Wange, R.L., Watts, J.D., Aebersold, R., and Samelson, L.E. (1996). Purification and characterization of human ZAP-70 protein-tyrosine kinase from a baculovirus expression system. J. Biol. Chem. *271*, 15753–15761.

Jiang, G., Giannone, G., Critchley, D.R., Fukumoto, E., and Sheetz, M.P. (2003). Two-piconewton slip bond between fibronectin and the cytoskeleton depends on talin. Nature *424*, 334–337.

Katsumi, A., Milanini, J., Kiosses, W.B., del Pozo, M.A., Kaunas, R., Chien, S., Hahn, K.M., and Schwartz, M.A. (2002). Effects of cell tension on the small GTPase Rac. J. Cell Biol. *158*, 153–164.

Klinghoffer, R.A., Sachsenmaier, C., Cooper, J.A., and Soriano, P. (1999). Src family kinases are required for integrin but not PDGFR signal transduction. EMBO J. *18*, 2459–2471.

Lee, H.S., Bellin, R.M., Walker, D.L., Patel, B., Powers, P., Liu, H., Garcia-Alvarez, B., de Pereda, J.M., Liddington, R.C., Volkmann, N., et al. (2004). Characterization of an actin-binding site within the talin FERM domain. J. Mol. Biol. *343*, 771–784.

Mayer, B.J., Hirai, H., and Sakai, R. (1995). Evidence that SH2 domains promote processive phosphorylation by protein-tyrosine kinases. Curr. Biol. *5*, 296–305.

Merkel, R., Nassoy, P., Leung, A., Ritchie, K., and Evans, E. (1999). Energy landscapes of receptor-ligand bonds explored with dynamic force spectroscopy. Nature *397*, 50–53.

Missbach, M., Jeschke, M., Feyen, J., Muller, K., Glatt, M., Green, J., and Susa, M. (1999). A novel inhibitor of the tyrosine kinase Src suppresses phosphorylation of its major cellular substrates and reduces bone resorption in vitro and in rodent models in vivo. Bone *24*, 437–449.

Miyake, I., Hakomori, Y., Misu, Y., Nakadate, H., Matsuura, N., Sakamoto, M., and Sakai, R. (2005). Domain-specific function of ShcC docking protein in neuroblastoma cells. Oncogene *24*, 3206–3215.

Nakamoto, T., Sakai, R., Honda, H., Ogawa, S., Ueno, H., Suzuki, T., Aizawa, S., Yazaki, Y., and Hirai, H. (1997). Requirements for localization of p130cas to focal adhesions. Mol. Cell. Biol. *17*, 3884–3897.

Oberhauser, A.F., Badilla-Fernandez, C., Carrion-Vazquez, M., and Fernandez, J.M. (2002). The mechanical hierarchies of fibronectin observed with single-molecule AFM. J. Mol. Biol. *319*, 433–447.

Okuda, M., Takahashi, M., Suero, J., Murry, C.E., Traub, O., Kawakatsu, H., and Berk, B.C. (1999). Shear stress stimulation of p130(cas) tyrosine phosphorylation requires calcium-dependent c-Src activation. J. Biol. Chem. *274*, 26803–26809.

Rief, M., Gautel, M., Oesterhelt, F., Fernandez, J.M., and Gaub, H.E. (1997). Reversible unfolding of individual titin immunoglobulin domains by AFM. Science *276*, 1109–1112.

Sakai, R., Iwamatsu, A., Hirano, N., Ogawa, S., Tanaka, T., Mano, H., Yazaki, Y., and Hirai, H. (1994). A novel signaling molecule, p130, forms stable complexes in vivo with v-Crk and v-Src in a tyrosine phosphorylation-dependent manner. EMBO J. *13*, 3748–3756.

Sakakibara, A., Ohba, Y., Kurokawa, K., Matsuda, M., and Hattori, S. (2002). Novel function of Chat in controlling cell adhesion via Cas-Crk-C3G-pathway-mediated Rap1 activation. J. Cell Sci. *115*, 4915–4924.

Sawada, Y., and Sheetz, M.P. (2002). Force transduction by Triton cytoskeletons. J. Cell Biol. *156*, 609–615.

Sawada, Y., Nakamura, K., Doi, K., Takeda, K., Tobiume, K., Saitoh, M., Morita, K., Komuro, I., De Vos, K., Sheetz, M., and Ichijo, H. (2001). Rap1 is involved in cell stretching modulation of p38 but not ERK or JNK MAP kinase. J. Cell Sci. *114*, 1221–1227.

Shin, N.Y., Dise, R.S., Schneider-Mergener, J., Ritchie, M.D., Kilkenny, D.M., and Hanks, S.K. (2004). Subsets of the major tyrosine phosphorylation sites in Crk-associated substrate (CAS) are sufficient to promote cell migration. J. Biol. Chem. *279*, 38331–38337.

Tamada, M., Sheetz, M.P., and Sawada, Y. (2004). Activation of a signaling cascade by cytoskeleton stretch. Dev. Cell *7*, 709–718.

Tang, D.D., and Tan, J. (2003). Role of Crk-associated substrate in the regulation of vascular smooth muscle contraction. Hypertension *42*, 858–863.

Thomas, S.M., and Brugge, J.S. (1997). Cellular functions regulated by Src family kinases. Annu. Rev. Cell Dev. Biol. *13*, 513–609.

Vogel, V., and Sheetz, M. (2006). Local force and geometry sensing regulate cell functions. Nat. Rev. Mol. Cell Biol. *7*, 265–275.

Wang, Y., Botvinick, E.L., Zhao, Y., Berns, M.W., Usami, S., Tsien, R.Y., and Chien, S. (2005). Visualizing the mechanical activation of Src. Nature *434*, 1040–1045.

Wisniewska, M., Bossenmaier, B., Georges, G., Hesse, F., Dangl, M., Kunkele, K.P., Ioannidis, I., Huber, R., and Engh, R.A. (2005). The 1.1 A resolution crystal structure of the p130cas SH3 domain and ramifications for ligand selectivity. J. Mol. Biol. *347*, 1005–1014.

Zhong, C., Chrzanowska-Wodnicka, M., Brown, J., Shaub, A., Belkin, A.M., and Burridge, K. (1998). Rho-mediated contractility exposes a cryptic site in fibronectin and induces fibronectin matrix assembly. J. Cell Biol. *141*, 539–551.

Journal of Cell Science

The C-terminus of ephrin-B1 regulates metalloproteinase secretion and invasion of cancer cells

Masamitsu Tanaka[1], Kazuki Sasaki[1,2], Reiko Kamata[1] and Ryuichi Sakai[1,*]

[1]Department of Growth Factor Division, National Cancer Center Research Institute, 5-1-1 Tsukiji, Tokyo 104-0045, Japan
[2]Department of Pharmacology, National Cardiovascular Center Research Institute, 5-7-1 Fujishirodai, Suita, Osaka 565-8565, Japan
*Author for correspondence (e-mail: rsakai@gan2.res.ncc.go.jp)

Accepted 28 April 2007
Journal of Cell Science 120, 2179-2189 Published by The Company of Biologists 2007
doi:10.1242/jcs.008607

Summary

Interaction of the Eph family of receptor protein tyrosine kinases and their ligands, ephrin family members, induces bi-directional signaling via cell-cell contacts. High expression of B-type ephrin is associated with high invasion potential of tumors, however, the mechanism by which ephrin-B promotes cancer cell invasion is poorly understood. We show that interaction of ephrin-B1 with the Eph receptor B2 (EphB2) significantly enhances processing of the extracellular domain of ephrin-B1, which is regulated by the C-terminus. Matrix metalloproteinase-8 (MMP-8) is the key protease that cleaves ephrin-B1, and the C-terminus of ephrin-B1 regulates activation of the extracellular release of MMP-8 without requirement of de novo protein synthesis. One possible mechanism by which ephrin-B1 regulates the exocytosis of MMP-8 is the activation of Arf1 GTPase, a critical regulator of membrane trafficking. In support of this hypothesis, activation of ephrin-B1 increased GTP-bound Arf1, and the secretion of MMP-8 was reduced by expression of a dominant-negative mutant of Arf1. Expression of ephrin-B1 promoted the invasion of cancer cells in vivo, which required the C-terminus of ephrin-B1. Our results suggest a novel function of the C-terminus of ephrin-B1 in activating MMP-8 secretion, which promotes the invasion of cancer cells.

Supplementary material available online at
http://jcs.biologists.org/cgi/content/full/120/13/2179/DC1

Key words: Eph, Ephrin, Metalloproteinase, Secretion

Introduction

The members of the Eph receptor family can be classified into two groups based on their sequence similarity and their preferential binding to ligands tethered to the cell surface either by a glycosylphosphatidyl inositol anchor (ephrin-A) or a transmembrane domain (ephrin-B) (Murai and Pasquale, 2003; Blits-Huizinga et al., 2004; Poliakov et al., 2004). The interaction of Eph receptor B2 (EphB2) protein tyrosine kinases and their ephrin-B ligands induces bi-directional signaling via the resultant cell-cell contacts. Ephrin-B has an intracellular domain, which includes sites for tyrosine phosphorylation via Src family kinases and a docking site for proteins with a PDZ domain (Lin et al., 1999; Cowan and Henkemeyer, 2001; Bong et al., 2004). These sites give ephrin-B ligands at least two ways of being involved in intracellular signaling. Although investigation of the functions of Eph receptors and ephrins have focused on the development of the vascular and nervous systems, the roles of Eph-ephrin pathways in epithelial cells and cancers have also attracted interest (Batlle et al., 2002; Klein, 2004; Batlle et al., 2005; Tanaka et al., 2005; Holmberg et al., 2006). Overexpression of B-type ephrin in cancer cells is reported to correlate with high invasion and high vascularity of tumors (Meyer et al., 2005; Castellvi et al., 2006; Nakada et al., 2006), and elevated expression of ephrin-B1 is observed in poorly differentiated invasive tumor cells and other tumors with poor clinical prognosis (Kataoka et al., 2002; Varelias et al., 2002). However, whether ephrin-B actually modifies tumor invasion in vivo has not been established, and the mechanism by which ephrin-B is involved in the invasion of cancer cells is unknown.

Some ephrins are cleaved by a protease. When ephrin-A5 binds with EphA3, their complex creates a recognition motif for a disintegrin and metalloproteinase (ADAM)10 membrane metalloproteinase, which allows effective cleavage of the extracellular domain of ephrin-A5 (Hattori et al., 2000; Janes et al., 2005). Protease-mediated cleavage also occurs for B-type ephrins; a rhomboid transmembrane serine protease RHBDL2 cleaves the transmembrane domain of ephrin-B3 (Pascall and Brown, 2004), and ephrin-B1 and ephrin-B2 are processed within the transmembrane region by the presenilin 1 (PS1)-γ-secretase system to release an intracellular peptide (Georgakopoulos et al., 2006; Tomita et al., 2006).

During the process of screening peptides secreted from pancreas cancer cell lines, we found evidence that the extracellular portion (ectodomain) of ephrin-B1 is secreted. This finding led us to study the mechanism of ephrin-B1 shedding within the ectodomain in cancer cells. In the present study, we show that the C-terminus of ephrin-B1 regulates the exocytosis of MMP-8, a key protease of ephrin-B1 cleavage, in response to the interaction with its receptor EphB2. An accumulating number of reports have shown that increased secretion of metalloproteinases often depends on their transcriptional activation (Chinni et al., 2006; Raymond et al., 2006; Reuben and Cheung, 2006). However, increase of MMP-8 secretion

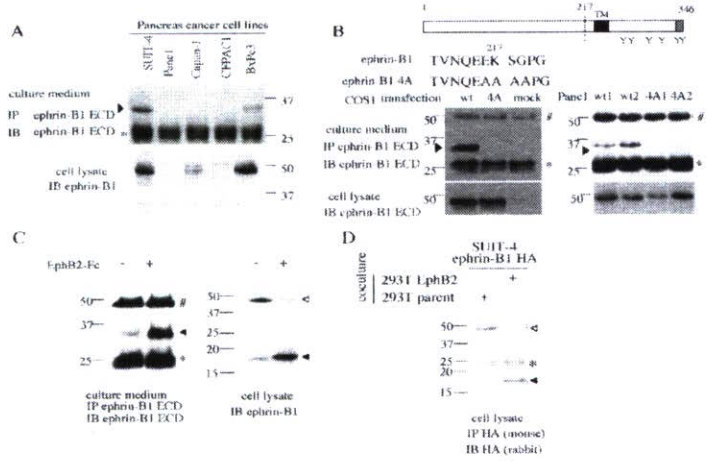

Fig. 1. The ectodomain of ephrin-B1 is secreted into the culture medium of human pancreas cancer cells. (A) Various pancreas cancer cell lines were cultured in medium containing 0.5% FBS. After 6 hours, conditioned medium was collected and subjected to immunoprecipitation (IP) and immunoblotting (IB) with polyclonal antibodies against the extracellular domain of ephrin-B1 (ephrin-B1 ECD). The immunoprecipitated 35 kDa ephrin-B1 fragment is indicated by an arrowhead. The expression of ephrin-B1 in each cell lysate was confirmed by immunoblotting (bottom). (B) A diagram of ephrin-B1 is shown at the top. TM, transmembrane domain; Y, tyrosine phosphorylation sites. Dotted line indicates the cleavage site of ephrin-B1, and the PDZ domain-binding motif is indicated as a gray box at the C-terminus. Four aa residues around the cleavage site were changed to alanine (ephrin-B1 4A) destroying the MMP-8 cleavage site. The conditioned medium of COS-1 cells transfected with wild-type (wt) or mutant ephrin-B1 (4A), or independent PANC-1 clones stably expressing ephrin-B1 were collected and subjected to immunoprecipitation and immunoblotting as described in A. (C) SUIT-4 cells were either treated with EphB2-Fc (4 μg/ml) for 2 hours (+) or left untreated (–). The ephrin-B1 fragment in the medium was detected as in A (left) or the cell lysates were subjected to immunoblotting with anti ephrin-B1 C18 (right panel). Open and filled arrowheads indicate uncleaved ephrin-B1 and its processed fragment (p17), respectively. (D) SUIT-4 cells were transiently transfected with ephrin-B1 tagged with HA at the C-terminus. Transfected SUIT-4 cells were overlayed on a monolayer of parent HEK293T cells or HEK293T cells stably expressing EphB2 for 2 hours. Cell lysates were prepared from co-cultured cells to detect HA-tagged p17 fragment derived from exogenously expressed ephrin-B1 in SUIT-4 cells by immunoprecipitation. # and * indicate the IgG heavy chain and light chain, respectively. Open and filled arrowheads indicate uncleaved ephrin-B1 and its processed fragment (p17), respectively.

induced by stimulation of ephrin-B1 did not depend on the elevation of MMP-8 expression level, but rather it was suggested to depend on the intracellular signaling mediated by ephrin-B1.

MMP-8, also known as neutrophil collagenase, is not only expressed in neutrophils, but it is also expressed in wide variety of cells, including chondrocytes, endothelial cells, synovial fibroblast and various cancer cells (Siller-Lopez et al., 2000; Stadlemann et al., 2003; Lint and Libert, 2006). MMP-8 cleaves all three α-chains of type I, II and III collagen and also a wide range of non-collagenous substrates, and plays important roles in inflammation and in cancer progression (Lint and Libert, 2006). Like other secretory proteins, proenzymes of soluble-type MMPs are secreted after the process of vesicle transport from Golgi to the plasma membrane, and then, extracellularly activated by removal of the propeptide domain (Sternlicht and Werb, 2001). In neutrophils, MMP-8 is stored in specific granules after being transported from Golgi, and released following activation by inflammatory mediators (Sternlicht and Werb, 2001), however, whether it is also the case in various cancer cells has yet to be fully investigated. Our analysis of the interaction between MMP-8 activity and EphB-ephrin-B1 signal transduction revealed a novel function of the C-terminus of ephrin-B1 in the secretion of MMP-8, which leads to the cleavage of ephrin-B1 and involves the negative regulation of the EphB-ephrin-B1 complex. Moreover, regulation of this MMP family member through the ephrin-B1 C-terminus may contribute to the highly invasive phenotype of ephrin-B1-expressing cancer cells by degradation of the extracellular matrix.

Results

The Ephrin-B1 ectodomain is secreted into the culture medium of pancreatic cancer cell lines

During screening of peptides secreted by the pancreatic cancer cell line SUIT-4, we identified,using MALDI-MS/MS analysis, three different peptides derived from ephrin-B1 sharing a common N-terminus. Analysis of these peptides indicated that ephrin-B1 undergoes limited cleavage between aa residues 217 and 218. Immunoprecipitation with antibodies against the extracellular domain of ephrin-B1 revealed a 35 kDa band from the conditioned media of two out of five pancreatic cancer cell lines. The 35 kDa fragment was also detected in COS-1 and PANC-1 cells when ephrin-B1 was expressed (Fig. 1A,B). These results indicate that the 35 kDa ectodomain fragment is released by cleavage of ephrin-B1 in these cell lines. The concentration of serum in the medium did not affect the cleavage of ephrin-B1 (data not shown). The cleavage site in ephrin-B1 estimated by MALDI-MS/MS was confirmed by the observation that substitution of the four amino acids (aa) at positions 216-219 (ephrin-B1$^{216\text{-}219}$) by alanine (ephrin-B1 4A), blocked the production of the 35 kDa ectodomain fragment in COS-1 and PANC-1 cells (Fig. 1B).

Cleavage of ephrin-B1 ectodomain is enhanced by interaction with its receptor EphB2, which is regulated by the C-terminus of ephrin-B1

Next, we examined whether the interaction of ephrin-B1 with its receptor EphB2 modifies the cleavage of ephrin-B1.

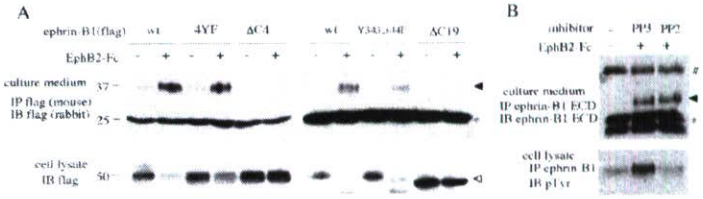

Fig. 2. Activation of ephrin-B1 cleavage requires its C-terminus. (A) Wild-type and various mutants of ephrin-B1 tagged with Flag at the N-terminus were expressed in Capan-1 cells by retrovirus-mediated gene transfer. The cells were treated with EphB2-Fc (2 μg/ml) for 1.5 hours (+) or left untreated (–) and conditioned medium was assayed for the presence of ephrin-B1 fragments by immunoprecipitation (IP) and immunoblotting (IB) with anti-flag antibody. The filled arrowhead indicates the ephrin-B1 ectodomain fragment. (Bottom) Expression of wild-type or mutated ephrin-B1 in cell lysates after treatment with EphB2-Fc. The open arrowhead indicates ephrin-B1 ΔC19. (B) SUIT-4 cells were treated with EphB2-Fc and PP2 or control PP3or left untreated, as indicated. Conditioned medium was collected after 2 hours and subjected to immunoprecipitation and immunoblotting. In the bottom panel, suppression of tyrosine phosphorylation of ephrin-B1 by PP2 treatment is shown. # and * indicate the IgG heavy chain and light chain, respectively.

Incubation of SUIT-4 cells with purified EphB2-Fc, a fusion protein of the extracellular domain of EphB2 with the Fc fragment of mouse IgG2b, significantly increased the amount of the 35 kDa fragment of ephrin-B1 in the conditioned medium (Fig. 1C, left). In EphB2-Fc-treated cell extract, a cellular fragment of ephrin-B1, produced by ectodomain shedding, was detected by immunoblotting with an antibody reacting to the C-terminal of ephrin-B1, as a band at 17 kDa (p17; Fig. 1C, right). The accumulation of p17 was also detected in ephrin-B1-expressing cells after contact with cells expressing EphB2. When ephrin-B1-expressing cells were overlayed on EphB2-expressing cells and co-cultured, significant reduction of uncleaved ephrin-B1 together with production of the p17 fragment was observed (Fig. 1D). This result indicates that cleavage of ephrin-B1 is also enhanced when ephrin-B1-expressing cells contact with heterologous cells expressing the EphB2.

In order to examine the processing mechanism of the ephrin-B1 ectodomain, several mutants of ephrin-B1 were analyzed. The cleavage of ephrin-B1 was also increased by EphB2-Fc treatment of Capan-1 cells expressing wild-type ephrin-B1 (Fig. 2A). However, expression of ephrin-B1 lacking the C-terminus (ΔC4 and ΔC19; the MMP-8 cleavage site at aa 217-218 is intact in these mutants), did not produce the 35 kDa ectodomain fragment in the culture medium upon treatment with EphB2-Fc (Fig. 2A). However, mutation of any of the four tyrosine residues in the cytoplasmic region (4YF) and tyrosines located at the C-terminus of ephrin-B1 (Y343, 344F) did not affect ephrin-B1 cleavage (Fig. 2A). In contrast to the significant reduction of full length wild-type or YF mutants of ephrin-B1 in cell lysates after EphB2-Fc treatment, level of C-terminally truncated ephrin-B1 mutants remained almost unchanged (Fig. 2A, bottom panels). We also observed similar results using PANC-1 cells, and confirmed that expression of ΔC mutants were localized on cell membrane (data not shown). In addition, treatment with PP2, an inhibitor of Src family kinases, significantly blocked tyrosine phosphorylation of ephrin-B1, but it did not affect cleavage of ephrin-B1 (Fig. 2B). Thus, the C-terminus of ephrin-B1, but not tyrosine phosphorylation of ephrin-B1, is required for induction of the proteolysis of ephrin-B1.

The Ephrin-B1 ectodomain is processed by MMP-8

The cleavage of ephrin-B1 was inhibited in PANC-1 cells expressing ephrin-B1, by incubation with the pan-matrix metalloproteinase (MMP) inhibitor GM6001, but not by inhibitors of other proteases including a cysteine protease, a serine protease, an aspartic protease or calpain (Fig. 3A). The amount of cleaved ephrin-B1 ectodomain was increased by treatment of DCI (3,4-dichloroisocoumarin), a serine protease inhibitor and TPCK (N$^{\alpha}$-tosyl-phe chloromethyl ketone), a chymotrypsin inhibitor of unknown function. As the inhibition of ephrin-B1 cleavage by GM6001 was also confirmed in SUIT-4 cells (data not shown), we further attempted to identify the metalloproteinase responsible. When SUIT-4 cells were treated with natural MMP inhibitors, TIMPs, at low concentration (100 nM), cleavage of ephrin-B1 was most effectively inhibited by TIMP-1 compared with TIMP-2 and TIMP-3 (Fig. 3B). TIMP-3, which is known to inhibit tumor necrosis factor-α converting enzyme (TACE) did not inhibit the cleavage of ephrin-B1 at all at concentrations from 5-250 nM (data not shown), whereas it completely inhibited the cleavage of TNF-α expressed in THP-1 cells at 100 nM (Fig. 3B, right panel). Among inhibitors of several MMPs expressed in SUIT-4 cells, including MMP-1, MMP-2 or 3, MMP-8 and MMP-9, only the inhibitor of MMP-8 blocked the cleavage of ephrin-B1 (Fig. 3C), and this effect was also seen in COS-1 cells and PANC-1 cells expressing ephrin-B1 (data not shown).

In order to examine whether MMP-8 cleaves ephrin-B1, ephrin-B1-Fc fusion protein, which consists of the entire extracellular region of ephrin-B1 and the Fc fragment of mouse IgG2b, was incubated with purified activated MMPs in vitro. Incubation of ephrin-B1-Fc with activated MMP-8 produced two fragments of ephrin-B1-Fc corresponding to the predicted sizes (Fig. 3D). However, other membrane-type metalloproteinases such as MT1-MMP and ADAM10, which are also expressed in SUIT-4 cells, did not cleave ephrin-B1-Fc in vitro (Fig. 3D).

Expression of MMP-8 protein was detected at approximately the same levels in all of the cell lines we examined (Fig. 4A, left), although it was detected at high level when the cells were replated and decreased after the cells reached confluence (Fig. 4A, right). When expression of

Journal of Cell Science

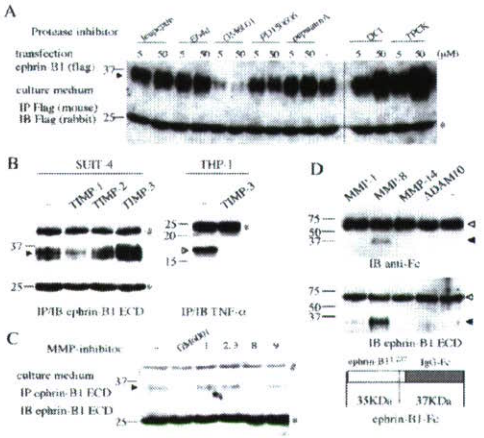

Fig. 3. Screening of a protease that cleaves the extracellular domain of ephrin-B1. (A) Panc-1 cells transiently expressing Flag-tagged ephrin-B1 were incubated with various protease inhibitors for 4 hours in medium containing 0.5% FBS: leupeptin and E64d (Loxistatin), a cystein protease inhibitor; GM6001, a pan-MMP inhibitor; PD150606, a calpain inhibitor; pepstatin A, an aspartic protease inhibitor; DCI (3,4-dichloroisocoumarin), a serine protease inhibitor; TPCK (N$^{\alpha}$-tosyl-phe chloromethyl ketone), a chymotrypsin inhibitor. The cleavage of ephrin-B1 ectodomain was examined as described in Fig. 2A. (B) Left: SUIT-4 cells were incubated with EphB2-Fc (2 μg/ml) together with or without TIMPs (100 nM for each) as indicated for 2 hours. The processed ephrin-B1 fragment was detected in the culture medium. Right: THP-1 cells were treated with PMA (10 ng/ml) together with or without TIMP-3 (100 nM) for 6 hours. Open arrowhead indicates the processed fragment of TNF-α in the medium detected by immunoprecipitation with anti TNF-α antibody. (C) SUIT-4 cells were treated with various MMP inhibitors as indicated (1 μM for MMP-8 inhibitor and 5 μM for others) for 4 hours. Ephrin-B1 fragment was detected in the medium. (D) Purified ephrin-B1-Fc protein was incubated with activated MMP in vitro for 1 hour at 37°C, separated by SDS-PAGE, and immunoblotted with anti-Fc mouse IgG or anti-ephrin-B1. Bottom: a schematic representation of ephrin-B1-Fc with the MMP-8 cleavage site indicated by a dotted line. Open and filled arrowheads indicate uncleaved ephrin-B1-Fc and the processed fragments, respectively.

MMP-8 was reduced in SUIT-4 cells by treatment of cells with siRNA, the amount of processed ephrin-B1 ectodomain in the culture medium was decreased (Fig. 4B). By contrast, overexpression of activated MMP-8 cDNA, in which the propeptide domain was removed, in SUIT-4 cells evidently increased the cleavage of ephrin-B1 (Fig. 4C).

As some MMPs and their substrates physically associate directly or indirectly and make a protein complex, interaction between MMP-8 and ephrin-B1 was examined (Sawicki et al., 2005; Yu et al., 2007). Ephrin-B1 was coprecipitated with MMP-8 from extracts of L ephrin-B1 cells by MMP-8-specific antibodies, but not by control normal rabbit IgG1, indicating that MMP-8 forms a complex with ephrin-B1 (Fig. 4D). However, association of MMP-8 with the receptor EphB2 was not detected (data not shown). These results also suggest that MMP-8 is the key metalloproteinase that cleaves the ephrin-B1 ectodomain.

Stimulation of ephrin-B1 activates secretion of MMP-8, which is regulated by the C-terminus of ephrin-B1

To understand the mechanism of activation of ephrin-B1 cleavage by EphB2, we next examined whether it is accompanied by an increase in MMP-8 expression. The level of intracellular expression of MMP-8 mRNA was not affected by treatment with EphB2-Fc or contact of ephrin-B1-expressing cells with EphB2-expressing cells for 4 hours or longer (Fig. 5A). Moreover, the amount of processed ephrin-B1 ectodomain produced in the medium was not altered by the addition of cyclohexamide or actinomysin D, inhibitors of de novo synthesis of mRNA and proteins, respectively (Fig. 5B). These results indicate that activation of ephrin-B1 cleavage by EphB2 does not depend on the increased amount of MMP-8. In addition, when the de novo synthesis of MMP-8 was blocked, the amount of intracellular MMP-8 protein decreased slightly after 4 hours or longer treatment of ephrin-B1-expressing cells with EphB2-Fc (Fig. 5C), which suggests that stimulation of ephrin-B1 activates extracellular release of MMP-8 protein from the cytoplasm. Actually, the amount of MMP-8 protein in the culture medium was remarkably elevated after incubation of the cells with EphB2-Fc as detected by immunoprecipitation (Fig. 5D).

In order to show directly that stimulation of ephrin-B1 increased exocytosis of MMP-8, which was already synthesized and present in the cytoplasm, SUIT-4 cells were pulse-labeled with [^{35}S]methionine. When pulse-labeled cells were treated with EphB2-Fc, a higher amount of labeled MMP-8 protein was detected in the medium compared to treatment of cells with Fc (Fig. 5E, left). However, secretion of labeled MMP-7, which was examined as a control, was not altered by EphB2-Fc treatment (Fig. 5E, right). In addition, the secretion of [^{35}S]methionine-labeled MMP-8 was also increased by EphB2-Fc treatment of Capan-1 cells expressing wild-type ephrin-B1, but it was not found in the media of cells expressing ephrin-B1 lacking the C-terminus (ΔC4 and ΔC19) (Fig. 5F, left). Consistently, the total amount of MMP-8 protein in the culture medium from cells expressing wild-type ephrin-B1 was higher than in the medium from ΔC4 ephrin-B1-expressing cells (Fig. 5F, right). These results suggest that stimulation of ephrin-B1 by EphB2 upregulates the process of MMP-8 exocytosis, and the C-terminus of ephrin-B1 regulates this event.

Stimulation of ephrin-B1 by EphB2 induces activation of Arf1 GTPase

To further confirm that activation of MMP-8 secretion is involved in the elevated ephrin-B1 cleavage in response to stimulation with EphB2, the cells were treated with brefeldin A, an inhibitor of membrane trafficking through the Golgi, which blocks the secretion of proteins (Tamaki and Yamashina, 2002). EphB2-stimulated cleavage of ephrin-B1 was apparently reduced by brefeldin A treatment (Fig. 6A). As a mode of action of brefeldin A is to inhibit activation of ADP ribosylation factor 1 (Arf1), a ras family GTPase, by blocking of the exchange reaction from Arf1-GDP to Arf1-GTP (Niu et al., 2005; Zeeh et al., 2006), we further examined the activity of Arf1 in ephrin-

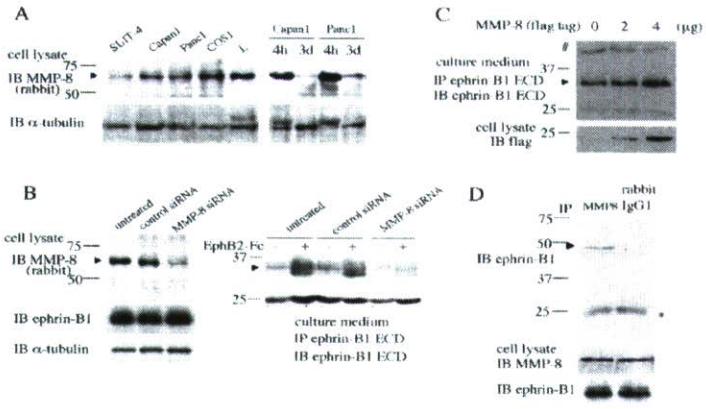

Fig. 4. MMP-8 is the key protease of ephrin-B1 cleavage. (A) Expression of MMP-8 in cell lysates. Left: The indicated cells were seeded on plates not to reach confluence. Cell lysates were prepared on the day after plating. Right: cell lysates were prepared 4 hours (4h) or 3 days (d3) after being plated on dishes. The cells were confluent on day 3 after plating. (B) SUIT-4 cells treated with either MMP-8 siRNA or control scrambled siRNA (control), or left untreated. The cells were detached 48 hours later, replated on new plates and further incubated for 24 hours. Left: Cellular levels of MMP-8 were analyzed 72 hours after treatment of SUIT-4 cells with siRNAs. Right: the culture medium was replaced with one fresh medium or medium containing EphB2-Fc (2 g/ml) and incubated for 2 hours to detect ephrin-B1 ectodomain in the medium. (C) SUIT-4 cells were transiently transfected with the indicated volume of a plasmid encoding Flag-tagged activated MMP-8 cDNA. After 48 hours of transfection, the medium was replaced and the cells were further incubated for 6 hours to detect processed ephrin-B1 ectodomain in the medium. The expression of transfected MMP-8 in each cell lysate was confirmed by immunoblotting with anti-Flag antibody (bottom). (D) The lysate of L ephrin-B1 cells was immunoprecipitated with anti-MMP-8 polyclonal antibody or control rabbit IgG1, and subjected to immunoblotting with anti-ephrin-B1 C18 antibody. HRP-conjugated anti-rabbit IgG (TrueBlot) was used as the secondary antibody for immunoblotting to avoid cross reaction with denatured rabbit IgG heavy chain of the antibody used for immunoprecipitation. The arrowhead indicates coprecipitated ephrin-B1. The asterisk indicates the IgG light chain.

B1-expressing cancer cells. To examine the amount of activated, GTP-bound Arf1, a pull-down approach was performed with an adaptor protein GGA3, which specifically binds to GTP-bound Arfs (Dell'Angelica et al., 2000). As a control experiment, we confirmed that constitutively activated Arf1 (Q71L), but not a dominant negative mutant of Arf1 (T31N) was coprecipitated with GST-tagged GGA3 (Fig. 6B, right panel). Incubation of SUIT-4 cells with EphB2-Fc increased the amount of Arf1-GTP coprecipitated with GST-tagged GGA3 (Fig. 6B). Similar results were also observed in PANC-1 cells expressing ephrin-B1, whereas treatment with EphB2-Fc did not affect activation of Arf1 in parent PANC-1 cells, which express ephrin-B1 in trace amounts (Fig. 6B). The amount of Arf1-GTP was also increased by EphB2-Fc treatment of Capan-1 cells expressing wild-type ephrin-B1 or ephrin-B1 4YF mutant, but not in cells expressing ΔC4 ephrin-B1 (Fig. 6C). These results suggest that stimulation of ephrin-B1 by EphB2 activates Arf1, and the signaling mediated by the C-terminus of ephrin-B1 is involved in this pathway. Furthermore, treatment of cells with brefeldin A, or overexpression of dominant negative mutant of Arf1, Arf1 T31N, decreased the secretion of MMP-8 in Capan-1 cells, indicating that Arf1 regulates the secretion of MMP-8 (Fig. 6D).

The C-terminus of ephrin-B1 is involved in the invasion by cancer cells

To investigate the biological implication of metalloproteinase activation caused by ephrin-B1-mediated signaling, we examined changes in the invasiveness of ephrin-B1-expressing cells with or without stimulation by EphB2 using an in vitro cell invasion assay. The invasion of collagen by Capan-1 cells was promoted by expression of ephrin-B1 and treatment of the cells with EphB2-Fc, and this invasion was inhibited by the addition of an MMP-8 inhibitor (Fig. 7A). On the other hand, the invasion by Capan-1 cells expressing ΔC4 ephrin-B1, or by parent Capan-1 cells was not significantly promoted by EphB2-Fc treatment (Fig. 7A).

We further examined whether expression of ephrin-B1 actually promotes cancer cell invasion in vivo using PANC-1 cells as a model system to study peritoneal dissemination. PANC-1 cells stably expressing wild-type ephrin-B1 (PANC-1 ephrin-B1) or ΔC4 ephrin-B1 (PANC-1 ΔC4) were established to compare their invasiveness with that of parent PANC-1 cells. Expression of wild-type or mutated ephrin-B1 did not affect BrdU incorporation into cells grown under normal two-dimensional cell culture conditions (data not shown). When these cells were injected intraperitoneally into nude mice, PANC-1 ephrin-B1 cells formed many tumor nodules in the mesenteric sheets and also in the peritoneal cavity, including the rectouterine region. By contrast, in mice injected with parent PANC-1 cells or PANC-1 ΔC4 cells, such tumors in mesentery sheets were fewer and smaller, and the total tumor volume involving the rectouterine region was much less (Fig. 7B,C, Table 1). The cells composing the mesenteric sheets express cognate receptors for ephrin-B1, EphB2 and

Journal of Cell Science

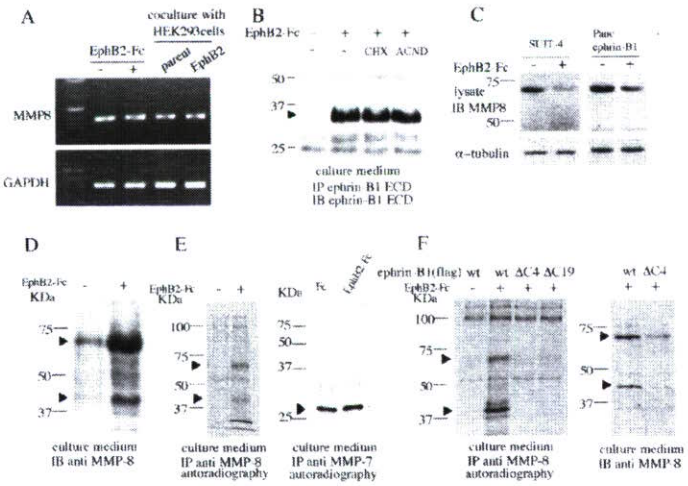

Fig. 5. Stimulation of ephrin-B1 with EphB2 increases MMP-8 secretion. (A) SUIT-4 cells were left untreated or were treated with EphB2-Fc or co-cultured with either parent or EphB2-expressing HEK293 cells for 4 hours. Cellular levels of MMP-8 were analyzed by RT-PCR using GAPDH as a control. (B) SUIT-4 cells were incubated with or without EphB2-Fc for 2 hours in the presence or absence of cycloheximide (CHX, 100 μg/ml) or actinomycin D (ACND, 5 μg/ml) to detect the ephrin-B1 ectodomain in the medium. (C) SUIT-4 cells or PANC-1 cells stably expressing ephrin-B1 were treated with actinomycin D (5 μg/ml) together with or without EphB2-Fc (2 μg/ml) for 4 hours. Cell lysates were prepared and intracellular expression levels of MMP-8 were analyzed by western blotting using α-tubulin as a loading control. (D) Conditioned medium of SUIT-4 cells were collected after the cells were treated with EphB2-Fc or left untreated for 4 hours in serum-free medium. Proteins secreted in the medium were precipitated with trichloroacetic acid (10%), resuspended in sample buffer, and subjected to immunoblotting with anti MMP-8 polyclonal antibody. Arrowheads indicate MMP-8 protein (proenzyme and activated). (E) SUIT-4 cells were metabolically labeled with [^{35}S]methionine, then treated with EphB2-Fc or control Fc for 2 hours. The amount of labeled MMP-8 (left panel) or MMP-7 (right panel) in the medium was evaluated through immunoprecipitation from the conditioned medium followed by SDS-PAGE and autoradiography. Arrowhead indicates MMP-8 (proenzyme and activated; left) or MMP-7 (right) in the medium. (F) Wild-type and mutants of ephrin-B1 were expressed in Capan-1 cells as in Fig. 2A, and [^{35}S]methionine-labeled MMP-8 was detected in the medium (left panel). Right: The total amount of MMP-8 in the conditioned medium of Capan-1 cells was evaluated using the trichloroacetic acid (TCA) precipitation procedure, followed by immunoblotting with anti MMP-8 antibody as in D.

EphB4 (see Fig. S1 in supplementary material). These results indicate that ephrin-B1 actually promotes cancer cell invasion, which requires the C-terminus of ephrin-B1. EphB2 and EphB4 expressed in cells of the mesenteric sheet might act as interaction partners for ephrin-B1 present on PANC-1 cells.

Discussion

The interaction of Eph family receptor protein tyrosine kinases with their ligands, ephrin family proteins, induces bi-directional signaling. In this study, we showed for the first time that ephrin-B1 regulates the activation and release of a metalloproteinase. We observed that binding of EphB2 to ephrin-B1 promotes secretion of MMP-8 without increasing the expression level of MMP-8. Activation of several molecules, such as Erk, p38 and PI 3-kinase or Akt cause transcriptional activation of metalloproteinases (Chinni et al., 2006; Raymond et al., 2006; Reuben and Cheung, 2006). In our study, however, activation of ephrin-B1 by EphB2 binding did not alter the phosphorylation levels of Erk-1, 2, p38 or Akt (data not shown), as also reported by others (Huynh-Do et al., 2002). Our observation that ephrin-B1-induced secretion of MMP-8 was sensitive to brefeldin A, which blocks the membrane trafficking of coated vesicles at the Glogi/trans-Golgi network suggests that ephrin-B1 signaling resulted in increased transport of MMP-8 from the cytoplasm to the cell surface (Tamaki and Yamashina, 2002).

Regulation of the secretion of MMP-8 enables ephrin-B1 signaling to play an important role in regulating MMP-8 activity. Like other soluble MMPs, MMP-8 is proteolytically activated extracellularly by removal of its propeptide domain, and physiologically relevant level of MMP protease activity requires efficient release of the protease to the cellular surface (Sternlicht and Werb, 2001). Although the molecular mechanism of the MMP-8 secretory pathway is not well understood, our data indicate that signaling mediated by the carboxyl-terminal region of ephrin-B1 is involved. Notably, removal of the C-terminus of ephrin-B1 resulted in significant reduction of MMP-8 secretion and cleavage of the extracellular domain of ephrin-B1. In addition, the C-terminus of ephrin-B1 regulates the signal leading to activation of Arf1, a critical regulator of membrane traffic in the secretory pathway and one target of brefeldin A (Tamaki and Yamashina, 2002; Donaldson et al., 2005). Arf1 GTPase regulates the membrane association of coat proteins involved in intracellular membrane trafficking, which is critical for the vesicle transport of secretory proteins at the Golgi (Donaldson et al., 2005). Actually we observed that treatment of cells with brefeldin A, or expression of Arf1 T31N inhibited the secretion of MMP-8. Therefore, as one possibility, secretion of MMP-8 is upregulated by activation of Arf1 GTPase through ephrin-B1 signaling, although the molecular mechanisms connecting ephrin-B1 and Arf1 are still not well understood. As ephrin-B1 has a docking site for the PDZ domain at the C-terminus, some protein containing PDZ domains may be involved in this pathway. As a consequence, the increase of secreted MMP-8 may trigger the degradation of extracellular matrix and the cleavage of ephrin-B1 as a possible feedback mechanism (Fig. 8). In our preliminary observations, Arf1 activation occurs as fast as 10 minutes after stimulation with EphB2-Fc, and some increase of MMP-8 in the culture medium was detected from 0.5 hours after addition of EphB2-Fc. By contrast, the cleavage of ephrin-B1 was observed at 1 hour, but not at 10 minutes after stimulation with EphB2-Fc, by immunoblotting of a cleaved C-terminal fragment of ephrin-B1, p17, in cell lysates (data not shown). Although we cannot determine the precise time point of MMP-8 secretion because of the limitation of the antibody's sensitivity, these observations are compatible with the model that ephrin-B1 reverse signaling induces Arf1 activation, which leads to MMP-8 release and ephrin-B1 cleavage. As extracellular activation of MMPs can be triggered by activation of other MMPs, there is the possibility that ephrin-B1-mediated signaling may synergistically promote activity of several MMPs. In addition, Arf1 GTPase may involve the intracellular transport of not only MMP-8, but also several other MMPs. Whether metalloproteinases other than MMP-8 are also upregulated by EphB2 stimulation of ephrin-B1 should also be investigated.

We show that the 35 kDa ephrin-B1 fragment in the culture medium of SUIT-4 cells was generated by cleavage at aa 218. From the experiments using natural inhibitors of metalloproteinases, TIMP-1 but not TIMP-2 and TIMP-3 effectively blocked the cleavage of ephrin-B1. Among these TIMPs, TIMP-3 most effectively inhibits the function of ADAM family metalloproteinase, including ADAM-17 (TACE), ADAM-10 and ADAM-TS4 (Amour et al., 2000; Brew et al., 2000; Hashimoto et al., 2001). In addition, membrane-type metalloproteinases (MT-MMPs) are preferentially inhibited by TIMP-2 and TIMP-3, but not by TIMP-1 (Brew et al., 2000). Our observation that cleavage of ephrin-B1 was most effectively inhibited by TIMP-1, but not by TIMP-2 or TIMP-3 suggests that it is unlikely that those members of the ADAMs family are critically involved. However, we cannot exclude that TIMP-3-independent ADAM metalloproteinases may contribute to the processing of ephrin-B1. Together with the observation that ephrin-B1 cleavage was at least partially inhibited by RNA interference of MMP-8, and it was increased by overexpression of MMP-8, our results suggest that MMP-8 is the key metalloproteinase that cleaves ephrin-B1 ectodomain.

In addition to an extracellular 35 kDa peptide derived from the N-terminal of ephrin-B1, stimulation of ephrin-B1-expressing cells with EphB2-Fc resulted in the production of a 17 kDa intracellular fragment (p17) derived from the C-terminus of ephrin-B1. As detection of p17 was abolished in L cells expressing the ephrin-B1 4A mutant (data not shown), p17 was generated by cleavage of ephrin-B1 within the extracellular domain at aa 218. Ephrin-B1 and ephrin-B2 are cleaved within the transmembrane region by presenilin-dependent γ-secretase, which releases an approximately 12

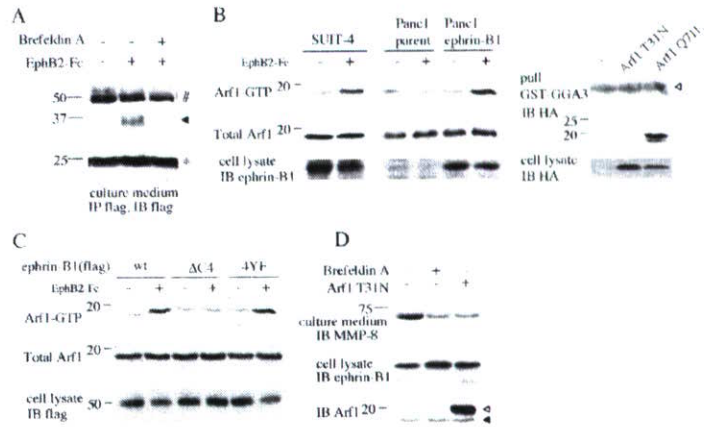

Fig. 6. Stimulation of ephrin-B1 with EphB2 activates Arf1. (A) Flag-tagged ephrin-B1 was expressed in Capan-1 cells. The cells were treated with or without EphB2-Fc (2 μg/ml) and brefeldin A (10 μg/ml) as indicated for 1.5 hours, and conditioned medium was assayed for the 35 kDa ectodomain of ephrin-B1. (B,C) The activity of Arf1 was analyzed in the indicated cells. (C) Wild-type or mutant ephrin-B1 was expressed in Capan-1 cells as in Fig. 2A. The cells were incubated with EphB2-Fc (4 μg/ml) for 20 minutes before being lysed. Arf1-GTP was pulled down with GST-GGA3 bound to glutathione-Sepharose. As controls, lysates of COS-1 cells transiently transfected with plasmids encoding Arf1 T31N or Arf1 Q71L, HA tagged at the C-terminus were analyzed (B, right panel). Open arrowhead indicates cross-reacted GST-GGA3 used for the pull-down assay. (D) Suppression of Arf1 activation decreased the MMP-8 secretion. Capan-1 cells stably expressing ephrin-B1 were used. In the right lane, Arf1 T31N was also transiently expressed in the cells by retrovirus mediated gene transfer. All cells were treated with EphB2-Fc together with (middle lane) or without brefeldin A for 4 hours, and the conditioned medium was subjected to TCA precipitation to detect MMP-8 through immunoblotting. The filled arrowhead indicates endogenous Arf1, and the open arrowhead indicates HA-tagged Arf1 T31N (bottom).

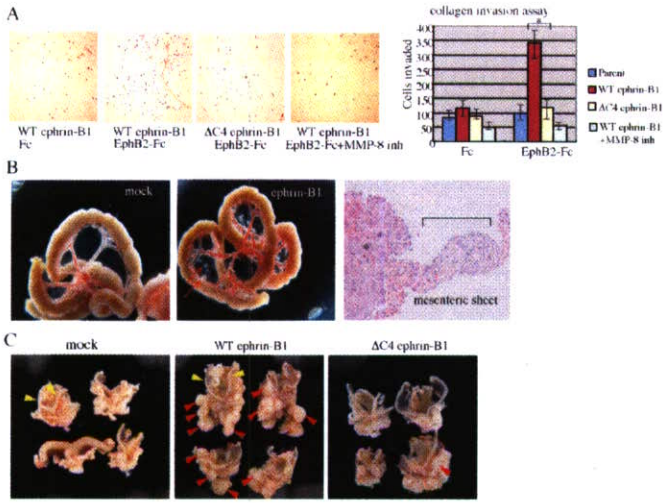

Fig. 7. The C-terminus of ephrin-B1 regulates the invasion of cancer cells. (A) Wild-type (WT) ephrin-B1 or ΔC4 ephrin-B1 mutant was expressed in Capan-1 cells. The cells were seeded onto a Transwell membrane coated with a collagen matrix (25 μg/cm^2) in serum-free medium containing control Fc or EphB2-Fc (4 μg/ml) with or without addition of the MMP-8 inhibitor (1 μM). In the lower chamber, medium containing 5% FBS was added as a chemoattractant. After 8 hours incubation, the wells were harvested and cells that had invaded the collagen were counted. Representative fields are shown. (Right) The results from three independent experiments, each in duplicate, are shown as the mean ± s.d. *P<0.01. (B) PANC-1 ephrin-B1 cells or PANC-1 cells transfected with a mock vector (mock) were injected intraperitoneally into nude mice. The representative appearance of intestinal loops 8 weeks after injection is shown. Arrows indicate disseminated tumor nodules in the mesentery. The right panel shows the histology of the tumors in the mesentery (×100). The asterisk indicates a tumor nodule. Microscopic invasion of cancer cells was observed in the mesenteric sheet (blanket). (C) Representative appearance of the tumors of panc1 cells expressing either mock vector, wild-type or ΔC4 ephrin-B1 in the rectouterine region was compared. Yellow and red arrowheads indicate uterine horns and tumor nodules, respectively.

kDa intracellular fragment (Georgakopoulos et al., 2006; Tomita et al., 2006). Although p17 may be further processed by γ-secretase and produce a small intracellular peptide, we did not detect such a product, possibly because of its rapid degradation or cell type-dependent differences in protease activity.

One possible function of ephrin-B1-mediated MMP-8 secretion is processing of ephrin-B1 and downregulation of EhpB2-stimulated ephrin-B1 intracellular signaling. Unlike wild-type ephrin-B1 protein, ΔC ephrin-B1 protein was not reduced after EphB2-Fc treatment, which seems to suggest that cleavage of ephrin-B1 contributes to the down regulation of ephrin-B1 after stimulation. However, recent reports show the trans-endocytosis of ephrin-B1 after engagement with EphB receptors, which regulates ephrin-B-mediated cell repulsion (Zimmer et al., 2003; Marston et al., 2003; Parker et al., 2004). We also observed that ephrin-B1 4A, which also triggers Arf1 activation and release of MMP-8, but is resistant to cleavage, was degraded and decreased in amount after stimulation with EphB2-Fc almost to the same degree with wild-type ephrin-B1 (data not shown). Because the C-terminus of ephrin-B1 may also modify its endocytosis, we cannot conclude at present that ephrin-B1 cleavage greatly affects the stability and turnover of the EphB-ephrin-B1 complex on the cell surface. Rather, the biological significance of ephrin-B1-mediated MMP-8 secretion is considered to be the promotion of the invasion potential of cancer cells via degradation of surrounding extracellular matrix. However, addition of the 35 kDa ephrin-B1 ectodomain prepared from conditioned medium of ephrin-B1 expressing COS-1 cells inhibited the motility of EphB2-expressing cells, similar to the effect of unclustered ephrin-B1-Fc, indicating the possible biological effect of secreted fragments on cell movement, whereas it did not affect cell proliferation (see Fig. S2 in supplementary material).

The potential significance of ephrin-B1 in cancer cell invasion is supported by our finding that ephrin-B1-mediated collagen invasion by Capan-1 cells was related to MMP-8. The inability of ΔC-ephrin-B1 to promote collagen invasion in the same assay revealed that signaling through C-terminus of ephrin-B1 affects the invasion ability of cancer cells. In addition, expression of ephrin-B1 in the pancreas cancer cells, PANC-1, promoted the dissemination of intraperitoneally injected cells into the mesentery and peritoneal cavity where they formed tumor nodules, demonstrating for the first time that ephrin-B1 actually promotes cancer cell invasion in vivo. Overexpression of B-type ephrins in cancer cells would affect cell-cell adhesion by their interaction with cell adhesion proteins such as claudin (Tanaka et al., 2005). Ephrin-B1-mediated intracellular signaling also results in aberrant

Table 1. Mesenterial dissemination after intraperitoneal inoculation of cancer cells

	Number of nodules*		
Cell line	0-10	10-30	30+
Mock	16	2	0
WT ephrin-B1	0	4	17
ΔC4 ephrin-B1	12	4	3

Data are shown as the number of mice with tumors in the mesentery.
*Number of tumor nodules larger than 2 mm in the mesentery per body.

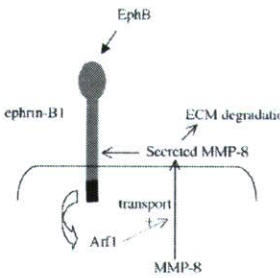

Fig. 8. Diagram showing the possible mechanism of ephrin-B1-mediated stimulation of MMP-8 secretion and cell invasion. When ephrin-B1 is stimulated by EphB receptors, Arf1 GTPase is activated through signaling mediated by the C-terminus ephrin-B1, which may stimulate the transport of MMP-8 for extracellular release. The increase of secreted MMP-8 triggers the degradation of extracellular matrix (ECM) and cleavage of ephrin-B1.

activation of RhoA and Rac1 (Tanaka et al., 2003; Tanaka et al., 2004; Lee et al., 2005). Together, events such as these would result in increased cell motility. These findings in conjunction with the ephrin-B1 induction of MMP-8 secretion, indicate that ephrin-B1 overexpression would result in an enhanced potential for invasion of surrounding tissues. For example, both MMP-8 and ephrin-B1 are frequently expressed in ovarian cancers, and their expression correlates with tumor grade and a poor prognosis (Castellvi et al., 2006; Varelias et al., 2002). Ephrin-B1 could also be involved in invasion of cancer cells circulating in the blood into sheets of endothelial cells which express EphB receptors and play a role in extravasation and metastasis. The inhibition of a specific cellular signal originating in ephrin-B1 stimulation may be a good candidate for regulating tumor invasion.

Materials and Methods

Plasmids, antibodies and reagents

Plasmids encoding full-length cDNAs of human ephrin-B1 and the Fc fusion protein construct of EphB2 and ephrin-B1 have been described previously (Tanaka et al., 2004). Fc fusion proteins were purified from the culture medium of COS-1 cells transfected with plasmids encoding EphB2-Fc or ephrin-B1-Fc using a protein A Sepharose column as described previously (Tanaka et al., 2004). Mutants of ephrin-B1 lacking the cytoplasmic tail (ΔC4 and ΔC19, truncation of four or 19 aa residues at the C-terminus, respectively) were generated using PCR-based techniques. Alanine substitution of four aa in the extracellular domain (aa 216-219) of ephrin-B1, ephrin-B1 4A, was performed using the Altered Sites Mutagenesis System (Promega). Generation of Ephrin-B1 with mutations of four tyrosine residues in the cytoplasmic domain (Y313, 317, 324, 329) and ephrin-B1 4YF, have been described previously (Tanaka et al., 2005). For making flag-tagged ephrin-B1, a DNA fragment encoding the Flag tag was inserted 3′ to the signal peptide of ephrin-B1 (aa 1-24). To generate a plasmid encoding human activated MMP-8, cDNA corresponding to nucleotides 336-824 of the reported sequence (GenBank accession number BC074988) was amplified with RT-PCR from a cDNA template derived from U937 cells. The amplified MMP-8 cDNA was tagged with the signal peptide and Flag at the 5′ terminus, and cloned into pcDNA3. GST-GGA3 was generated by cloning of PCR-amplified cDNA corresponding to aa 1-313 of human GGA3 short isoform (GenBank accession number AF219139) into pGEX4T2 (Amersham Pharmacia). The plasmids encoding wild-type Arf1 and Arf1 T31N bearing the HA epitope at the C-terminus were donated from J. S. Bonifacino (National Institute of Child Health and Human Development, NIH, Bethesda, MA). To generate the recombinant retrovirus, cDNAs were subcloned into pDON-AI vector (Takara). Monoclonal and polyclonal antibodies that recognize the Flag tag were purchased from Sigma and Affinity Bioreagents (Affinity Bioreagents, Golden, CO), respectively. Antibodies that recognize the HA tag were from InvivoGen (InvivoGen, San Diego, CA; monoclonal antibody) and Santa Cruz Biotechnology Inc. (polyclonal antibody). Rabbit polyclonal antibody that recognizes ephrin-B1 (C18) was purchased from Santa Cruz Biotechnology, Inc. The goat polyclonal antibody against ephrin-B1, which reacts with the entire extracellular domain, was purchased from R&D Systems. The polyclonal antibody against tyrosine-phosphorylated ephrin-B1 (ephrin-B1 pY317, aa residues 314-321) was raised in rabbits and affinity-purified as described previously (Tanaka et al., 2005). EphB2 and EphB4 polyclonal antibodies were from R&D Systems. Polyclonal and mouse monoclonal antibodies for MMP-8 were purchased from Chemicon and Daiichi Fine Chemical (Takaoka, Japan), respectively. The monoclonal antibody for phosphotyrosine (4G10) and Arf1 was from Upstate Biotechnology and Affinity Bioreagents, respectively. TrueBlot anti-rabbit IgG secondary antibody was purchased from eBioscience (San Diego, CA). Cyclohexamide and actinomycin D were purchased from Sigma. Purified TIMP-1, and 2 were purchased from Calbiochem, and TIMP-3 was from Sigma. The protease inhibitors shown in Fig. 3 and purified MMP-1 (proenzyme), MMP-8 (proenzyme), MT1-MMP (catalytic domain, aa 89-265) and ADAM10 (mature active ectodomain, aa 19-673) were purchased from Calbiochem. The MMP-8 inhibitor is (3R)-(+)-[2-(4-methoxybenzenesulfonyl)-1,2,3,4-tetrahydroisoquinoline-3-hydroxamate]. Src family kinase inhibitor 4-amino-5-(4-chlorophenyl)-7-(t-butyl)pyrazolo[3,4-d]pyrimidine (PP2) and the structural analog 4-amino-7-phenylpyrazolo[3,4-d]pyrimidine (PP3) were purchased from Calbiochem.

Cell culture, transfection and retrovirus infection

SUIT-4 (Kawano et al., 2004) and the other pancreas carcinoma cell lines were cultured in RPMI1640 supplemented with 10% fetal bovine serum. Mice fibroblast L cells and COS-1 cells were cultured in DMEM with 10% fetal bovine serum. For transient expression assays, COS-1 cells and SUIT-4 cells were transfected with plasmid DNA using Lipofectamine 2000 reagent (Invitrogen). Recombinant retroviral plasmid, pDON-AI was cotransfected with pCL-10A1 retrovirus packaging vector (IMGENEX) into 293gp cells to allow the production of retroviral particles. Capan-1 cells were infected with retroviruses for transient expression of ephrin-B1 or Arf1 mutants, and used for experiments 48 hours after infection. For some experiments, Capan-1 cells stably expressing wild-type ephrin-B1 were established after retrovirus infection through the selection in medium containing G418 (600 μg/ml). L cells stably expressing ephrin-B1 or EphB2 were established as described and cultured in medium containing hygromycin B at a concentration of 400 μg/ml (Tanaka et al., 2005). PANC-1 cells stably expressing ephrin-B1 were established through selection in medium containing puromycin at a concentration of 2 μg/ml for 2-3 weeks. Well isolated colonies were characterized further.

In vitro siRNA treatment

Stealth siRNA (Invitrogen) of MMP-8 was synthesized as follows. Sense: 5′-AAGGCAUGAGCAAGGAUUCCAUUGG-3′; antisense: 5′-CCAAUGGAAUCC-UUGCUCAUGCCUU-3′. The control siRNA (scramble II duplex: 5′-GCG-CGCUUUGUAGGAUUCGdTdT-3′) was purchased from Dharmacon. SiRNAs were incorporated into cells using Lipofectamine™ 2000 according to the manufacturer's instructions (Invitrogen). Assays were performed 72 hours post treatment.

Peptidomic analysis of secretory proteins

SUIT-4 cells were cultured in serum-free RPMI1640 medium and the conditioned medium was collected. Cleared supernatant was loaded onto a SepPak C18 cartridge (Waters) for peptide extraction. Peptides bound to the cartridge were eluted with 0.1% trifluoroacetic acid (TFA)/60% acetonitrile (ACN) and lyophilized. The resultant sample was reconstituted with the same solvent and applied to an HPLC gel filtration column (Pharmacia). Fractions containing peptides with a molecular mass below 8,000 Da were subjected to reductive alkylation as described previously (Sasaki et al., 2002) and desalted with an Empore disk cartridge (3M). The desalted material was separated with a 75 mm × 100 mm C18 column (LC Packings, Sunnyvale, CA) before matrix assisted laser desorption ionisation (MALDI)-MS/MS analysis using an Ultimate HPLC pump and gradient programmer (LC Packings). The solvent system was 5% acetonitrile (ACN) (solvent A) and 95% ACN (solvent B); both contained 0.1% TFA. A linear gradient from 5% B to 60% B over 50 minutes was used. Eluates were spotted at 20-second intervals using Probot (LC Packings) on a MALDI target plate. Mass spectra were obtained in reflector mode on a (MALDI-TOF/TOF 4700 mass spectrometer (Applied Biosystems). Ion signals above S/N 25 observed in the MSMS spectra were selected for MSMS ion search against human entries in the NCBI nr database using the Mascot (Matrix Science) search algorithm with no enzyme specification, with the mass tolerance of precursor ions and product ions set at 100 ppm and 0.25 Da, respectively.

Immunoprecipitation and immunoblotting

Cell lysates were prepared with protease inhibitors in PLC buffer [50 mM HEPES (pH 7.5), 150 mM NaCl, 1.5 mM $MgCl_2$, 1 mM EGTA, 10% glycerol, 100 mM NaF, 1 mM Na_3VO_4 and 1% Triton X-100]. To precipitate the proteins, 1 μg of

Journal of Cell Science